The Dissertation Committee for Marcelo Arturo Somos Valenzuela Certifies that this is the approved version of the following dissertation:

Vulnerability and Decision Risk Analysis in Glacier Lake Outburst Floods (GLOF). Case Studies: Quillcay Sub Basin in the Cordillera Blanca in Peru and Dudh Koshi Sub Basin in the Everest Region in Nepal

Committee:

Daene C. McKinney, Supervisor

David R. Maidment

Ben R. Hodges

Ginny A. Catania

Randall J. Charbeneau

Vulnerability and Decision Risk Analysis in Glacier Lake Outburst Floods (GLOF). Case Studies: Quillcay Sub Basin in the Cordillera Blanca in Peru and Dudh Koshi Sub Basin in the Everest Region in Nepal

by

Marcelo Arturo Somos Valenzuela, B.S; M.S.E.

DISSERTATION

Presented to the Faculty of the Graduate School of

The University of Texas at Austin

in Partial Fulfillment

of the Requirements

for the Degree of

DOCTOR OF PHILOSOPHY

THE UNIVERSITY OF TEXAS AT AUSTIN

AUGUST, 2014

Dedication

To my mother Marina Victoria Valenzuela Reyes for showing me that I could always achieve a little more.

A mi madre Marina Victoria Valenzuela Reyes por mostrarme que siempre podia lograr un poco mas.

Acknowledgements

There are many people to whom I want to thank for this achievement. I start with my children Sebastian and Antonia for their patience and unconditional love despite the difficult times we have experienced in the last 5 years, I hope that someday this achievement will lead to better opportunities for you and justify to be apart for all these years. Thank to my fiancée, Stephanie, for her love, for her tenacity and intelligence that inspire me, but most of all for giving me our beautiful son Julian whose smile makes us happy every day. To my supervisor Dr. Daene C. McKinney for his support, his time, his friendship and for allowing me to travel and see other places through the HiMap project. My friend Alvaro who I met when everything looked difficult to achieve; thank you for being always there when I needed you. To Miriam and Cony for giving me a home when I needed in Chile. Thanks to Zacapa FC: Torpedo, Diavolo, Johnny, Wiki, Mate, Evitala and many others who brought joy and laughs to light the way while I was in Austin. My parents for giving me the tools to finish the PhD.

Special thanks to my dissertation committee for their comments and taking the time to review my work. To all who have made this work possible such as the Fulbright Commission, Conicyt-Chile, Graduate School of the University of Texas at Austin, The Mountain Institute, CRWR, USAID, Ministry of Environment of Peru, Inter-American Development Bank, Himalayan Research Expeditions, Cesar Portocarrero for his kindness and for sharing his knowledge and expertise, Dr. McKinney's research group, and many others who have been in this process and much earlier too.

Hay muchas personas a las cuales quisiera agradecerles este logro. Quiero comenzar con mis hijos Sebastián y Antonia por la paciencia y amor incondicional a pesar de los momentos difíciles que hemos vivido en estos últimos 5 años, espero que este logro algún día se traduzca en mejores oportunidades para ustedes y la distancia haya valido la pena. Agradecer a Stephanie por su amor, por su tenacidad e inteligencia que me inspiran, pero por sobre todo por darme nuestro hermoso hijo Julián cuya sonrisa nos alegra cada día. A mi supervisor el Dr. Daene C. McKinney por su apoyo, su tiempo, su amistad y por permitirme viajar y conocer otros lugares a través del proyecto HIMAP. A mi amigo Álvaro a quien conocí cuando todo se veía difícil de lograr, gracias amigo por estar siempre ahí cuando te he necesitado. A la señora Miriam y Cony por entregarme un hogar cuando lo necesité en Chile. A Zacapa FC, Diávolo, Johnny, Wiki, Mate, Evítala y muchos otros que trajeron alegría y risas para alumbrar el camino mientras estuve en Austin. A mis padres por darme las herramientas necesarias para terminar el Doctorado.

Agradecer al comité de disertación por sus comentarios y darse el tiempo de revisar mi trabajo. A todos quienes han hecho posible este trabajo como la Comisión Fulbright, Conicyt, Escuela de Graduados de la Universidad de Texas en Austin, el Instituto de Montaña, CRWR, USAID, Ministerio de Medio Ambiente del Perú, Banco Interamericano de Desarrollo, Himalayan Research Expeditions, Cesar Portocarrero por su amabilidad y disposición a compartir su experiencia y conocimiento, al grupo de investigación del Dr. McKinney. Y muchos otros que han estado en este proceso y mucho antes también.

Vulnerability and Decision Risk Analysis in Glacier Lake Outburst Floods (GLOF). Case Studies: Quillcay Sub Basin in the Cordillera Blanca in Peru and Dudh Koshi Sub Basin in the Everest Region in Nepal

Marcelo Arturo Somos Valenzuela, Ph.D.
The University of Texas at Austin, 2014

Supervisor: Daene C. McKinney

Glacial-dominated areas pose unique challenges to downstream communities in adapting to recent and continuing global climate change, including increased threats of glacial lake outburst floods (GLOFs) that have substantial impacts on regional social, environmental and economic systems increasing risk due to flooding of downstream communities. In this dissertation, two lakes with potential to generate GLOFs were studied, Imja Lake in Nepal and Palcacocha Lake in Peru. At Imja Lake, basic data was generated that allowed the creation of a conceptual model of the lake. Ground penetrating radar and bathymetric surveys were performed. Also, an inundation model was developed in order to evaluate the effectiveness of a project that seeks to reduce flooding risk by lowering the lake at least 3 meters. In Peru, a GLOF inundation model was created. Also, the vulnerability of the people living downstream in the City of Huaraz was calculated, and the impacts of an early warning system were evaluated. The results at Imja indicated that the lake deepened from 98 m in 2002 to 116 m in 2012. Likewise, the lake volume increased from 35.8 to 61.6±1.8 million m^3 over the past decade. The GPR survey at Imja

and Lhotse-Shar glaciers shows that the glacier is over 200 m thick in the center of the glacier. The modeling work at Imja shows that the proposed project will not have major impacts downstream since the area inundated does not reduce considerably unless the lake is lowered by about 20 m. In Huaraz, the results indicate that approximately 40646 people live in the potentially inundated area. Using the flow simulation and the Peru Census 2007, a map of vulnerability was generated indicating that the most vulnerable areas are near the river. Finally, the potential number of fatalities in a worst case GLOF scenario from Lake Palcacocha was calculated to be 19773 with a standard deviation of 1191 if there is no early warning system and 7344 with a standard deviation of 1446 people if an early warning system is installed. Finally, if evacuation measures are improved the number reduces to 2865 with a standard deviation of 462.

TABLE OF CONTENTS

LIST OF TABLES

LIST OF FIGURES

Chapter 1: Introduction

Continued atmospheric warming induces striking changes of most glaciers around the world (WGMS 2008). The formation of new lakes in de-glaciating high-mountain areas (Linsbauer et al. 2012) strongly influences landscape characteristics and represents a significant hazard related to climate change (Richardson and Reynolds 2000; Kattelmann 2003; Haeberli et al. 2010).

Numerical models indicate that mountain glaciers are likely to continue vanishing (Zemp et al. 2006); for example, a fifth of Canada's Arctic Archipelago glaciers may disappear by the end of the century (Lenearts et al. 2013); up to 50 percent of the Andes glaciers may have already been lost to climate-induced melting (Rabatel et al. 2013); that Himalayan glaciers are losing mass as well, although with notable exceptions in the Karakoram and Northwestern Himalaya (Bolch et al. 2012). Major effects of this trend in glacier recession are increased variability in water supplies in some areas (Huss 2011) and flooding risks from lakes formed at receding glaciers (Clague and Evans 2000; Haeberli et al. 2010).

According to the Intergovernmental Panel on Climate Change (IPCC 2001) "Numerous studies worldwide show a widespread, and well documented, retreat of mountain glaciers in non-polar regions of the world during the 20th century." Coudrain et al. (2005), Casassa et al. (2009), and Armstrong (2010) note that mountain glaciers are an excellent indicator of climate change. When glaciers melt the runoff increases, increasing the risk of flooding in zones adjacent to downstream rivers. These melting processes also lead to the formation of new glacier lakes at or on the terminus of glaciers (Awal et al.

2010) in high elevations in rugged terrain of remote areas (Bajracharya et al. 2008; Chen et al. 2010). Glaciers have been receding due to climate change, in some cases causing the formation of glacier lakes of increasing volume. In some cases, there can be increasing the risk of failure of terminal moraines due to the weakening of ice cores combined or due to an increase in trigger mechanisms (e.g., rock and ice avalanches) in such places (Horritt and Bates 2002). Newly formed glacier lakes are often contained by loose boulders and soil dams, and this can present a risk of a Glacial Lake Outburst Flood (GLOF) in some cases (Sakai et al. 2003; Bajracharya et al. 2007b; Osti and Egashira 2009; Shrestha et al. 2010). A GLOF is a sudden release of water, many orders of magnitude higher than the normal flow, from the glacier lake due to a triggering mechanism (often a breach of the moraine dam) (Ives 1986; Carrivick 2006). GLOFs represent one of the most significant hazards related to glacier recession and temperature rise due to climate change (Richardson and Reynolds 2000; Kattelmann 2003). GLOFs can affect fragile mountain ecosystems as well as economic activities due to the large magnitude and power of the flood flow comprised of water and (Bajracharya et al. 2007b).

There is a necessity to evaluate the impact of GLOFs and validate models that describe such events; however, this is difficult because of the lack of information Attention has been primarily focused on past events, and satellite image information, but not on the field information, hydrodynamic characteristics and continuum mechanics of the floods (Osti and Egashira 2009).

1.1 SITUATION AND ISSUES

Antarctic and Greenland ice sheets hold 99 percent of the land glacier mass in the world; however, they represent just 17 percent of the ice mass loss worldwide. High Mountain of Asia, the second greatest glaciered area represent 10 percent of the ice mass loss worldwide (Gardner et al. 2013). Glacier-dominated mountains play a significant role in providing water to large populations, especially in the Himalayas (Singh and Bengtsson 2004; Barnett et al. 2005) and Andes regions (Bradley et al. 2006). Continued and increasing glacier melting may initially increase runoff in some areas, but lack of a glacial buffer ultimately will cause decreased reliability of dry season stream flow (Bradley et al. 2006) affecting water supply, agriculture, hydropower, and ecosystems.

Glacial-dominated areas pose unique challenges to downstream communities in adapting to recent and continuing global climate change, including reduced dry season flows and increased threats of glacial lake outburst floods (GLOFs), both of which have substantial impacts on regional social, environmental and economic systems increasing risk and vulnerability due to flooding and water availability in downstream communities. These impacts can induce changes in interlinked local and global political economies depending on the vulnerability (i.e., sensitivity, exposure and adaptive capacity) to the hazard (Gallopín 2006; O'Brien et al. 2006; Adger 2006).

Research is needed on these systems to understand the interaction of hazards and vulnerability in the social-ecological system that includes two-way, participatory input and involvement, communicating biophysical science research to local communities and reciprocally transmitting local knowledge and understanding back to physical scientists in equitable ways (O'Brien et al. 2006; Vogel et al. 2007). Especially over the past several

decades, hundreds of lower altitude (< 5200 m) Himalayan and Peruvian glaciers have been melting, leaving behind new glacier lakes that are holding millions of cubic meters of water. Usually contained by dams of loose boulders and soil, these lakes present a risk of GLOFs. Triggering factors for GLOFs include "…lake area expansion rate; up-glacier and down-valley expansion rate; dead-ice melting; seepage; lake water level change, and surge wave by rock fall and/or slide and ice calving" (Watanabe et al. 2009). GLOFs unleashes stored lake water often causing enormous devastation downstream that can include high death tolls, as well as the destruction of valuable farmland and costly infrastructure (e.g., hydroelectric facilities, roads, and bridges).

Examples of GLOFs include the 1941 GLOF disaster in Huaraz, Peru that killed nearly 6,000 people within minutes (Carey 2005; Carey 2010); the 1985 Langmoche outburst in the Sagarmatha (Mt. Everest) National Park, Nepal that destroyed the Thami hydroelectric facility, hundreds of hectares of cropland, and dozens of bridges downstream (Vuichard and Zimmermann 1986; Vuichard and Zimmermann 1987); and 1998 outburst of the Sabai Tso in the Hinku valley, Makalu-Barun National Park, Nepal that destroyed trails and seasonal settlements for 100 km downstream (Cox 1999; Osti and Egashira 2009), damage that is still visible in satellite images taken a decade later. Many countries with glaciated mountain ranges have experienced GLOF events, from Canada and Italy to Nepal and Peru (Clague and Evans 2000; Richardson and Reynolds 2000; Huggel et al. 2003; Carey 2005; Bajracharya and Mool 2009; Carey 2010; ICIMOD 2011; Carey et al. 2012). Nepal has experienced numerous GLOFs in the past (Ives 1986; Byers 1987; Bajracharya et al. 2007a). The frequency of GLOF events has increased in recent decades (Eriksson et al. 2009; ICIMOD 2011), but only recently has

the problem received a significant level of attention (Bajracharya et al. 2007b; Eriksson and Xu 2008; ICIMOD 2009).

Although the call for the greater use of holistic, basin-wide approaches to both water resources management and hazards reduction is increasing in Nepal (ICIMOD 2009), experience in dangerous lake analysis, control, management, and utilization remains limited and nascent (Byers et al. 2013). Peru, on the other hand, has more than 50 years of experience reducing risk in high elevation glacial lake and installing safety systems. However many of those systems, which were successful when they were installed, need to be revised since the conditions of the environment have changed dramatically during the last decades. An example is the case of Palcacocha Lake safety system installed in 1971, which successful kept the lake in a volume of 500.000 cubic meters. However, the glacier tongue retreated during the last decades increasing the lake volume to 17 million cubic meters.

Additionally, much uncertainty exists regarding appropriate methods for lowering the levels and decreasing the volumes of dangerous lakes to safe levels. This uncertainty is perhaps related to the mixed results and tremendous expense (~ $4 million) of the Tsho Rolpa lake project in the Rowaling valley in the late 1990s, Nepal's only effort to date to manage a glacial lake (Bell et al. 2000; Matambo and Shrestha 2011). As a result, some have argued that engineering methods, such as controlled breach or siphons, are too expensive for the Himalaya and that, early warning systems are the only practical solution (ICIMOD 2011).

Additionally, local people living below these new lakes are increasingly voicing their concerns and fears for their lives and safety. They have experienced glacial lake

outbursts as recent as 1998 that caused severe property and infrastructural damage as well as the tragic loss of life (Ives 1986; Vuichard and Zimmermann 1986). Furthermore, local communities are becoming increasingly frustrated that they rarely have if ever, been consulted or involved in the decades of glacial lake scientific field research. Researchers do not share their results with them, and accessible only in scientific journals or the internet, and that there is a growing sense of uncertainty and confusion experienced by the community as a result (Khadka 2012; Byers et al. 2013). Local perspectives have also rarely been integrated into management plans and solutions. Clearly, a science-driven, community-centered approach to the study of potentially dangerous lakes is long overdue, which will be applicable to other sites around the globe facing similar hazards.

1.2 RESEARCH OBJECTIVES

The aims of this dissertation are to generate information that allow communities downstream Palcacocha Lake in Peru and Imja Lake in Nepal to understand the level of hazard related to GLOFs; to generate tools that allow authorities and communities to evaluate qualitatively or quantitatively the effectiveness of proposed risk reduction measurements; to increase awareness to this worldwide growing hazard related to glacier melting and lake formation, which is threatening infrastructure, as well as human life.

This goal of this research is to apply flood risk methodologies for the risk evaluation of GLOFs. The objectives of this dissertation research are to:

1. Generate basic physical information that allows us to understand and model potential GLOF events from Imja Lake predicting future conditions.

2. Evaluate the effectiveness of an UNDP proposal to reduce Imja Lake risk lowering the lake by 3 meters.
3. Quantify the magnitude of a potential GLOF from Lake Palcacocha in Peru and map the vulnerability using INDECI framework.
4. Evaluate the benefits of an early warning system (EWS) in the risk reduction in Huaraz including uncertainty analysis.

It is important that this work helps, especially, local communities in Peru and Nepal, who have been affected by changes in their environments due to global warming. Allowing them to understand the level of risk to which they are exposed and helping local governments and international agencies to develop projects that fulfil the goal of reducing risk saving expensive infrastructure, and especially saving people's life.

1.3 DISSERTATION OUTLINE

This dissertation is divided into four chapters: Chapter 1 is the Introduction, the objectives and the contributions to the state of the art are indicated. Chapter 2 and 3 are the core of this dissertation document. This study covers two lakes one in Peru and one in Nepal; therefore, this geographic division is used to divide these 2 chapters. Objectives 1 and 2 are addressed in Chapter 2. Objectives 3 and 4 are addressed in Chapter 3. Chapter 4 provides a discussion of the work in Peru and Nepal addressing how this research helps to answer the objectives proposed at the beginning of this work. At the end of the document, there are an Appendix that describes the equations for the inundation model Flo-2D and a list of references.

1.4 CONTRIBUTION TO THE STATE OF THE ART

This research presents 6 contributions to the state of the art

1. It updates the bathymetry of Imja Lake, which was measured successfully for the last time in 2002. Also, this research generates information related to the depth thickness of Imja-Lotse shar glaciers, which could potentially be the future depth of the Lake if the glaciers continue retreating.
2. It evaluates the effectiveness of a project that UNDP and the Nepal government are proposing for reducing the risk at Imja Lake lowering water level by 3 meters replicating the work done in Tsho Rolpa Lake in Nepal. There are no scientific criteria that justify for replicating that work; therefore, this research seeks to fill that gap.
3. It updates the GLOF hazard map in Huaraz, which will be used to delineate public policies related to increase the preparedness of the people in Huaraz.
4. It adapts a life loss risk analysis framework use for the Corps of Engineering (USACE) to the information available in Huaraz including uncertainty analysis.
5. Evaluate the effectiveness of a EWS in Huaraz and proves the necessity of information dissemination and training in order to reduce the evacuation time in case that a GLOF is generated at Palcacocha Lake
6. It brings awareness and proposed solutions to this growing problem generated by Global Warming in high elevation environments.

Chapter 2: Imja Lake in Nepal [1]

2.1 INTRODUCTION

The formation of glacier lakes in the Nepal Himalaya has been growing since the early 1960s. Accompanying this increase in the number and size of glacier lakes is an associated number of GLOF events. Table 1 lists known GLOF events in Nepal (Ives et al. 2010; Shrestha and Aryal 2010). Kattelmann (2003) estimates that since 1960 GLOFs occur on average every three to four years in the eastern Himalaya. The appearance and danger posed by glacier lakes in this region have prompted national and regional groups to assess the increasing GLOF risk to communities downstream of the lakes. Glacial lakes in Nepal that need further investigation due to their GLOF risk include Tsho Rolpa, Lower Barun, Imja, Lumding, West Chamlang, and Thulagi lakes (Yamada 1998; Ives et al. 2010).

---

[1] Some of the information from Sections 2.1 to 2.5 is part of a journal paper that is currently under review. The complete reference citation is "Somos-Valenzuela MA, McKinney DC, Rounce DR, Byers AC (2014) Changes in Imja Tsho in the Mt. Everest region of Nepal. Cryosph Discuss 8:2375–2401. doi: 10.5194/tcd-8-2375-2014". This article has 3 other authors whose contributions are as it follows. Dr. Daene C. McKinney worked in the field data collection, literature review and writing of the paper. David Rounce contributions are the analysis of the evolution of Imja Lake using Landsat imagery, writing and comments on the final paper. Dr. Alton Byers contributed to the field work, data collection and comments to the final version of paper.

Table 1: GLOF Events in Nepal (Yamada 1998; Ives et al. 2010; Shrestha and Aryal 2010).

Date	River basin	Name of lake	Cause
450 years ago	Seti Khola	Machhapuchhare	Moraine collapse
Aug. 1935	Sun Kosi	Taraso	Moraine collapse, seepage
Sept. 1964	Arun	Gelhaipco	Moraine collapse, ice avalanche into lake
1964	Sun Kosi	Zhangzangbo	Moraine collapse, seepage
1964	Trisuli	Longda	
1968	Arun	Ayaco	Lake burst 3 times (’68, ’69, ’70)
Sept. 1977	Dudh Koshi	Nare	Moraine collapse
1980	Tamur	Punchan	
Jun. 1980	Tamur	Nagmapokhari	Moraine collapse
Jul. 1981	Sun Kosi	Zhangzangbo	Moraine collapse, ice avalanche into lake
Aug. 1982	Arun	Jinco	Moraine collapse, ice avalanche into lake
Aug. 1985	Dudh Koshi	Dig Lake	Moraine collapse, ice avalanche into lake
Jul. 1991	Tama Koshi	Chubung	Moraine collapse, ice avalanche into lake
May 1995	Kaligandaki		
Sept. 1998	Dudh Koshi	Tama Pokhari	Ice avalanche
Aug. 2003	Madi River	Kabache Lake	Moraine collapse
Aug. 2004	Madi River	Kabache Lake	Moraine collapse

In the Mt. Everest region of Nepal, 24 new glacial lakes have formed, and 34 have grown significantly during the past 50 years (Bajracharya et al. 2007b; ICIMOD 2011). Accompanying this increase in the number and size of glacier lakes is an increase in concern over the potential impact of glacier lake outburst floods (GLOFs) (Ives et al. 2010; Shrestha and Aryal 2011). The appearance and possible danger posed by glacier lakes in this area has prompted calls for assessments of the potential risk to communities downstream of the lakes, and in some cases implementation of risk reduction actions, e.g., at Lake Rolpa (RGSL 2003) and proposed for Imja Lake (UNDP 2013). The Khumbu region of Nepal (Figure 1) has experienced two GLOF events in recent years – Nare in 1977 and Dig Lake in 1985 – both of which caused several deaths and the loss of substantial downstream infrastructure (Fushimi et al. 1985; Ives 1986; Vuichard and Zimmermann 1986; Hammond 1988; Ives et al. 2010). Twelve new and/or growing lakes within the Dudh Kosi watershed of the Khumbu region have been designated as potentially dangerous glacial lakes based on the use of time-lapse satellite imagery (Bajracharya et al. 2007b; Bolch et al. 2008; Watanabe et al. 2009; ICIMOD 2011).

Imja Lake in the Khumbu is often mentioned as a potentially dangerous glacier lake (PDGL) and its GLOF risk has been investigated for more than 20 years (Armstrong 2010). This lake has been reported by Fujita et al. (2009) and Watanabe et al. (2009)as a stable lake. However in September 2011, Dr. Watanabe and people from downstream villages agreed that many surface ponds on the terminal moraine were coalescing into bigger pounds and eventually will form part of the main water body, which could weaken the terminal moraine (Goldenberg 2011).

2.2 STUDY AREA: IMJA LAKE

Imja glacier is located in the Imja Khola watershed in the Khumbu region of the Nepal Himalaya (27.9 ^{o} N, 86.9 ^{o} E), about 9 km south of Mt. Everest (Figure 1). Hammond (1988), in one of the first studies in the region concerned with glacial lakes, identified twenty-four lakes and numerous other meltwater ponds in the Khumbu region in 1988. Most of these lakes began forming in the late 1950s to early 1960s, and have expanded considerably since then, especially Imja Lake (Figure 2). For example, the 1963 Schneider map of the Everest region does not show a lake on the Imja glacier, but rather five small meltwater ponds on the surface near the glacier's terminus (Hagen et al. 1963). The expansion of Imja Lake since the mid-1950s has also been documented through the use of repeat oblique photography (Byers 2007) and remote sensing (Mool et al. 2001).

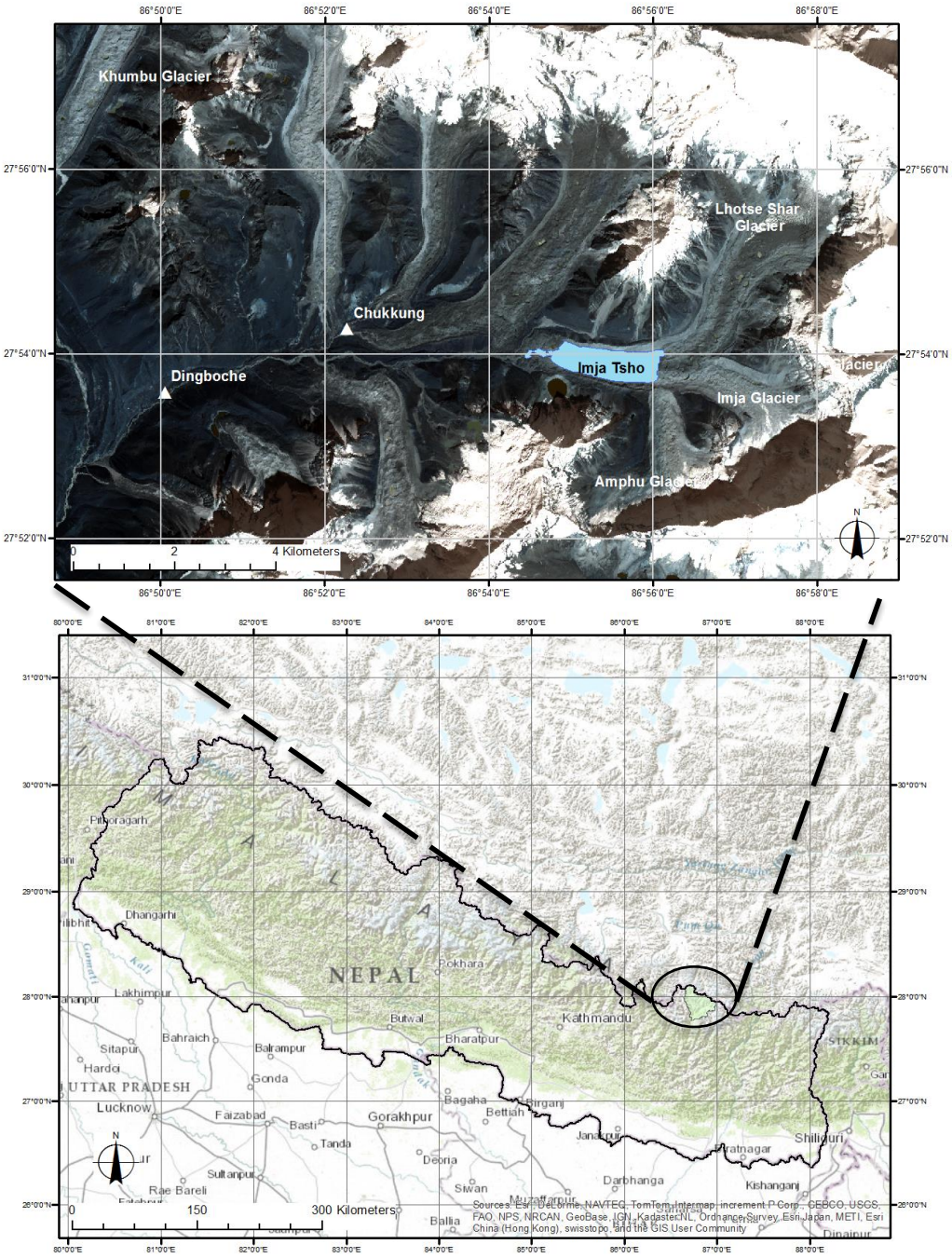

Figure 1: Location of Imja Khola basin within Nepal (Somos-Valenzuela et al. 2014b)

Figure 2: Imja Glacial Lake, September 2012 with Imja glacier to the right, Imja Glacial Lake in the center, and former glacier tongue and outlet at the front left (Photograph by Daene C. McKinney).

A number of authors have discussed the lake's historic development in detail (Yamada 1998; Quincey et al. 2007a; Watanabe et al. 2009; Ives et al. 2010; Lamsal et al. 2011). (Bolch et al. 2011) studied the mass change for ten glaciers in the Khumbu region south and west of Mt. Everest, and found that the Imja glacier area (including the Lhotse Shar/Imja glacier) exhibited a specific mass balance of -0.5±0.09 m/yr., the largest loss rate in the Khumbu region. Nuimura et al. (2012) also report significant surface lowering of the glaciers of the Imja area, with –0.81±0.22 m/yr. for the Lhotse-Shar/Imja glacier. This high annual mass loss rate appears to result from a complex combination of processes that include recently accelerating calving of the glacier terminus and

comparatively thin debris cover (Bolch et al. 2011) that results in the daily transfer of heat directly from the heated debris to the ice below (Sakai and Fujita 2010).

Imja Lake is bounded to the east by the Imja glacier, to the north and south by lateral moraines, and to the west by the ice within the moraine. The lateral moraine troughs act as gutters, trapping debris derived from rock fall, snow avalanches, and fluvial transport (Hambrey et al. 2008). Imja Lake is dammed by a 700 m wide by 600 m long, ice-cored, debris-covered, former glacier tongue through which water exits by means of an outlet lake complex (Watanabe et al. 1994; Watanabe et al. 1995). The incision of the outlet channel complex has lowered the lake level by some 37 m over the last four decades (Watanabe et al., 2009; Lamsal et al, 2011). The bottom of Imja Lake is most likely dead ice, and the presumed melting of this ice has caused the lake level to fall in past decades (Watanabe et al. 1995; Fujita et al. 2009). Fujita et al. (2009) Fujita et al. (2009) concluded that the lake level was stable for the period 1992-2002 by in-situ survey. Watanabe et al. (2009) concluded that the lake level exhibited a continuous lowering for the recent two decades.

Knowledge of the vertical lowering of the Imja glacier, lake, and former glacier tongue is minimal at best. Lamsal et al. (2011), however, report that the average lowering of the glacier surface for the period 1964 to 2006, in the area west of the lakeshore, was 16.9 m. The average glacier lowering east of the lakeshore during this period was 47.4 m. The former glacier tongue still contains ice as clearly evidenced by outcrops of bare ice, ponds formed by melt water from ice in the moraine, traces of old ponds, and results of a GPR survey (Yamada and Sharma 1993). It is likely that the outlet lake complex is evolving into a new arm of the lake (Benn et al. 2012). The outlet flow from the lake

forms the Imja Khola (river), which is a tributary of the Dudh Koshi River. As illustrated in Figure 3, Imja Lake has expanded over the last 50 years mostly through calving of the eastern end of the glacier (Hambrey et al. 2008). The western, down-valley expansion has stabilized in recent years while the eastern expansion continues unabated (Watanabe et al., 2009). For example, we witnessed extensive calving of the eastern glacier terminus, estimated at more than 200 m of ice loss, between May and September of 2012, which is quite unusual and extreme since the average calving retreat during the last decade is 52.6 meters (Somos-Valenzuela et al. 2014b). Somos-Valenzuela et al. (2014c) use normalized differential water index (NDWI) and Landsat imagery to calculate the decadal area changes for Imja Lake from 1992 to 2012 (Table 2 and Figure 3).

Table 2: Imja Lake Decadal Area Expansion 1992-2012 (Somos-Valenzuela et al. 2014b).

Year	Debris Covered Bergs (no.)	Melt Ponds (no.)	Lake Pixels (no.)	Perimeter Pixels (no.)	Area (km^2)	Max Error (km^2)	Error (%)	Decadal Expansion Rate (km^2/yr.)
1992[1]					0.60			
1992[3]	0	12	720	162	0.648	0.073	11.3	
2002[2]					0.868			0.026
2002[3]	0	28	963	202	0.867	0.091	10.5	0.022
2012[3]	15	2	1397	231	1.257	0.104	8.3	0.039

[1] (Yamada and Sharma 1993)
[2] (Fujita et al. 2009)
[3] (Somos-Valenzuela et al. 2014b)

Figure 3 shows the Imja Lake areal evolution from 1963 to 2012, showing some acceleration in the growth rate during the last decade.

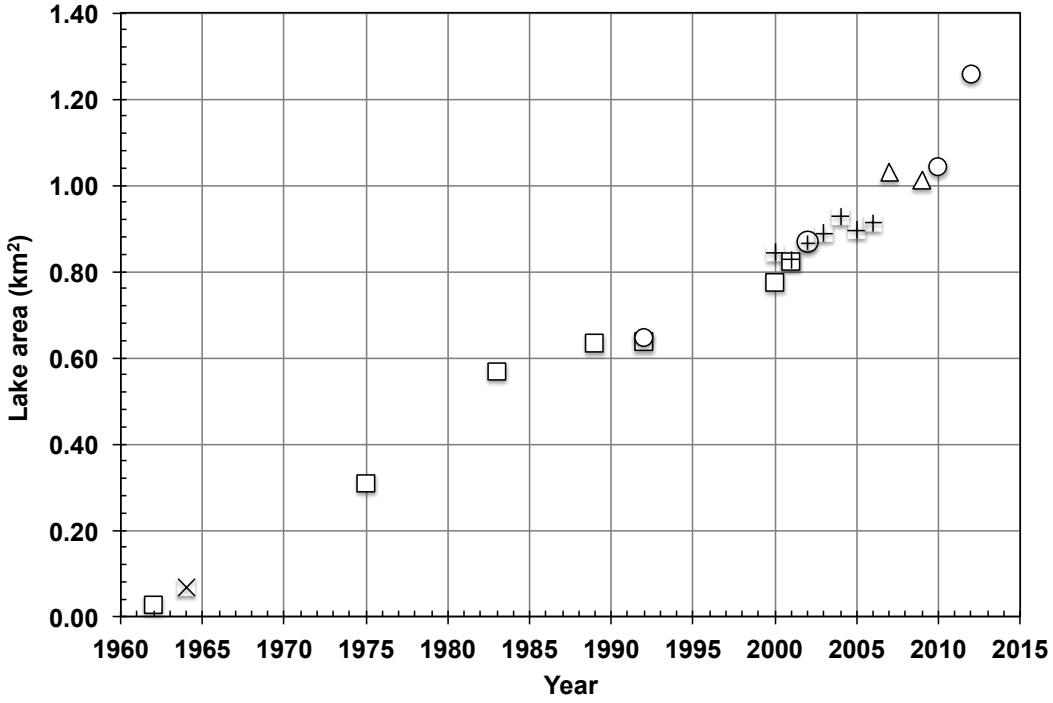

Figure 3: Imja Lake Area Expansion 1962-2012 (Source: □ - Bajracharya *et al*. (2007); ◇ - Yamada and Sharma (1993); ＋ - Fujita *et al*. (2009); × - Lamsal *et al*. (2011); △ - Watanabe *et al*. (2009); and ○ - Somos-Valenzuela et al. (2014b)

2.2.1 Imja: A Potentially Dangerous Glacial Lake?

Imja Lake is among the most studied glacial lakes in Nepal, if not the world (e.g. Hammond 1988; Chikita et al. 2000; Sakai et al. 2003; Sakai et al. 2007; Quincey et al. 2007b; Byers 2007; Bajracharya et al. 2007a; Hambrey et al. 2008; Bolch et al. 2008; Fujita et al. 2009; Ives et al. 2010; Lamsal et al. 2011; Benn et al. 2012). During the past two decades, the lake's growth has led to concerns among some researchers regarding the

possibility of a GLOF event, while a number of other researchers maintain that the risk is minimal**.** Yamada and Sharma (1993), for example, mention Imja Lake as one of the most dangerous lakes in Nepal, noting that ice is present in the terminal moraine and that the moraines are mostly unconsolidated. Watanabe et al. (1994; 1995) reported rapid melt of the debris-covered ice and significant changes in the outlet that may lead to an outburst of the lake if the outlet complex ice continues melting and the terminal moraine sinks. Bajracharya, et al. (2007) called for urgent mitigation measures to reduce the risk of the lake due to its rapid growth. Imja Lake has consistently been ranked in the top three lakes on the Potentially Dangerous Glacial Lakes (PDGLs) list in Nepal, along with Tsho Rolpa and Thulagi Lakes (ICIMOD 2011). On the other hand, Budhathoki et al. (2010) suggested that the risk of a GLOF is only moderate. Hambrey et al. (2008) state that the possibility of a GLOF is very low because of the low risk of calving waves, the wide, gradually changing moraine with adequate freeboard, and a free-draining channel. Watanabe et al. (2009) and Fujita et al. (2009) concluded that Imja is relatively stable. Watanabe et al. (2009) note that the terminal moraine and dead-ice area are of greatest significance and the lateral moraines can be disregarded. Although slow at the time of their reporting (2008-9), continued melting of dead ice in the western shoreline area could cause the lake to burst. They note that a greater possibility for triggering a GLOF by seepage, especially along the spillway, but no signs of seepage was found during their visits to the site. However, we witnessed seepage in two areas of the terminal moraine on three separate occasions in 2011-2012. In addition, Watanabe et al. (2009) note that Imja Lake is most likely to be secure from surge-wave overtopping of the lateral moraines, and that surge waves would not easily overtop the terminal moraine except for the area along

the spillway. However, it is not the threat of overtopping of the lateral moraines that is of concern, but rather the reflection of the resulting waves toward the outlet. Fujita et al. (2009) note that despite the stable downstream shoreline of Imja Lake over the last two decades, continued lowering will cause downstream expansion of the lake, though the lowering rate of the damming moraine seems to be slower that in the late 1980s. This downstream expansion could increase the risk of GLOF. Benn et al. (2012) note that if the outlet channel incision dominates the outlet evolution, the lake may completely drain safely; whereas, if moraine dam narrowing dominates, a GLOF may occur.

The reasons for such a disparity of opinions regarding the level of risk that Imja Lake presents are not entirely clear, but may be related to the wide range of sampling techniques employed, short term nature of the average field expedition, challenging working conditions, or exclusive reliance on remote sensing methods alone. Nevertheless, the risk has been serious enough to prompt the Government of Nepal to engage in a new GLOF risk reduction project, in partnership with the United Nations Development Program in Nepal (UNDP 2013).

2.3 JUSTIFICATION AND AIMS OF OUR WORK IN IMJA LAKE

Imja Lake is of particular interest for several reasons. This lake represents one of the most dramatic examples of glacial lake formation during the second half of the last century growing up to more than 63 million cubic meters in 60 years approximately, presenting one of the fastest glacial lake expansion rates in the world. Imja Lake has been studied for several scientists and yet there is not a complete consensus to the level of risk that it represents for local communities and the economy of Nepal. Although this

disparity in previous risk assessment results, the government of Nepal declared that the lake is in high risk. Consequently UNDP and the Nepalese government are implementing a risk reduction project that aims to lower the lake in at least 3 meters following a previous risk reduction effort in Tsho Rolpa Lake. That previous effort was unsuccessful, and there is no physical and reliable information that indicated that Imja Lake presents the same conditions than Tsho Rolpa Lake presented at the moment of its project design and implementation. Therefore, the aims of the work at Imja Lake are to: perform basic data collection at Imja Lake and glacier in order to have a better physical representation of the system analyzed; estimate Imja Lake Hazard level using a combination of methodologies that allow to have a more holistic approach combining the strength and weakness of different methods; analyze the effectiveness of the risk reduction plan proposed by the government of Nepal and UNDP.

2.4 FIELD WORK

One of the first problems detected in the work at Imja Lake was the lack of the necessary information that could allow running GLOF simulations and predicting future expansion of the lake. Fortunately, trough the High Mountain Glacial Watershed Research program funded by USAID, three visits to Imja Lake were made on September 2011, May 2012 and September 2012. Performing ground penetrating radar (GPR) and lake bathymetry surveys as well as first hand observation in order to create a better understanding of the size of the problem analyzed.

2.4.1 GPR

In order to better understand the structure of the moraine and glacier structure at Imja Lake, ground penetrating radar (GPR) surveys were conducted there during May and September 2012.

2.4.1.1 Methods

GPR is a geophysical technique developed for non-invasive investigation of subsurface features (Davis and Annan 1989) Using GPR, transmitted energy is reflected at the interface of different materials and the reflection is picked up by a receiver and displayed as a plot of signal amplitude against two-way travel time (Davis and Annan 1989; Woodward and Burke 2007). Pulse frequencies used in glaciological applications of GPR normally range from range 5 – 200 MHz. The interface between materials of different permittivity causes reflection of the radiation, with a high permittivity difference between materials results in more reflection. The delay between the time that the GPR transmitter emits its signal and the time reflections return to the receiver is a function of the distance to and from the target and the speed of propagation through the material. Velocities can range from $33x10^6$ m/s in fresh water, to $60x10^6$ m/s for saturated sand, to $110x10^6$ m/s for loose debris and frozen sediments, to $167x10^6$ m/s for ice, and $300x10^6$ m/s in air. Imaging of the subsurface is possible due to the large contrast between the electromagnetic properties of rock, ice, water, and sediments. GPR pulses can penetrate 50 – 1000 m in depth and much deeper in clean ice, depending on the antenna used and the electrical and dielectric properties of the materials being irradiated (Davis and Annan 1989; Neal 2004; Sass 2007).

The GPR surveys described here were carried out using a custom built, low-frequency, short-pulse, ground-based radar system (Catania et al. 2010) refitted from sleds deployment over dry, polar ice to back-pack deployment on wet, temperate ice. Gades et al. (2000) used a similar system on the debris-covered Khumbu glacier near Imja Lake. The GPR transmitter used here was a Kentech Instruments Ltd. GPR pulsar outputting 4kV signals with a 12v power source. The receiving antenna is connected to an amplifier and a National Instruments USB-5133 digitizer. The digitizer output signal is input to a National Instruments Lab View program for immediate processing in the field. GPS signals are correlated with the GPR signals in the Lab View application. Using a common offset deployment, the GPR pulses are transmitted and received through weighted dipole antennae threaded inside climbing webbing (Gades et al. 2000) oriented in-line and operating at 5 MHz (10 m half-length), 10 MHz (5 m half-length), 20 (2.5 m half-length) MHz or 20 MHz (1 m half-length), depending on which antenna provides the best resolution for the depth of the moraine and ice. Both GPR and GPS signals are post-processed using MatLab programs.

The following data processing steps were performed on the data:

Topographic correction

Pre-trigger points removed

Deglitch

Demean with smoothing of mean trace

Detrend

Band pass filter

Convert two-way travel time to depth using a radar velocity in ice of 167×10^6 m/s

Depth strip

Normalize by maximum absolute value

Gades et al. (2000) used a similar GPR system to measure ice thickness on the Khumbu glacier of Nepal, but it was not configured for moving transects. Ice thickness measurements were made using the highest frequency that allowed bed reflection detection; the lowest used was 5 MHz. Longer wavelength (lower frequency) increases the amount of energy that passes through the surface debris layer and decreases the amount of energy scattered from within the ice; however, it also decreases the resolution. Gades et al. (2000) noted errors in their GPR measurements arising from three main sources: migration, inability to select the precise bed reflection location, and uncertainty in the GPR wave velocity within the glacier.

2.4.1.2 Survey Description

GPR survey transects were taken on both sides of the Imja Lake outlet complex, longitudinal surveys on each side of the lake outlet, and surveys near the lateral moraines. Table 3 lists the GPR transects at the terminal moraine. Figures 4 and 5 show the layout of the main GPR transects. Surface elevations were measured by GPS during the GPR transects. The GPS data were collected using both a Garmin BU-353 and a handheld Garmin Etrex Vista HCx unit.

Table 3: List of GPR Transects Taken at the Terminal Moraine of Imja Lake in May-September 2012.

Label	Date	File	Length (m)	Frequency (MHz)
Imja Glacier	25 May 2012	day4-3	210	10
A	22 May 2012	day1-34	341	10
B	23 May 2012	day2-1	389	5
C	23 May 2012	day2-2	483	5
D	23 May 2012	day2file3_5	200	5
E	23 May 2012	day2file4	130	5
F	23 May 2012	day2file5	236	10
G	23 May 2012	day2-7	469	10
H	26 May 2012	day5-3B	238	10
I	24 May 2012	day3-78	762	5
I-2	Sept 25, 2012	Fall12_1-2	512	10
J	26 May 2012	day5-4	146	10
K	26 May 2012	day5-5	142	10
L	26 May 2012	day5-6	217	10

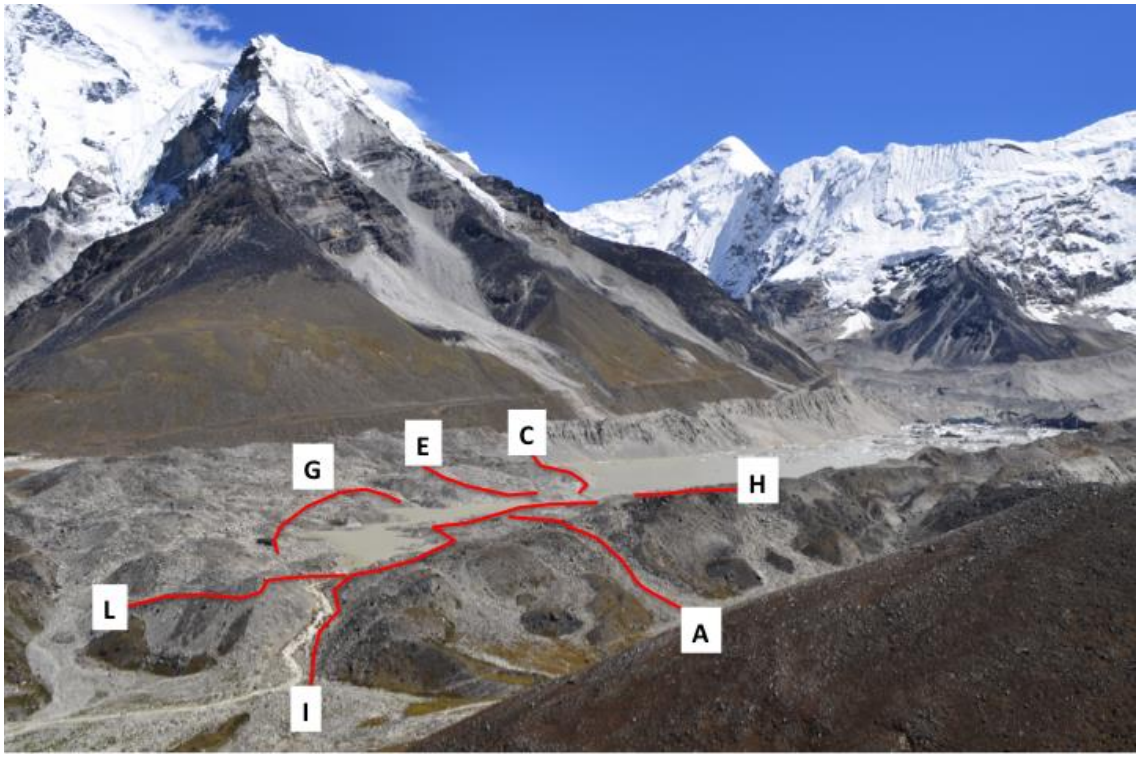

Figure 4: Imja Glacial Lake, September 2012. Imja glacier is at the right, Imja Glacial Lake in the center, and former glacier tongue and outlet at the front left (by Daene McKinney).

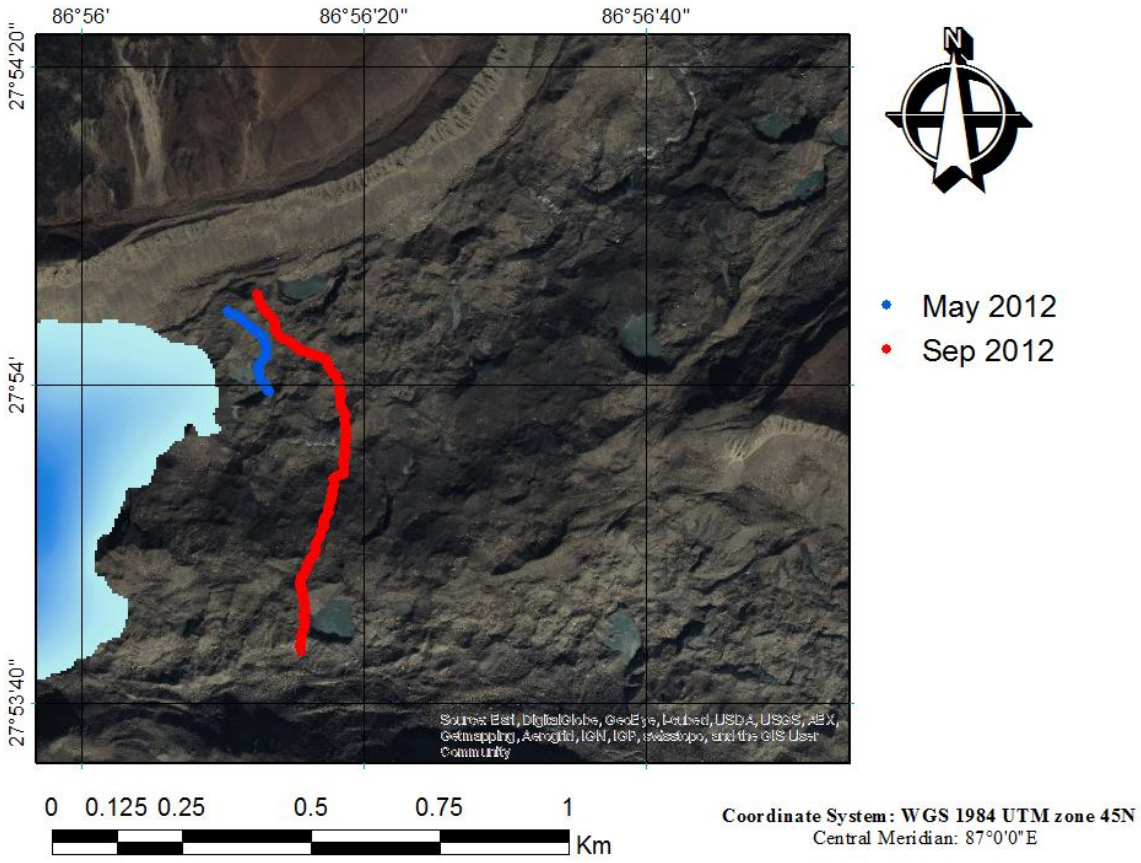

Figure 5: GPR transects at Imja glacier May 25, 2012 (Blue) and September 25, 2012 (Red).

2.4.1.3 GPR results

Imja Glacier GPR Survey

Figure 6 and 7 show GPR transect across the Imja Glacier from north to south, illustrating the transition from layered ice to bedrock both images have the same information they differ in the vertical axis. In in the vertical axis of Figure 6 the two way travel time (TWTT) is used. In in the vertical axis of Figure 7 depth was used, which was

calculated assuming a velocity of propagation through the ice of $167x10^6$ m/s, typical of ice. Figure 8 shows the glacier, near the GPR transect, with a thin layer of debris overlying the thick ice formation.

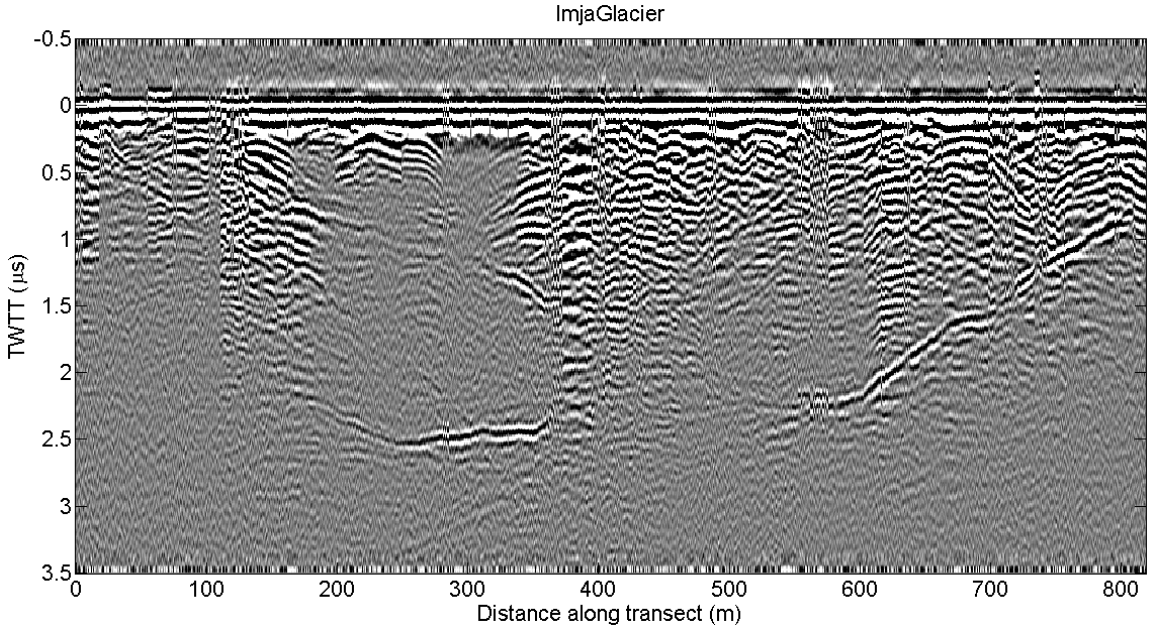

Figure 6: GPR transect at Imja glacier at Imja Lake crossing from north to south on September 25, 2012 using a 10 MHz antenna using the two ways travel time (TWTT) in the vertical axis.

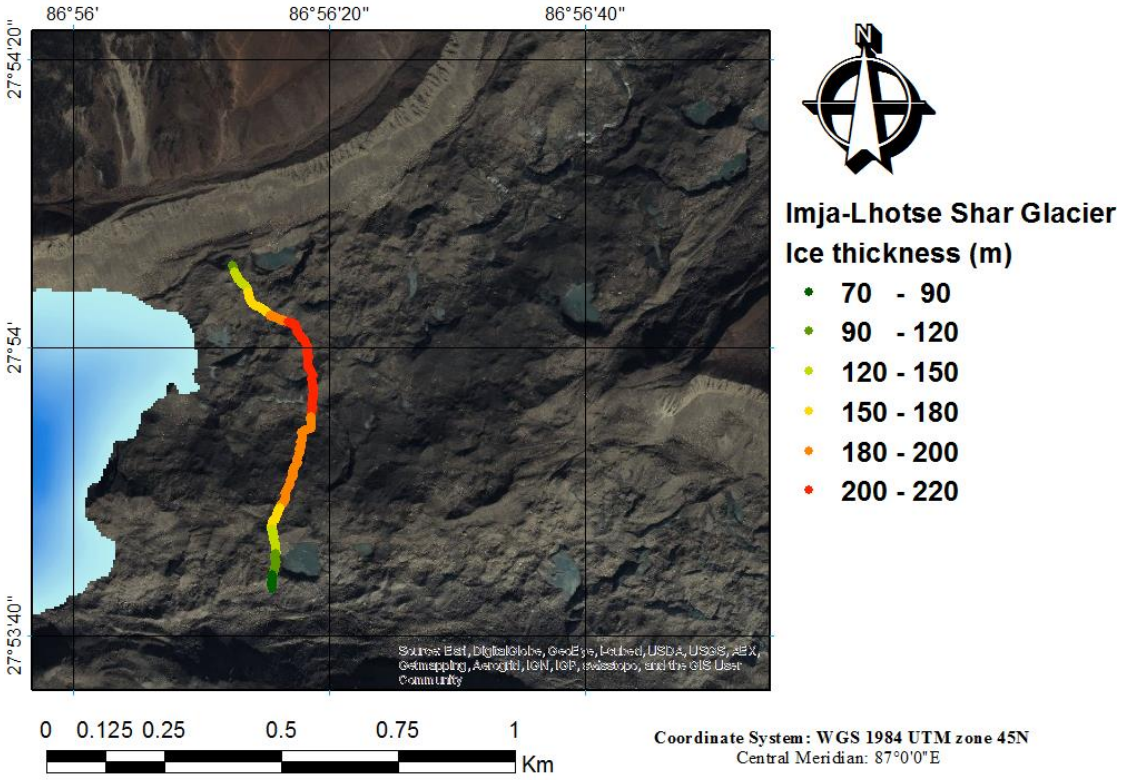

Figure 7: GPR transect at Imja glacier at Imja Lake crossing from north to south on September 25, 2012 using a 10 MHz antenna assuming a velocity in ice of $167x10^6$ m/s.

Figure 8: Photo of Imja Glacier near the location of the GPR transect showing the thin debris cover and ice structure beneath (Credits Daene McKinney).

Imja Terminal Moraine GPR Results

What can be seen in the Figure 9 is probably a buried wedge-shaped ice block that has previously been identified as being present (north of about 225 m circled in red). If we use an ice velocity of 167×10^{-6} m/s we calculated an approximate ice thickness of around 35 m. However, this is an approximate value since the moraine is not all ice; there is debris everywhere so the velocity should be lower. This means that the depths indicated in Figure 9 (lower) should be smaller.

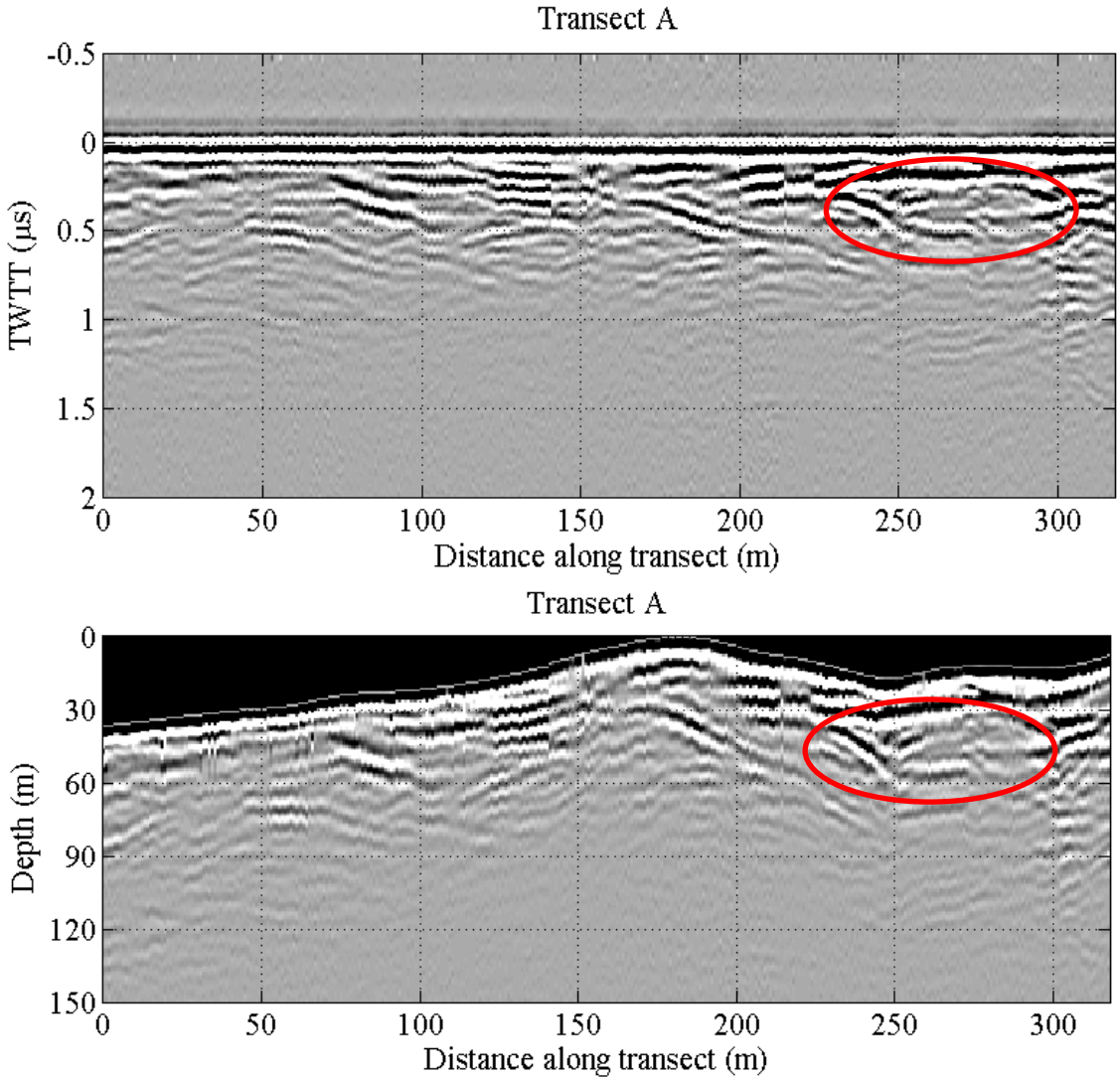

Figure 9: Transect A, Upper figure shows the TWTT in the y axis, the bottom figure shows an estimation of the depth assuming that the propagation velocity is 167×10^{-6} m/s

Although the extensive GPR data collection that we performed at the terminal moraine, the results unfortunately are not as satisfactory as we expected. In the next 3 sets of GPR radar grams we can observe that there is not conclusive information that can

allow us to map the ice thickness. The same happen with the remaining transect; therefore, we are not showing all of them since they don't give extra information.

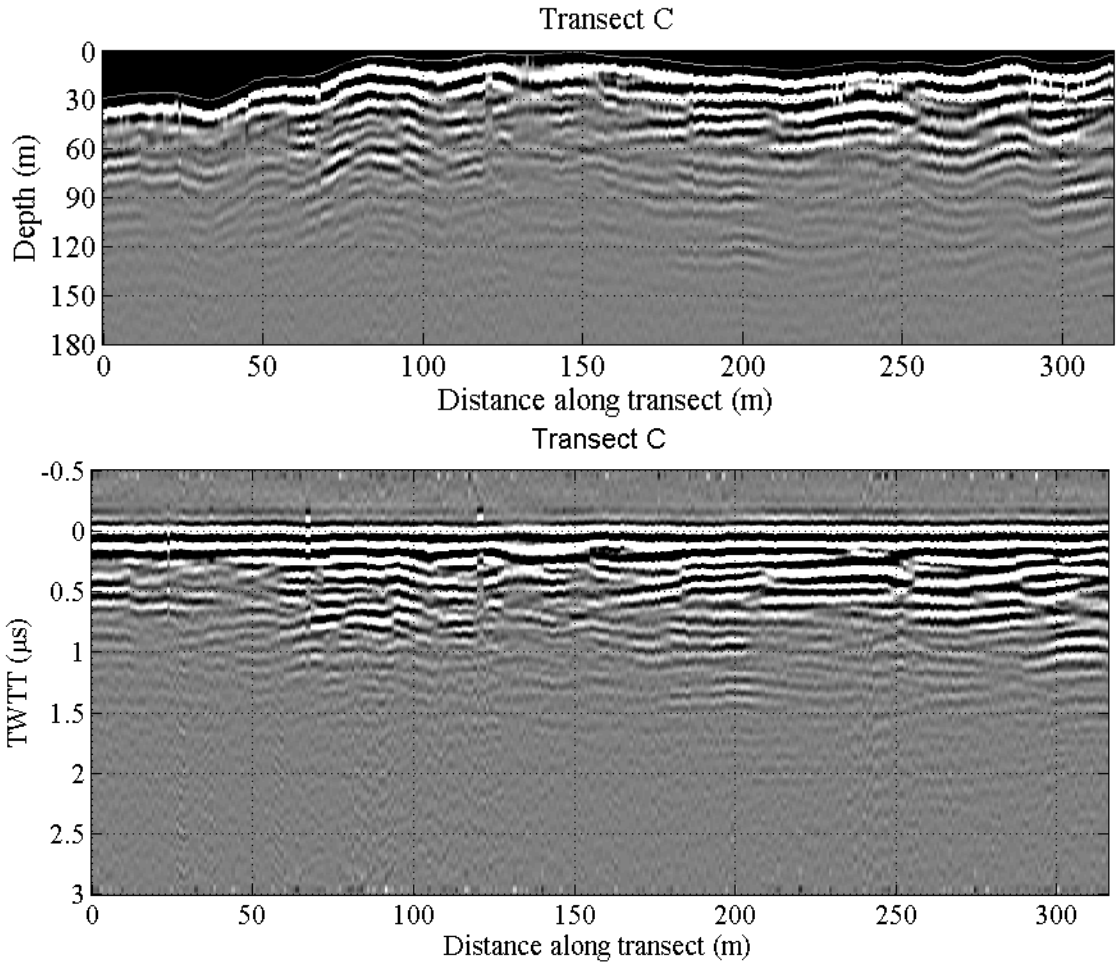

Figure 10: GPR Transect C (Day2file2) at Imja Lake moving from south to north on the terminal moraine above the north-west shore with a 5 MHz antenna and assuming a velocity of $167x10^6$ m/s.

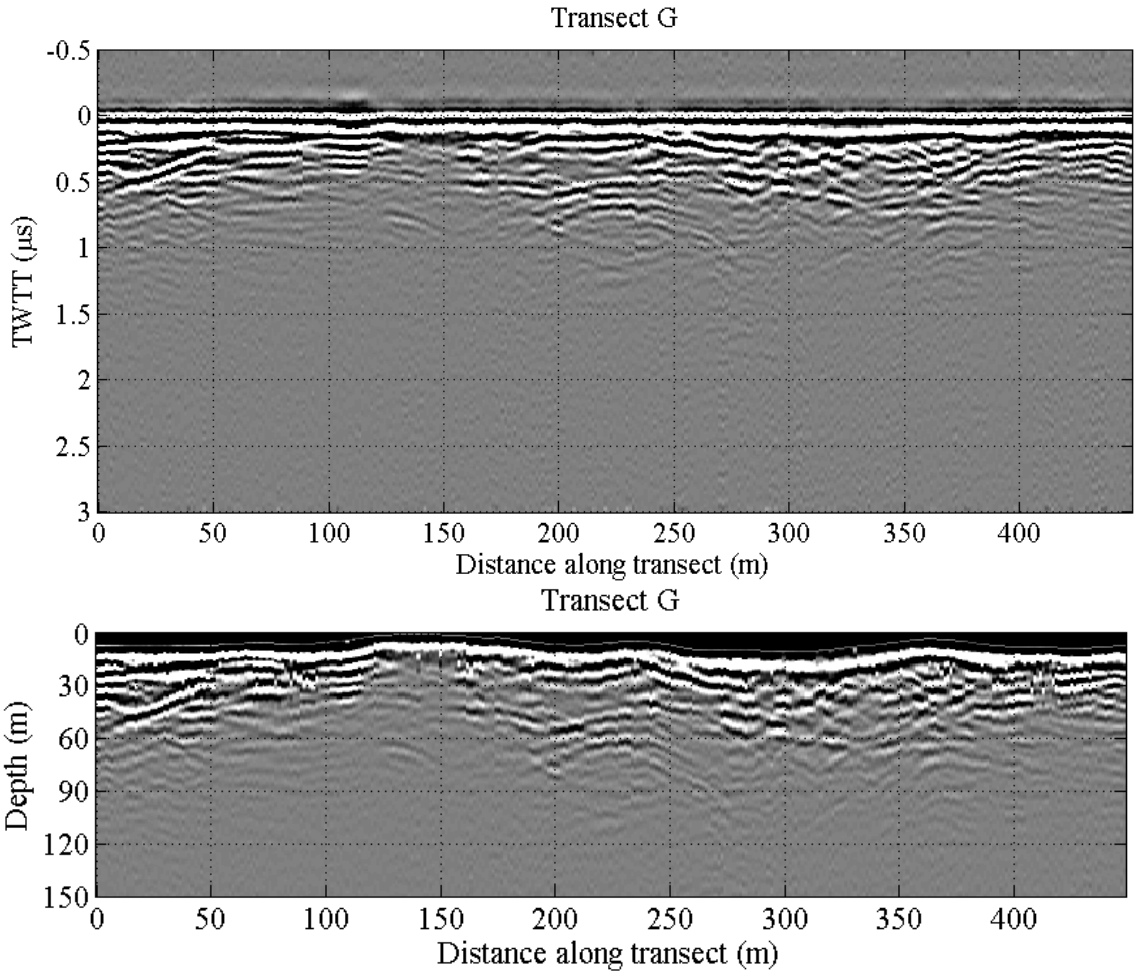

Figure 11: GPR transect G (Day2file7_8) at Imja Lake on the north side of the outlet using a 10 MHz antenna and assuming a velocity of $167x10^6$ m/s.

We have no doubt that in the area where transect H (Figure 12) is located, there is ice underneath. The picture in Figure 13 shows an exposed ice wall that proves that there is ice underneath. However we cannot see in the radargram any interesting or conclusive information that allow us to say something else than that there is ice beneath the debris cover.

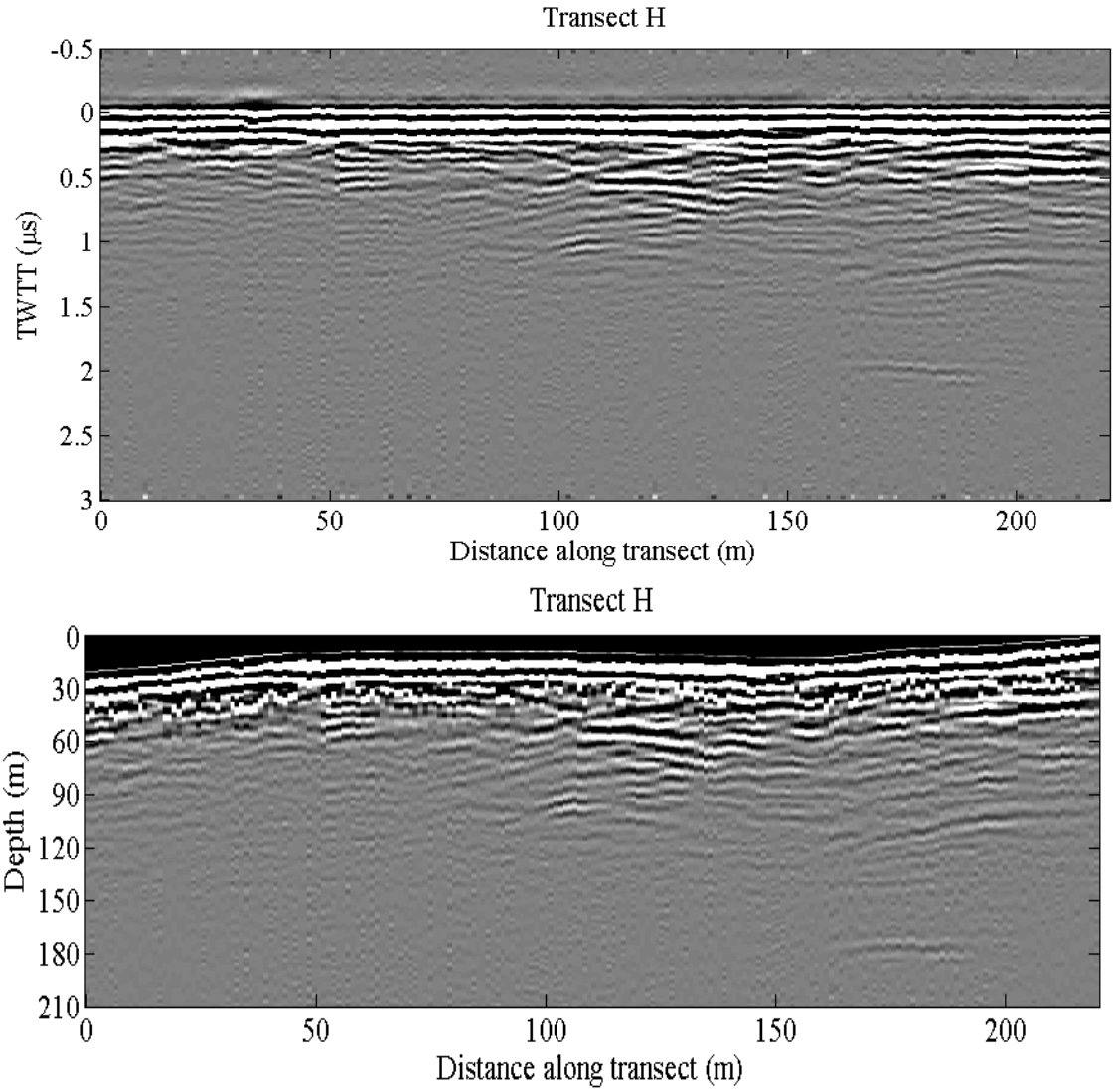

Figure 12: GPR transect H (Day5file3_B) at Imja Lake on the south side of the outlet using a 10 MHz antenna and assuming a velocity of $167x10^6$ m/s.

Figure 13: Ice is visible below GPR transect H seen from a small peninsula near the shore of the lake.

2.4.2 Bathymetry

2.4.2.1 Methodology

We conducted a bathymetric survey of Imja Glacial Lake between September 22 and 24, 2012 using a Biosonic Echo Sounder MX sonar unit mounted on an inflatable raft. The sonar used has a maximum range of 100m. Several transects were measured across the lake, as well as the lake outlet complex of the former glacier tongue of the lake (Figure 14).

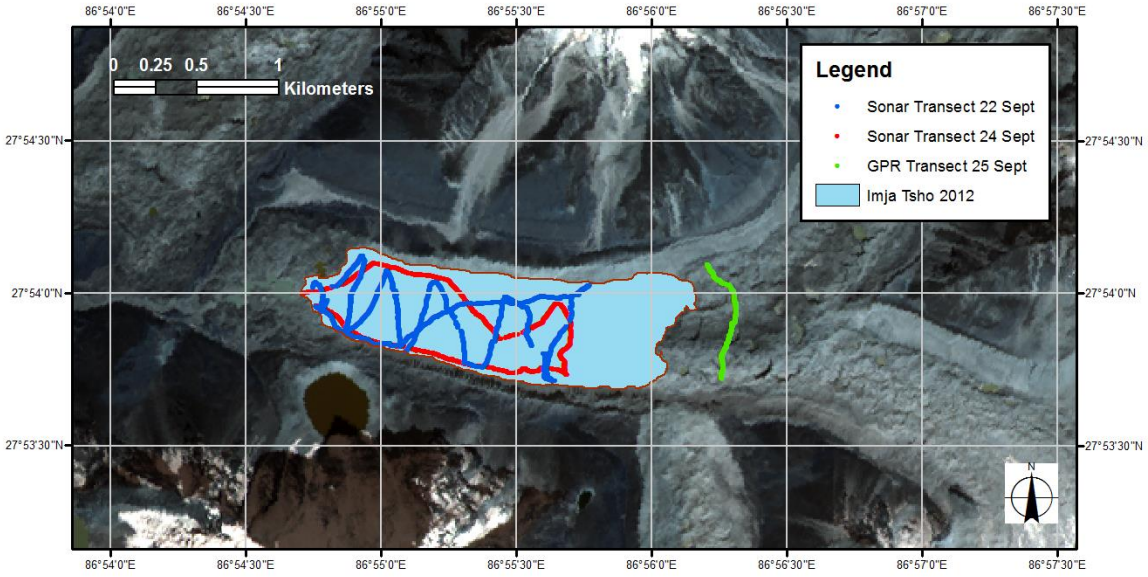

Figure 14: Sonar bathymetric survey transects at Imja Lake September 22 (red) and 24 (blue) and the GPR transect at Imja-Lhotse Shar glacier September 25 (green). The background is an ALOS image from 2008.

For areas with depths greater than 100 m where the equipment could not measure the depth it did record the position of those points. To estimate the depth of the lake in these areas, interpolations were made with values of the shallower, measured points by establishing transects are established crossing the lake from north to south over these depth areas. The lake bottom shape along these transects is assumed to be parabolic fit and an interpolation is fit to the measured points and used to estimate the depths at the missing points.

Figure 15: Icebergs blocking the access to the east end of Imja Lake during the bathymetry survey

Additionally during the survey, large icebergs blocked access to the eastern end of the lake (Figure 15), so interpolation was used to fill in missing values in this area. Robertson et al. (2012) found that ice ramps at the glacier end of glacial lakes tend to have slopes 11-30 degrees and exhibit subaqueous calving. To fill in the missing values, we assume that the lake bottom in the eastern part of the lake is comprised of an ice ramp sloping up toward the glacier terminus and that the ice ramp has a slope of 10-30 degrees in the first 150 m near the glacier; 10-20 degrees in the next 150 m, and 2-5 degrees until the measured points are reached. Three transects, north to south, at 150, 300 and 450m from the eastern shoreline with the shape of the eastern-most measured transect are used for interpolation. The lake depth at the points along the three lines were calculated so

that they agree with the slopes described by Robertson et al. (2012). Since these slopes have maximum and a minimum values, each point along these lines also has a maximum and a minimum value as well that can be used in the uncertainty calculations described below.

In calculating the uncertainty associated with the lake volume, we consider the uncertainty in the depth measurements, and the uncertainty in the slope of the ice ramp, but not the uncertainty in the lake area. The uncertainty of the lake volume calculations are estimated using a range of depth for each point that was interpolated in areas deeper than 100 m or estimated from ice ramp slopes on the eastern end of the lake. In the areas where the depth of the lake was measured with the sonar device, we could directly calculate the maximum and minimum values using the error of the equipment. Using the points measured, interpolated in areas deeper than 100m and calculated using the slope of the ice ramp we interpolate two 5m resolution raster files using the tool TopoToRaster in ArcGIS software, one for the maximum depth values and one for the minimum depth values. Therefore now we have 2 values representing the maximum and minimum depth for each cell of $25m^2$. We assume that the depth in each cell follows a uniform probability distribution (USACE 2003), so that any depth within the maximum to minimum depth range has an equal probability of being the actual depth of the cell. In order to calculate the volume of the lake we used a Monte Carlo simulation with 2000 samples, which allows us to include the uncertainty in our measurement and assumptions; and calculate the expected value and standard deviation of the water volume.

2.4.2.2 Bathymetry Results

Figure 16 shows a contour map of the depth of the bottom of Imja Lake derived from the sonar measurements taken during the two days of surveys. Water depths of 20-60 m were measured near the western edge of the lake (outlet end) and 30-100+ m deep near the eastern (glacier) end of the lake. Because of the thick iceberg coverage on the eastern edge of the lake, transects there were not possible. Elevations deeper than 100 m within the 100 m-contour in Figure 16 were interpolated from the surrounding values; the slope at the up-glacier end (eastern) of the lake has also been approximated. Apparently, the lake bottom has continued to lower as the ice beneath the lake has melted.

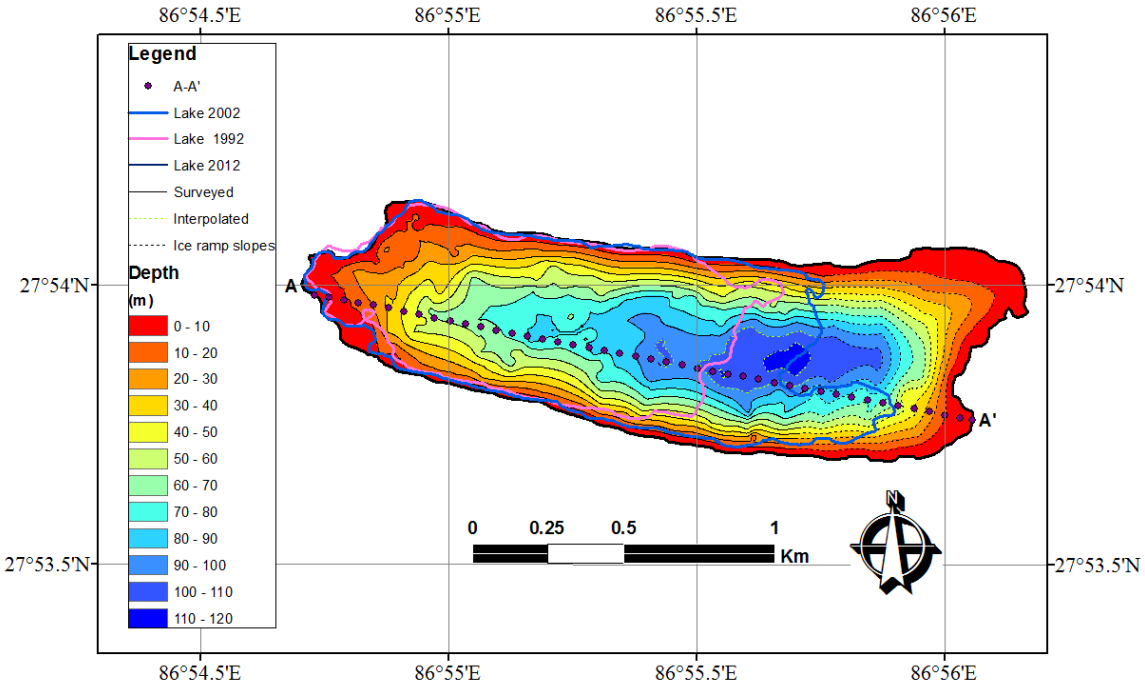

Figure 16: Bathymetric survey results from Imja Lake in September 2012.

The results of the 2012 bathymetric survey are shown in Table 4, and illustrate

considerable variability between those conducted in 2012 and 1992/2002. For example, the previous maximum depth measured in 1992 was 98 m (Yamada and Sharma 1993), compared with an interpolated depth of 116 m measured by our survey. Additionally, the estimated volume of water in the lake nearly doubles that from the 2002 estimates, i.e., from 35.8±0.7 million m^3 in 2002 to 61.6±1.8 million m^3 in 2012. The accuracy of the 1992 data are unknown; however, Fujita et al. (2009) estimated the uncertainty of the 2002 data to be ±0.7 million m^3 by assuming the depth measurement error to be 0.5 m. However, as shown in Figure 15, the consistency of the 2002 and 2012 data from 500 to 1,750 m distance (western part) supports the observations and measurements of a rapid acceleration in growth in the eastern part of the lake.

Table 4: Comparison of Imja Lake 2012 Bathymetric Survey Results with Previous Studies.

Study	No. of measurement points	Volume (10^6 m^3)	Average Depth (m)	Maximum Depth (m)
1992 (Yamada and Sharma, 1993)	61	28.0	47.0	98.5
2002 (Sakai et al., 2003)	80	35.8±0.7	41.6	90.5
2012 (Somos-Valenzuela et al. 2014b)	10,020	61.6±1.8	48.0±2.47	116.3±0.25

Yamada and Sharma (1993) did not report any elevation of the lake or surrounding area. Sakai et al. (2003) report “Glacial Lake is located at the termini of the

Imja Glacier (27°59'N, 86°56'E) in the Khumbu region of eastern Nepal at an altitude of 5010 m.a.s.l." Fujita et al. (2009) report that a number of surveys of the Imja Glacial Lake end-moraine in 2001 (laser) and 2007 (GPS) showed no significant change in the lake level (within 0.2 m in height) between 2001 and 2007. Sakai made a topographic map in 2000-one year before their bathymetric survey--that showed the lake level was 5009 m (Sakai et al. 2007, Figure 5, p. 34). Sakai et al. (2003) plot the data of 1992 and 2002 as having the same water level elevation, so we can assume that the water elevation (5009 m) did not change from 1992 to 2002. I assume that the 1992 and 2002 lake elevations (5009 m) are similar to that of 2012 (5010 m). Sakai et al. (2005) state that the shoreline did not change from 1992 to 2002. Showing the profiles together in Figure 17 gives a good idea of the changes in the lake (maximum depth, length of the lake), which makes this figure truly illustrative.

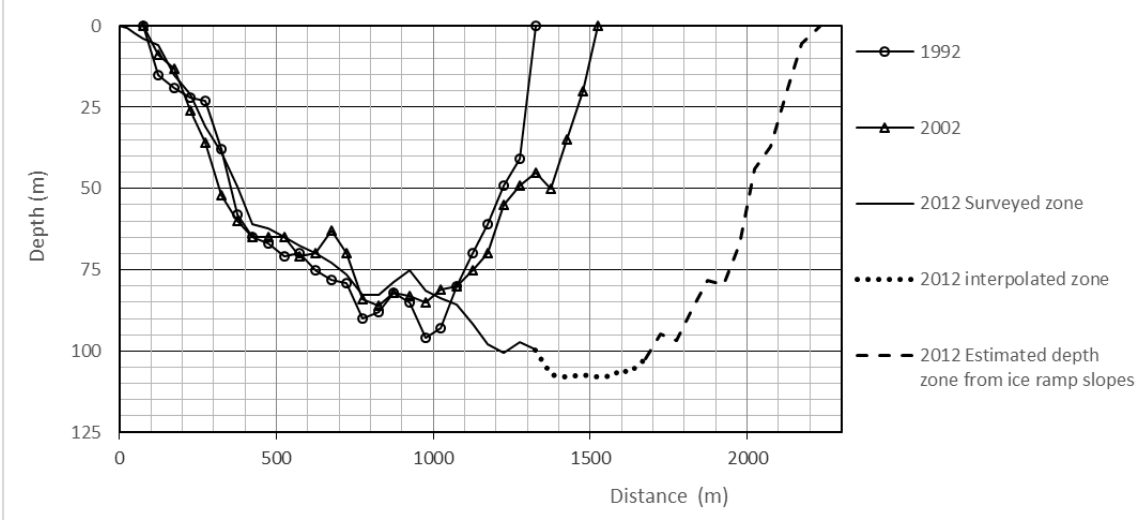

Figure 17: Cross-section A-A' of 2012 bathymetric survey data for Imja Lake compared to 1992 (Yamada and Sharma 1993) and 2002 (Sakai et al. 2003) surveys.

Table 5 shows that the volume of the lake in 2012 was 70 percent larger than in 2002, increasing at a rate of 2.51 million m^3/yr. Compared to the prior surveys, our results also show that the eastern section of the lake has deepened over the last decade (2002-2012) as the ice beneath has melted, with the average depth increasing by 0.86 m/yr. In the same period, the maximum depth has increased 28 percent, and continues to increase at an annual rate of 2.55 m/yr.

One of the important factors in assessing the GLOF risk of Imja Lake is the immense volume that could be released in the event of a flood, and accurate bathymetric data are essential for estimating that volume. We estimate that the volume of a GLOF today would be 33.25 ± 1.25 million m^3, an increase from the previous estimate of 21 million m^3 in 2002 (Sakai et al. 2003). However, even though the potential water that could be released in a GLOF has increased, the probability of GLOF occurrence may not necessarily have increased.

Table 5: Comparison of Imja Glacial Lake Characteristics Over Two Decades

Decade	Volume Increase (%)	Volume Expansion Rate (Million m^3/yr.)	Area Expansion Rate (Km^2/yr.)	Average Depth Change Rate (m/yr.)
1992-2002	30	0.78	0.026	-0.54
2002-2012	70	2.51	0.035	0.86

Based on the results of the bathymetric survey, the volume of Imja Lake for different elevations of the water surface was estimated (Figure 18, upper). In addition, this allowed us to estimate the "potential GLOF water" (PGW) or the amount of water that could be released from the lake in the event of a GLOF occurrence. The PGW is 33.25 ± 1.25 million m^3 if the lake surface elevation decreases from the current lake water level (5010m) to the elevation of the valley floor below the lake (4975m) It may happen that the final elevation of the lake water surface after a GLOF will be higher than the valley floor, depending on the depth of the breach produced by the GLOF. Figure 16 (lower) illustrates the resulting PGW as a function of the final water surface elevation.

Sakai et al. (2003) reported that if the Imja Lake moraine damming the lake water completely collapsed, the lake elevation would drop about 30 m and the water above that level would discharge as PGW. The PGW values in 1992 and 2002 were estimated to be 15×10^6 m^3 and 21×10^6 m^3, respectively (Sakai et al. 2003). Therefore the 2002 PGW was estimated to be 40% larger than the 1992 PGW, and the 2012 PGW is 40.5% larger than the 2002 value.

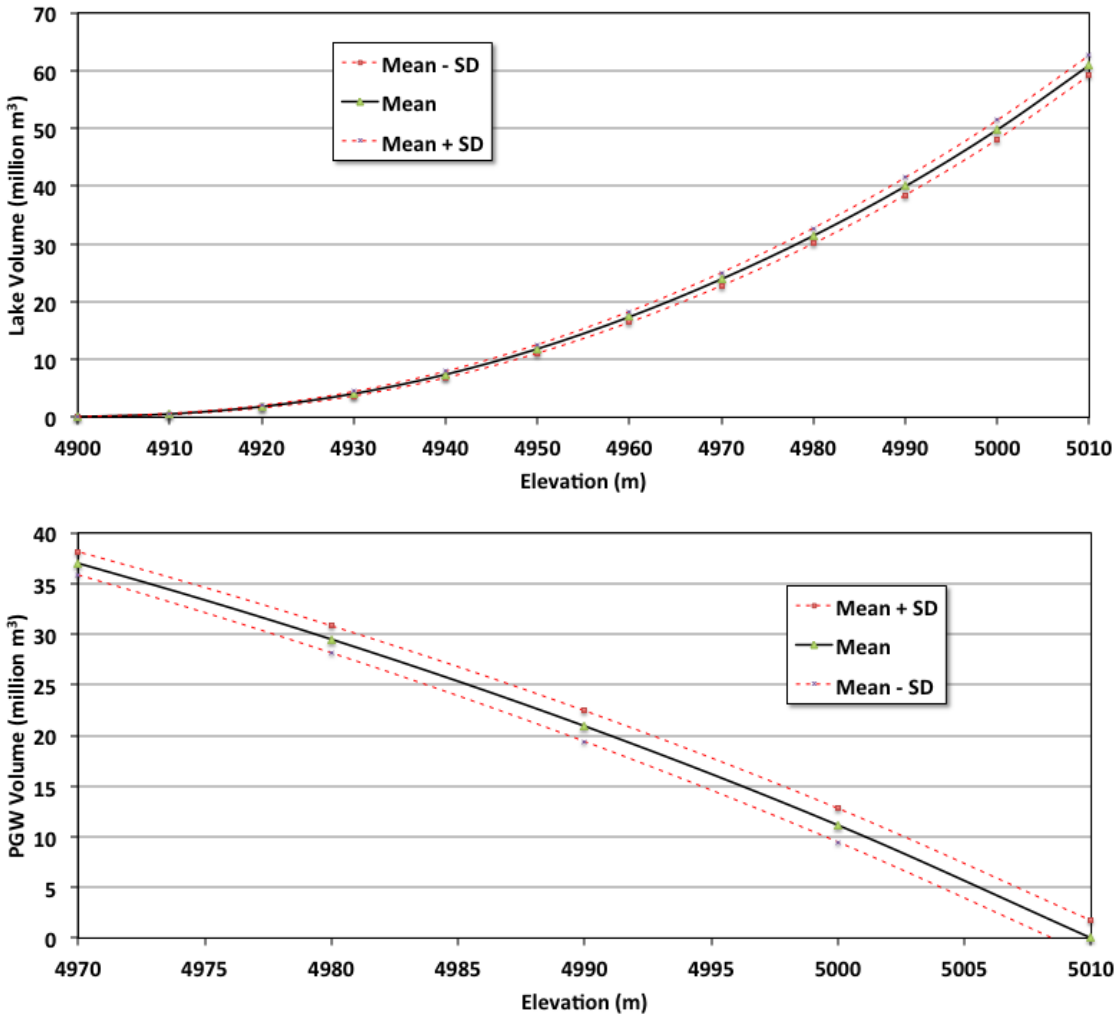

Figure 18: Top: Mean (solid black line) and ±1 standard deviation (dashed red line) of lake volume (million m^3) versus lake surface elevation (m). Bottom: Mean and ±1 standard deviation of "Potential GLOF Water" (PGW) volume (million m^3) versus post-GLOF water elevation (m) of Imja Glacial Lake.

2.5 CONCEPTUAL MODEL OF IMJA LAKE

Figure 19 shows a vertical cross-section of a conceptual model of Imja Lake

created from recent sonar bathymetric survey and ground penetrating radar survey data (Somos-Valenzuela et al. 2014b) as well as a 5 m resolution DEM with an accuracy of ± 4m maximum created from ALOS PRISM stereo data by Lamsal et al. (2011) for the topography of the glacier and the end moraine. The bottom of the Imja Glacier was determined by a GPR survey. The exact boundaries of the debris and ice areas and the lower bedrock and the glacier ice are unknown and shown as such in the figure using question marks (?). Two distinct zones with different depths are illustrated in Figure 19: zone A, from 500 to 1,750 m (western part), and zone B, from 1,750 m to 2,800 m (eastern part). The exact separation between these two zones is unknown, but it is estimated from the bathymetric data to occur at about 1,750 m on Figure 19. Reasons for the differences in depth between the two zones are not entirely clear, but may be related to the presence or non-presence of ice at the lake bottom. That is, a lack of dead ice at the bottom of zone A would arrest all further deepening, while the presence of ice at the bottom of zone B would account for its continued deepening. This might also be due to a thick debris cover on the ice at the bottom of zone A. When the lake grew to form the western part (zone A), the growth rate was much smaller. Therefore, more debris might have deposited on the lake bottom. Later, when zone B was formed, the rapid growth may not have resulted in thick debris to form on the lake bottom. The debris volume on and in the glacier also might be smaller.

Figure 19 also supports the hypothesis of subaqueous calving in zone B that we have observed at the lake. Climate change creates higher temperatures resulting in an increase in the elevation of the rain-snow boundary, a reduction in solid precipitation, and an increase in glacial melt rate. The mid-ablation zones of glaciers experience increased

mass loss and reduced ice flux from up-glacier leading to the development of glacial lakes (Benn et al. 2012). As glacier lakes expand, their growth undergoes a transition from shoreline melting to rapid calving retreat (Kirkbride 1993). Calving occurs in a cyclic pattern where waterline notches develop and grow upward by flake calving, which induce crevasse propagation and full-height slab calving that restores the vertical profile to the waterline and forms a submerged ice foot that undergoes subaqueous calving (Kirkbride and Warren 1997) . We witnessed this cyclic calving process at Imja Lake during three field visits in 2011 and 2012. Benn et al. (2001) observed these four calving processes and reported that waterline melting exerts a strong influence on calving rates at Ngozumpa Glacier, Nepal Himalaya, but found the location and spacing of weaknesses within the calving front to be significant as well to full-height slab calving. Warren and Kirkbride (2003) proposed, and Röhl (2006) further supported with field measurements, that water temperature and circulation provides a thermal undercutting mechanism that controls calving speeds. Röhl (2006) also reported water-level fluctuations, debris supply, and cliff geometry influence the rate of thermal notch development. Sakai et al. (2009) found the thermal undercutting to be controlled by water temperature and wind-driven currents, which are a function of the fetch length, using a simplified lake model of supraglacial lakes in the Nepal Himalaya. When sub aerial calving and melt losses exceed those below, a subaqueous ice ramp develops. These ramps are overlain with a thick layer of debris, which reduces the melting of the ice ramp and the buoyant forces that act to break up the ramp, thereby allowing the ice ramps to extend far from the calving front (Robertson et al. 2012). Subaqueous calving events have been observed in supraglacial lakes in the Nepal Himalaya (Benn et al. 2001) and frequently in New Zealand (Kirkbride

and Warren, 1997), but their contribution to glacier mass loss is difficult to fully quantify due to their transient nature (Robertson et al. 2012) and challenges associated with modeling subaqueous melt rates (Benn et al. 2007).

Figure 19 illustrates the difficulty in defining the boundary between the area underlain by ice as opposed to ice and rock or just rock. The horizontal line in Figure 19 shows that at least half the lake volume will not discharge in the event of a GLOF. The "potential GLOF water" (Figure18) may not drain from the lake all at once in a GLOF and the timing or the hydrograph of the drainage is important in order to estimate the critical water volume that might cause serious GLOF damage downstream. The increasing "potential GLOF water" does not necessarily increase the GLOF occurrence probability. Additional lake bottom melting in zone B will deepen the lake and add to the "safe" pool of water.

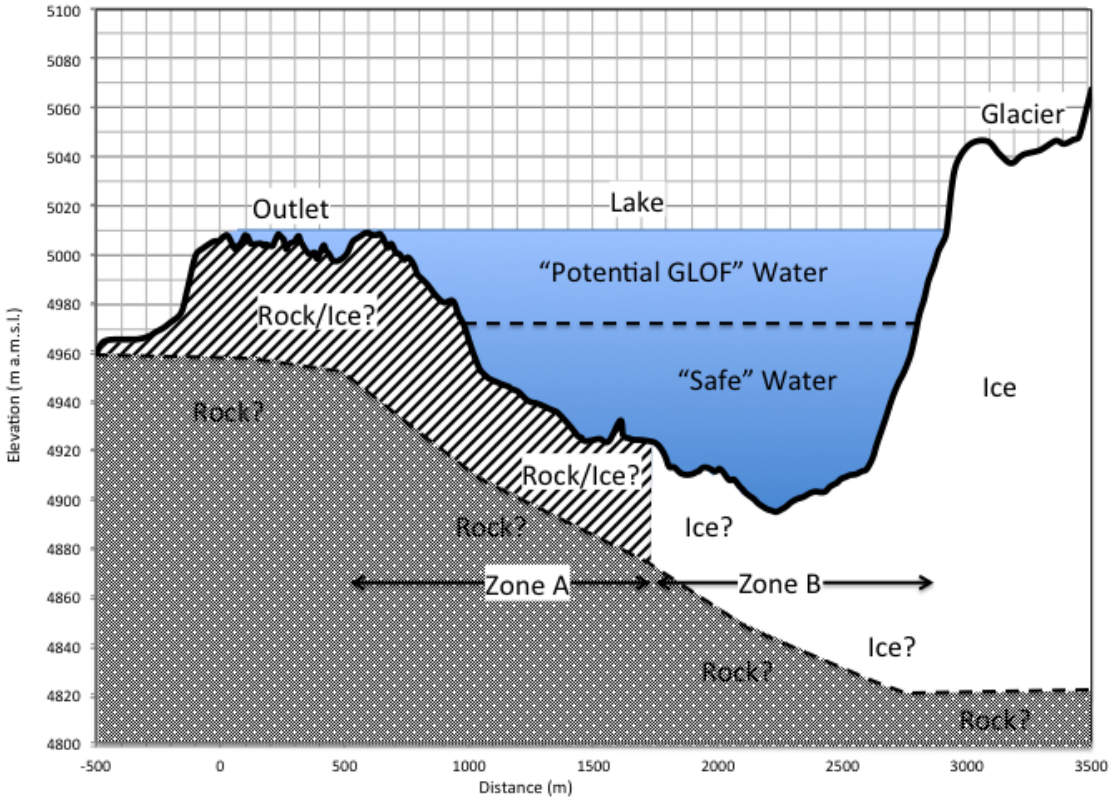

Figure 19: Conceptual model of Imja Glacial Lake created from recent bathymetric survey and ground penetrating radar survey data, as well as a 5 m resolution DEM with an accuracy of ± 4m maximum created from ALOS PRISM stereo data by Lamsal et al. (2011) for the topography of the glacier and the end moraine.

2.6 CHARACTERIZING IMJA LAKE HAZARD LEVEL

Several methodologies have been proposed for characterizing glacier lake hazard (Grabs and Hanisch 1993; Mool et al. 2001; Huggel et al. 2002; RGSL 2003; Huggel et al. 2004; Kääb 2005; Bajracharya et al. 2007a; Richardson 2010; ICIMOD 2011; Emmer and Vilímek 2013); mostly following the basic framework suggested by Grabs and Hanisch (1992). The Grabs and Hanisch (1992) framework includes: (1) establishing a

glacier lake inventory, (2) agreeing upon GLOF risk indicators, (3) estimating GLOF risk and the vulnerability of downstream infrastructure and communities, (4) comparing lake drainage alternatives and selecting one for implementation, (5) developing monitoring and early warning systems, and (6) performing further investigations as necessary.

The potential risk of a GLOF from Imja Lake has been investigated by numerous authors (Ives 1986; Hammond 1988; Yamada and Sharma 1993; Watanabe et al. 1994; RGSL 2003; Hambrey et al. 2008; Fujita et al. 2009; Watanabe et al. 2009; Budhathoki et al. 2010; Ives et al. 2010; ICIMOD 2011). Since the mid-1980s, Imja Lake has been the source of considerable disagreement regarding its GLOF potential and threat to downstream communities. Yamada and Sharma (1993), for example, describe Imja Lake as one of the most dangerous lakes in Nepal. During field visits, they observed the presence of glacier ice in the outlet, and that the moraines are comprised mostly of unconsolidated debris materials as well as ice-major indicators of risk, according to Grabs and Hanisch (1993). Watanabe et al. (1994, 1995) reported rapid melting of the debris-covered ice and significant changes in the outlet position of the lake. Reynolds Geo-Sciences Ltd. (RGSL) (2003) developed a vulnerability assessment scheme that was applied to Imja Lake, resulting in the conclusion that if a GLOF were to occur it would cause extensive damage for about 90 km downstream. Bajracharya et al. (2007a) called for urgent mitigation measures to reduce the GLOF risk of Imja Lake on the basis of its rapid growth. Based on data from 2000-2006, however, Hambrey et al. (2008) state that the risk of a moraine breach at Imja is very low because: (1) there is a low risk of calving waves, (2) the outlet is wide relative to its height, (3) that although the outlet has an ice-core that narrows as it melts, there exists sufficient ice-free moraine and freeboard to

ensure a stable lake with a free-draining channel and low hydraulic gradient, and (4) changes to the moraine are gradual, so it can be easily monitored. After twenty years of study of Imja Lake, Japanese researchers likewise concluded that it was relatively stable (Watanabe et al. 2009; Fujita et al. 2009). Budhathoki et al. (2010) evaluated the hazard potential of Imja Lake based on the methodologies suggested by ICIMOD (2001), Huggel et al. (2002), and RGSL (2003). They concluded that there is a moderate risk of a GLOF from Imja Lake. Reporting on fieldwork performed in 2009, ICIMOD (2011) found the lake to be relatively stable but in need of regular monitoring.

The describe disagreements in Imja Lake hazard assessment are results of the wide range of criteria and methodologies available, many of them were developed for different areas and conditions, and they don't consider all the parameters involved in the hazard assessment. For example, O'Connor et al. (2001) consider 2 parameters in the evaluation of hazard level, while ICIMOD (2011) considers 26 parameters. In addition, previous hazard assessments at Imja Lake just considered current condition without the evaluation of the future evolution of the lake. For this work, we use a combination of hazard evaluation methods in order to include different lake characteristics, doing this we pursue to avoid biases or personal judgment in our assessment, which may be another source of uncertainties and differences in previous results. It is important to avoid anchoring in our judgment especially in a sensitive case like the one we are analyzing. Emmer and Vilimek (2013) did a similar work in the Peruvian Andes; they selected a variety of qualitative, quantitative and semi quantitative methods combining them to estimate the level of hazard that different lakes present in Peru. We also include a hazard assessment for a future scenario, since it is hypothesized that Imja Lake is becoming

more dangerous as it is growing toward the steepest slopes. In this work we are using six qualitative, one semi quantitative and one quantitative method for the Imja Lake hazard assessment.

2.6.1 Qualitative methods

The most simple method use in this work is O'Connor et al. (2001), which has two parameters that describe the level of hazard at a glacier lake. The levels of hazard are low medium and high according to the Table 6. The process refers to the glacier as a potential source of avalanches; therefore, although Imja Lake is in contact with the glacier, we initially consider that it does not constitute a source of hazard. For a future scenario, this would be different since the lake will reach the avalanche zone, so the lake is considered in contact with the glacier. In addition, since the lake is drained by a natural channel above the moraine the freeboard is considered inexistent.

The second method used is the one described by Costa and Schuster (1988). This method consists of four variables (Table 7), which need to be evaluated to estimate the level of hazard at the lake. Clague and Evans (2000) (Table 8) use six parameters to define hazard, three of them describe the internal characteristics such us moraine/lake geometry relationship, and three are related to avalanches or external features. Grabs and Hanish (1993) describe the fourth combination of parameter use in this work. They combine eleven parameters that consider moraine stability and potentiality of avalanches (Table 9). Some of the parameters cannot be assessed for a future scenario with the information available; therefore, we assume they won't change from the current lake conditions.

Xin et al. (2008) evaluated the hazard from Longbasaba and Pida lakes in Chinese Himalayas using 8 parameters (Table 10). They give critical values for 7 out of 8 parameters to compare and determine the level of hazard that a lake represent. The parameter with no critical value is ignored in our analysis since we have not clarity of the ranges that need to be used.

The ICIMOD (2011) approach for characterizing glacier lake hazard includes the lake and glacier characteristics listed in Table 11 (ICIMOD 2011), based primarily on physical criteria derived from remotely sensed data. Table 10 has been filled in for Imja Lake based on information available in 2013. Imja Lake exhibits 16 of the 26 potentially dangerous glacial lake (PDGL) indicators on the list at the current state and 21 when the lake reaches the avalanche zone.

2.6.2 Semi-quantitative methods

Table 12 presents the results of applying the empirical scoring method of Reynolds Geo-Sciences Ltd. (RGSL 2003) to further refine the Imja Lake hazard estimate. The resulting score from Table 12 is compared with the threshold values from Table 13 to determine the level of Hazard from Zero to Very high.

2.6.3 Quantitative methods

Wang et al. (2011) defines a quantitative method based on remote sensing, which was develop after the analysis of 78 lakes in the Tibetan Plateau. The method consists in the evaluation of five parameters that need to be compared to the limits define in Table 14. The method assumes that a GLOF will be trigger by an ice avalanche from the mother glacier. Although it is believed that in the future at Imja Lake the main triggers will

come from the steep slopes at the side of the lake instead of the mother glacier, the method was included in order to have a wider range of methods that can lead us to a more robust conclusion when we estimate the consolidated level of hazard. The weighting of the stability parameters (Table 15) was calculated using a fuzzy consistent matrix. The weighting values are multiply by the percentile in which the parameter calculated is located according to the threshold given by Table 15. If the result falls between 0-0.5 the lake is considered safe, 0.5-0.7 medium risk, 0.7-0.8 high potential and 0.8-1.0 very high potential for GLOF. Since the water at Imja Lake is in contact with the glacier the Slope between lake and glacier is the same than the mother glacier snout mean slope as it is described in Wang et al. (2011). The level of hazard for the current lake condition is medium. This method does not consider the size of the lakes or another trigger but ice avalanches from the mother glacier; therefore its level of hazard stays in the medium level for the future scenario considered as well (Table 16).

Table 6: Combination of the two binary criteria by O'Connor et al. (2001)

Contact with the glacier	**Dam Freeboard**	**Outburst potential**
No	High	Low
Yes	High	Medium
No	Low	Medium
Yes	Low	High

Table 7: Costa and Schuster (1988) methods under Imja current and future conditions.

Lake condition or parameter affecting the moraine dam	**Current Scenario**	**Future Scenario**	**Source**
Buried Ice present in moraine dam	yes	yes	Hambrey et al. (2008), Somos-Valenzuela et al. (2014c)
Unstable young moraines, no presence of vegetation	yes	yes	Watanabe (2009),
Steep slope moraine > 40^{o}	no	no	Lamsal et al. (2011)
Possibility of rock/ice avalanches into the lake	no	yes	Field observations

Table 8: Clague and Evans (2000) methodology applied to Imja Lake.

Lake condition or parameter affecting the moraine dam	Imja Current Scenario	Imja Future Scenario	Source
Small width-to-height ratio of dam	No	No	Watanabe (2009)
Dam lacks armored overflow channel	Yes	Yes	Field Observation
Outflow occurs mainly by seepage through the dam	No	No	Field Observation.
Reservoir surface is normally at or just below the crest of the dam	Yes	Yes	Field Observation
One or more highly crevassed glaciers cling to steep slopes	No	Yes	Watanabe (2009); Field Observation.
Slopes above the lake are subject to rock falls	No	Yes	Field Observation

Table 9: Grabs and Hanish (1993) method description.

Lake condition or parameter affecting the moraine dam	Current Scenario	Future Scenario	Source
Lake dammed by young, unstable and unconsolidated moraines	Yes	Yes	Watanabe (2009)
Lake in contact with active ice body of a glacier	Yes	Yes	Field observation
Glacier is advancing	No	No	Hambrey (2008)
Glacier tongue is steep	No	Yes	Lamsal et al. (2011)
Glacier is dissected by many deep crevasses	Yes	Yes	Field observation
Unconsolidated, high and steep lateral moraines	Yes	Yes	Field observation
Evidence of general slope failures above the lake	No	N/A	Field observation
High lake water levels and strong dam seepage	No	N/A	Field observation
Evidence of recent multiple small outbursts	No	N/A	Field observation
Large ice bodies and/or sand/gravel lenses in moraine which are likely for melting or being washed out during excessive seepage	Yes	Yes	Hambrey (2008)

Table 9 (Continued)

Lake condition or parameter affecting the moraine dam	Current Scenario	Future Scenario	Source
High probability of slope or ice failures with sudden quantified mass wastage into the lake	No	Yes	Field observations
Kinetic energy and height of surge wage overtops the moraine crest	No	yes	Watanabe (2009)
Excessive seepage and piping occurs during lake water level increases	No	No	Field observation

Table 10: Xin et al. (2008) stability criteria.

Lake condition or parameter affecting the moraine dam	Critical Value	Current Scenario	Future Scenario	Source
Top width of dam 600	< 600 m	No	No	Watanabe et al (2009), Lamsal et al. (2011)
Distal flank steepness	> 20°	Yes	Yes	Calculated from Lamsal et al. (2009)
Iced cored moraine	Yes	yes	yes	Hambrey (2008)
Ratio of Dam width to height	0.1 - 0.2	No	No	Calculated from Lamsal et al. (2011)
Slope of glacier snout	> 8°	No	Yes	Field observation, Lamsal et al. (2011)
Temperature and precipitation	High T, wetness High T, dryness	No	Yes	Temperature is increasing weakening slope stability (IPCC 2007)
Ratio of freeboard to dam height	0	Yes	Yes	Field observations, freeboard is considered to be 0
Lake-glacier proximity	< 500 m	Yes	Yes	Field observations.

Table 11: Dangerous Lake and Glacier Characteristics (adapted from ICIMOD 2011).

Lake condition or parameter affecting the moraine dam	Current Scenario	Future Scenario	Source
Large size and rapid expansion	Yes	Yes	(Somos et al. 2014b)
Increasing water level	No	No	(Watanabe et al. 2009)
Intermittent activity of supra-glacial lakes	No	No	(Watanabe et al. 2009
Position of lake in relation to moraines and associated glacier	Yes	Yes	(Lamsal et al. 2011)
Narrow crest	No	Yes	(Lamsal et al. 2011)
No drainage outflow or outlet not well formed	No	No	Field work
Steep moraine walls	Yes	Yes	(Lamsal et al. 2011
Existence and stability of ice core and / or permafrost within moraine	Yes	Yes	(Hambrey et al. (2008)
Height of moraine	Yes	Yes	(Lamsal et al. 2011)
Mass movement (or potential for it) on the moraine slopes	Yes	Yes	(Watanabe et al. 2009)

Table 11 (Continued)

Lake condition or parameter affecting the moraine dam	Current Scenario	Future Scenario	Source
Lake breached in the past and refilling	No	No	Field Observations
Seepage through moraine walls	Yes	Yes	Field Observations
Condition of associated glacier	Yes	Yes	Field Observations
Hanging glacier in contact with or close to lake	No	Yes	This study
Large glacier area	Yes	Yes	Google Earth
Rapid glacier retreat	Yes	Yes	(Watanabe et al. 2009)
Debris cover on lower glacier tongue	Yes	Yes	Field observations
Slope of glacier tongue	No	Yes	This study
Presence of crevasses of ice from the glacier front	Yes	Yes	Field observations
Ice bergs breaking off glacier terminus and floating into lake	Yes	Yes	Field observations
Potential rock fall and / or slide sites around the lake	No	Yes	This study

Table 11 (Continued)

Lake condition or parameter affecting the moraine dam	Current Scenario	Future Scenario	Source
Large snow avalanche sites immediately above	No	Yes	This study
Neo-tectonic and earthquake activity	Yes	Yes	
Climatic conditions, especially large inter-annual variations	No	Yes	
Recent moraines of tributary glaciers that were previously part of a former glacier complex, and with multiple lakes that have been developed due to retreat of several glaciers in close proximity	Yes	Yes	
Sudden advance of a glacier towards a lower tributary or main glacier that has a well-developed frontal lake	No	Yes	

Table 12: Lake Outburst Hazard Scoring System Applied to Imja Lake (after RGSL 2003).

Factor	Potential Score				Current Scenario		Future Scenario		Source
					Score	Score	Score	Score	
	0	2	10	50	Best case	Worst case	Best case	Worst case	
Volume of lake	N/A	Low	Mod.	Large	50	50	50	50	Somos-Valenzuela et al. (2014c)
Lake level relative freeboard	N/A	Low	Mod.	Full	10	50	10	50	Field observations
Seepage evident through dam	None	Min.	Mod.	Large	10	10	10	10	Field observations
Ice-cored moraine dam	None	Min.	Partial	>Mod.	50	50	50	50	Somos-Valenzuela et al. (2014c)
Calving risk from ice cliff	N0	Low	Mod.	Large	0	2	10	50	Field Observations

Table 12 (Continued)

Factor	Potential Score				Current Scenario		Future Scenario		Source
					Score	Score	Score	Score	
	0	2	10	50	Best case	Worst case	Best case	Worst case	
Ice/rock avalanche	N/A	Low	Mod.	Large	0	2	50	50	Field Observations Haeberli (1983)
Supraglacial or englacial drainage	None	Low	Mod.	Large	0	0	0	0	Field Observations
Compound risk (e.g., earthquake)	None	Slight	Mod.	Large	10	50	10	50	Bolch *et al.*, 2008
Total					**130**	**214**	**190**	**310**	

Table 13: Hazard Rating Based on Empirical Scoring System (RGSL 2003).

Outburst likelihood score and hazard rating				
0	50	100	125	150+
Zero	Minimal	Moderate	High	Very High
		>>>>>> Outburst could occur at any time <<<<<<		

Table 14: Quantitative Stability Method (Wang et al. 2011)

	Limit Values				**Weight (w)**
	I	II	III	IV	
Interval Weight	0.25	0.5	0.75	1	
Area of mother glacier (km^2)	< 0.25	0.5-1	1-2.5	> 2.5	0.07
Distance between lake and glacier (m)	> 600	300-600	80-300	< 80	0.27
Slope between lake and glacier (degrees)	< 12	12-17	17-21	> 21	0.22
Slope of downstream face of dam (degrees)	< 10	10-14	14-22	> 22	0.195
Mother glacier snout steepness (degrees)	< 14	14-19	19-26	> 26	0.245

Table 15: Quantitative Stability Method Application (Wang *et al.*, 2011)

Factor	Scenario		Limit Values		Weight (w)	Total Weight		Source
	Current	Future	Current	Future		Current	Future	
Area of mother glacier (km^2)	2.12	1.28	0.75	0.75	0.07	0.0525	0.0525	Alos Image (28/10/2008) Aster L1 Image (9/2013)
Distance between lake and glacier (m)	0	0	1	1	0.27	0.27	0.27	Alos Image (28/10/2008)Aster L1 Image (9/ 2014)
Slope between lake and glacier	4.5	11.2	0.25	0.25	0.22	0.055	0.055	Alos Image (28/10/2008) Lamsal *et al*. (2011)
Slope of downstream face of dam (degrees)	12.1	12.1	0.5	0.5	0.195	0.0975	0.0975	Alos Image (28/10/2008) Lamsal *et al*. (2011)
Mother glacier snout steepness	4.5	11.2	0.25	0.25	0.245	0.06125	0.06125	Alos Image (28/10/2008) Lamsal *et al*. (2011)
Total						**0.5363**	**0.5363**	

2.6.4 Results Hazard level

Sixth qualitative, one semi quantitative and one quantitative method were used to estimate the level of hazard that Imja Lake represents for the current conditions of the lake and a future scenario when the lake reaches the avalanche zone with an area of at least 2 km2. The qualitative methods are summarized in Table 16. According with the consolidated scores, which can go from 0 to 1; at the current conditions Imja Lake represents a medium hazard for a potential GLOF with a score of 0.47. However in the future scenario analyzed the lake will become dangerous with a score of 0.76.

The semi quantitative method used in this work agrees with the result from the qualitative analysis. Using RGSL (2003) matrix we calculated that Imja Lake scores 130 and 190 for the current and future scenario, with a maximum score of 214 and 310 respectively. Therefore, according to RGSL (2003) methodology Imja Lake represents high outburst likelihood for the current condition, and it will represent very high outburst likelihood for the future conditions analyzed.

Finally, we applied Wang et al. (2011) quantitative method. The results are that Imja Lake has an outburst probability of 0.5363 for the current and future scenario analyzed, which represent a medium level of risk. These results agree in the current lake conditions with the qualitative and semi quantitative analysis. The level of hazard does not change in the future because the method does not consider others trigger but the calving from the mother glacier, which likely won't generate big avalanches into the lake in the future scenario analyzed.

Table 16: Qualitative method summary, the arithmetic and the standard Deviation are calculated using the scores for the 6 qualitative methodologies following Emmer and Vilímek (2013) calculations.

Time	O'Connor et al (2001) (2)		Costa and Schuster (1988) (4)		Clague and Evans (2000) (6)		Grabs and Hanish (1993) (11)		Wang et al. (2008) (8)		ICIMOD (2011) (26)		Arithmetic mean	Standard Deviation
Present	1/2	0.50	2/4	0.50	2/6	0.33	5/13	0.38	4/8	0.50	16/26	0.62	0.47	0.10
Future	2/2	1.00	3/4	0.75	4/6	0.67	8/13	0.62	6/8	0.75	21/26	0.81	0.76	0.13

2.7 IMJA LAKE GLOF MODELING

In this section, we describe the development of a new hydraulic model for predicting the results of a potential GLOF from the lake in terms of the hazard to downstream communities and the uncertainties in the calculation of the dam breach parameters involved in the hydrograph generation. In this study we considered six scenarios, current lake conditions, lowering the water level in 3, 10 and 20 meters, and evaluation of two future scenarios projected from the changes that Imja Lake has experienced during the last 30 years with the level as it currently is and lowered by 20 m, and discuss a method for reducing the GLOF risk.

2.7.1 Methodology

2.7.1.1 Data

Digital Elevation Model

For this work, we have three sources of topographic information for the inundation model. The first one is a 5 meters DEM derive from a 2008 Alos Image from the lake to Dingboche, which is the first significant settlement downstream (Figure 20) (Somos-Valenzuela et al. 2014b). A 5 by 5 meters resolution DEM generated from a 2008 ALOS image (Lamsal et al. 2011) that contains the elevation of the moraine surrounding the lake (Figure 20). These five meters DEM give us good resolution and quality terrain data for the inundation modeling; however, they cover just 5 km of river downstream the lake. The goal was to extend the model until Phakding 38.5 km downstream the lake. Therefore, initially a 30m x 30m resolution Advanced Space borne

Thermal Emission and Reflection Radiometer (ASTER L1) digital elevation model (DEM) (Tachikawa, 2011) was used to represent the topography of the watershed and provide a basis for delineating the basin and streams. However, ASTER L1 data has too many unrealistic features such as several ponds all the way from Imja Lake to Phakding. Such ponds don't exist according to our field work observations; therefore, we decided not to use that source of information. In replacement, we used topographic maps published by the topographic Survey Department of Nepal in 1996 in order to have a first approximation of the inundation downstream. A digital elevation model (DEM) from 40m interval contour maps was produced (Bajracharya et al. 2007b; Bajracharya et al. 2007a). The modeled portion of the river has a length of 38.5 km from the lake outlet to a point 5 km downstream of the village of Phakding.

Bathymetry of the lake was derived from the results of the 2012 sonar survey of Imja Lake (Somos-Valenzuela et al. 2014c). Imja Lake has a water surface elevation of about 5010 m. In the 2012 bathymetric survey of the lake, water depths of 20-60 m were measured near the western edge of the lake (outlet end) and 30-116 m deep near the eastern (glacier) end of the lake. The water available to drain from the lake in a GLOF event is now at least 33 million m3 (Somos-Valenzuela et al. 2014c). The base of the outlet at the start of the valley below Imja Lake is about 4970 m (Lamsal et al. 2011).

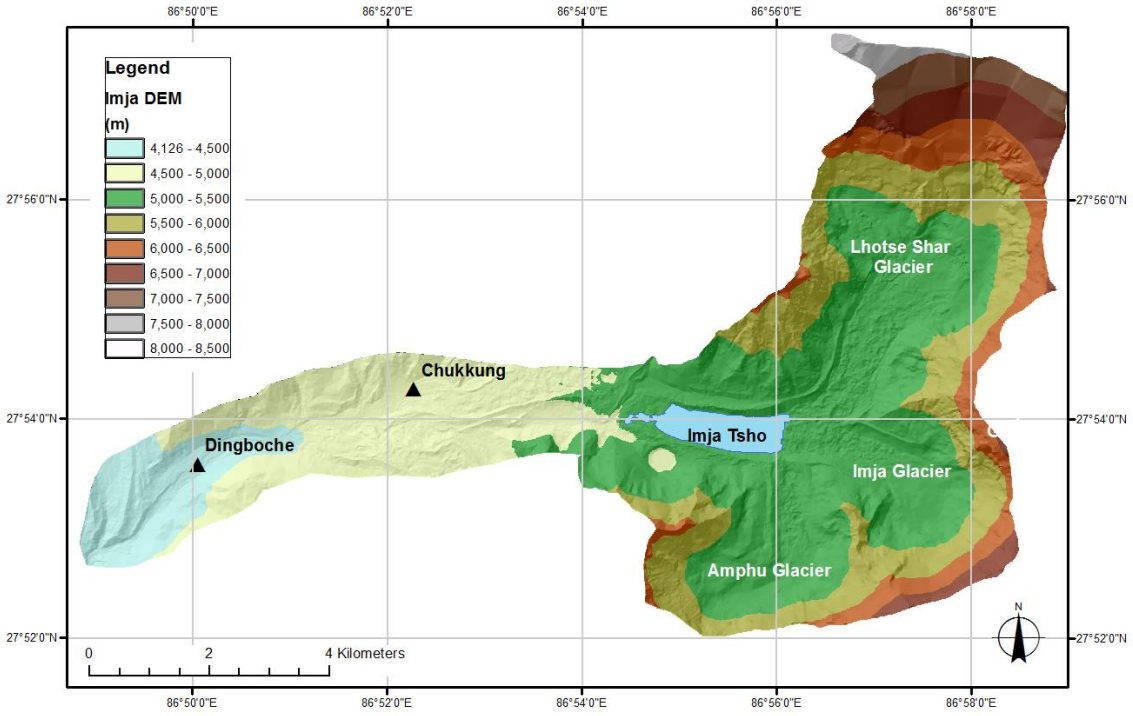

Figure 20: Digital Elevation Model of Imja Lake area of the Khumbu region of Nepal.

Land Cover and Roughness Coefficients

Flow resistance in river channels depends on different factors such as: meandering, bed channel materials, cross-sectional area and its variation, obstructions, and vegetation (Chow 1959). For the inundation model, values of Manning's roughness coefficient need to be estimated and included as input to the simulation (Flo-2D, 2009; USACE, 2010). Estimates of roughness coefficients can be done *in situ*. However, this is time consuming and can be inefficient for large rivers; also, the spatial variability of roughness may be misrepresented (Hossain et al. 2009; Forzieri et al. 2011). As an alternative, automatic classification of vegetation indices (VIs) derived from spectral images can be combined with high resolution terrain elevation maps (Forzieri et al. 2010;

Forzieri et al. 2011). The VI is used to classify the different land cover classes present in the river basin and the elevation map is used to estimate cover texture, which is used to estimate roughness values. Roughness values can be assigned to different land covers either manually or automatically (Forzieri et al. 2010; Forzieri et al. 2011).

ICIMOD generated land cover maps from 2006 ASTER imagery (Bajracharya and Uddin 2010) for the Sagamartha National park (Figure 21). We assigned the roughness coefficient values for eight categories as shown in Table 17. Cenderelli and Wohl (2001) calculated roughness coefficients for the Imja Khola and found values of 0.15 and 0.30 for the river bed and floodplain, respectively, which agrees with the values that the Flo-2D manual recommends for the land covers in the study area (Table 17). In addition, in order to understand the influence of this parameter on the inundation five scenarios were simulated in which the roughness coefficient values were varied from 0.05 to 0.6.

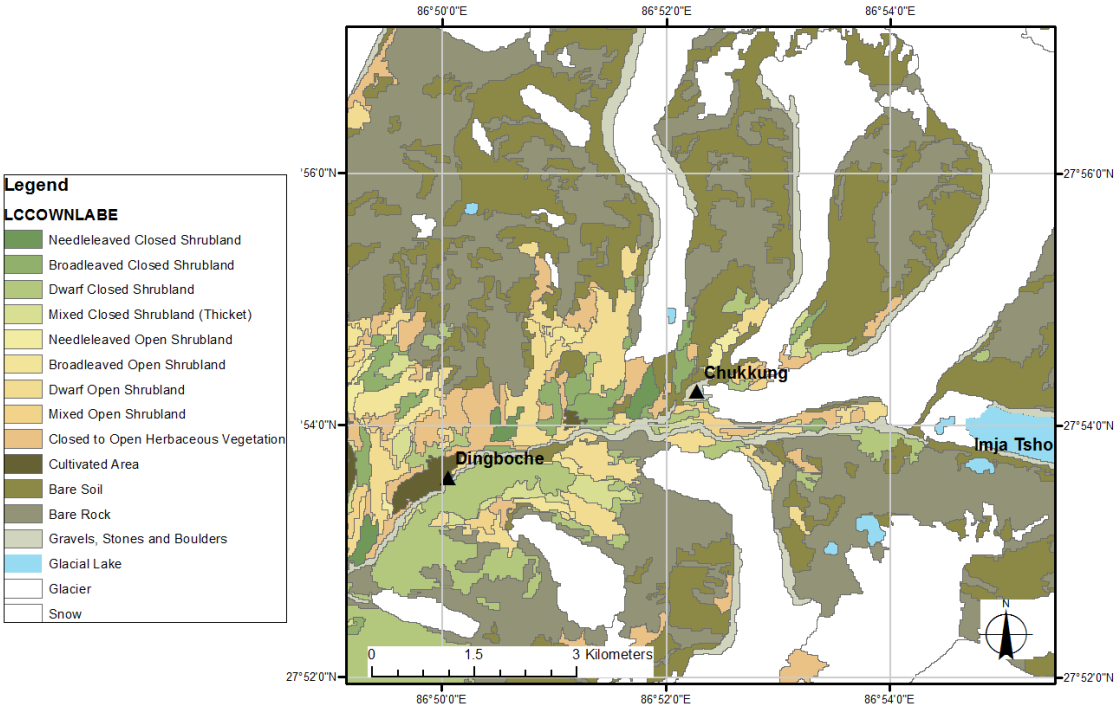

Figure 21: Dudh Kosi land cover classes (Bajracharya and Uddin 2010).

Table 17: Roughness Coefficients for the Main Land Cover Classes in the Study Area (Bajracharya and Uddin, 2010; Flo-2D, 2012)

Land Cover	Upper Bound	Lower Bound
Bare Rock	0.13	0.05
Bare Soil	0.1	0.03
Shrub land	0.4	0.3
Forest	0.4	0.17
Herbaceous Vegetation	0.3	0.2
Cultivated Area	0.2	0.1
Water Bodies	0.05	0.03
Gravels, Stones and Boulders	0.3	0.2

2.7.1.2 Future Expansion of Imja Lake

It is clear that Imja Lake will keep growing in area and volume. The lake will expand to a point in which avalanches will be able to enter the water and produce waves increasing the probability of dam breaching at Imja Lake. It arbitrary was decided to analyze a future scenario when the lake has an area of 2 km^2. Watanabe et al. (2009) estimated that Imja Lake lineal expansion is 43 m/year, and areal expansion is 0.03 km^2/year. If the lake follows Watanabe et al. (2009) areal rate of expansion (0.03 km^2/year), it may reach the area of 2 km^2 by year 2040. In a rough estimate, considering that for the current conditions, area=1.21 km^2 and a 35 meters moraine cut the GLOF water volume is 33.5 million m^3; the potential GLOF volume when the lake area reaches 2.0 km^2 will be in the order of 55.1 million m^3. It is important to remember that for a

GLOF calculation is most important to know the volume available above the breach bottom elevation than the total volume which includes the water unable to leave the lake when the moraine breaches.

2.7.1.3 Breach Model

Kattelmann and Watanabe (1998) discuss potential GLOF triggers at Imja Lake: (1) surge waves generated by ice or rock avalanches into the lake that overtop the dam; (2) slow melting of the ice core within the dam; (3) seepage and piping through the dam; and (4) progressive thinning of the moraine by landslides and earthquakes. Portocarrero (2014) notes that glacier or ice avalanches falling into glacial lakes that, in turn, cause the lakes to overflow have triggered most GLOFs. Surge waves from rock and ice avalanches into Imja Lake from the surrounding high mountain peaks are not a danger at the present time because of the wide valley configuration surrounding the lake and the current distance of the glacier terminus from the mountains (Watanabe et al. 2009; Hambrey et al. 2008). However, the factors that may trigger a GLOF there include hydrostatic pressure or seismic effects causing a failure of the ice-cored moraine dam. (Kattelmann and Watanabe 1996) list earthquakes as a potential Imja Lake GLOF trigger because of the high seismicity of the region. When ice melts or fractures, the hydrostatic pressure and water act directly against the moraine and if it does not have the right conditions, the pressure will cause an intense filtration and piping process with potentially catastrophic consequences. Seepage from the base of the southern portion of the outlet dam was observed during three visits between 2011 and 2012. This suggests that at present a piping could be a potential trigger at Imja Lake, especially in conjunction with an

earthquake. In the future, if the lake water elevation stays at the same level, as it has been the case for several years, there may be a chance that avalanches of rock and ice will be able to reach the lake producing waves that could eventually overtop the moraine complex. The moraine characteristics relevant to potential Imja Lake GLOF simulation calculations are given in Table 18.

Table 18: Moraine Characteristics Used in the GLOF Simulation Scenarios.

Description	**Current Conditions**	**Lowering 3 m**	**Lowering 10 m**	**Lowering 20 m**	**Future Scenario**
Moraine Height (h_d, m)	35	32	25	15	35
Breach height (h_b, m)	35	32	25	15	35
Water height (h_w, m)	35	32	25	15	35
GLOF Volume (V_w, m^3)	$33.5x10^{06}$	$29.5x10^{06}$	$22.4x10^{06}$	$12.5x10^{06}$	$55.1x10^{06}$

Breach Equations

Predicting a dam or embankment breach is difficult. According to Wahl (1998) "breach simulation and breach parameter prediction contain the greatest uncertainty of all aspects of dam-break flood forecasting." Reclamation (U.S.B.R. 1988) grouped the analysis methods into four categories: (1) physically-based methods (e.g., NWS-BREACH), (2) parametric models (e.g., FLDWAV), (3) empirical equations, and (4) comparative analysis.

For locations close to the dam, discharge, inundation levels, and flood arrival time can vary abruptly depending of the characteristic of the breach process, breach width and breach time formation. However, for locations well downstream from the dam, the flood peak arrival time is a function of the breach formation time but the peak discharge and

inundation levels are insensitive to changes in these breach parameters (Petrascheck and Sydler 1984; U.S.B.R. 1988).

To model a potential GLOF from Imja Lake, we use a combination of dam breach analysis methods. Due to the absence of actual GLOF data, empirical equations are used to represent the moraine breach by the shape of the breach, its final size, and the time required for its development and these are predicted by empirical equations (Wahl 2004). These predicted breaching parameters are used in a HEC-RAS dam break model (USACE 2010) to simulate the progression of the breaching process and the resulting GLOF hydrograph, similar to the FLDWAV model (Fread and Lewis 1998; Zhou et al. 2005), which is a more broadly recognized model for dam breach process simulations. GLOF hydrographs from the breaching were computed with the dam break model in HEC-RAS (USACE 2010). These hydrographs were adjusted to match the peak discharge values from the empirical equations.

There are a number of breach equations in the literature (Wahl 2004). However, the Froehlich equations (Froehlich 1995) were selected because Wahl (2004) found these equations to have the lowest uncertainty among a large number of equations studied. Additionally, Osti and Egashira (2009) demonstrated that the Froehlich equations provided good agreement for the Tam Pokhari GLOF, which is the latest GLOF occurred in the area. The Froehlich equations were used to compute predicted, lower bound and upper bound values for the breach parameters. The predicted values of breach width (B, m), failure time (t_f, hr) and peak discharge (Q_p, m^3/s) are given by (Froehlich 1995)

$$B = 0.1803 k V_w^{0.32} h_b^{0.19} \quad (1)$$

$$t_f = 0.00254 V_w^{0.53} h_b^{-0.9} \quad (2)$$

$$Q_p = 0.607 V_w^{0.295} h_w^{1.24} \quad (3)$$

Where h_b is the height of the breach (m), V_w is the water volume (m^3), k is the overtopping multiplier: $k = 1$ for no overtopping, and $k = 1.4$ for overtopping, and h_w is the depth of water above breach invert at time of failure (m).

Wahl (1998) analyzed the main empirical equations available for dam breach parametric calculations and presented an uncertainty analysis in Wahl (2004). Equations to calculate upper and lower bounds on the breaching parameters are defined as (Wahl, 2004)

$$Upper\ Bound = Predicted\ Value * 10^{(-error+2Se)} \quad (4)$$

$$Lower\ Bound = Predicted\ Value * 10^{(-error-2Se)} \quad (5)$$

Where, the *Predicted Value* is the value of B, t_f, or Q_p estimated by Eqs. (1-3), *error* is the mean prediction error (Table 19), and 2*Se* is the width of the uncertainty band (Table 19).

Table 19: Froehlich Equations Prediction Error and Uncertainty Bounds (Wahl, 2004).

Parameter	**Mean Prediction Error**	**Uncertainty Band** (+/-2Se)
Breach Width (m)	0.01	0.39
Failure Time (hr)	-0.22	0.64
Peak Discharge (m^3/s)	-0.04	0.32

2.7.1.4 Inundation Model

In the work reported here, a model of the Imja Khola (River) was developed using Flo-2D an unsteady debris flow model (Flo-2D, 2009) (see Appendix A for Flo2D model description). Flo-2D is a volume conservation flood routing model developed by O'Brien et al. (1993) that can be used for delineating flood hazards, regulating floodplain zoning or designing flood mitigation, among other advantages, the model can deal with mud/debris flows and urban flooding. Although the geometry of the model grid is two-dimensional, the Flo-2D considers flow in eight directions and solves a one-dimensional equation in each direction independently of the other seven directions. Continuity and momentum equations are solved with a finite difference method using an explicit time-stepping scheme; therefore, the Courant-Friedrich-Lewy (CFL) condition is used to ensure numerical stability. Several publications show that the Flo-2D model is advantageous for the simulation in which sediments are able to change the flow rheology (O'Brien et al. 1993; FLO-2D 2009; Mussetter Enginnering Inc. 2009; Calvo and Savi 2009; Lin et al. 2011; Valderrama and Vilga 2012; Peng and Lu 2013; Wu et al. 2013).

In order to assess the magnitude of a potential GLOF from Imja Lake and the hazard to downstream communities within the Sagamartha (Everest) National Park, including Dingboche, the first major settlement downstream of the lake, two-dimensional, unsteady simulations of GLOF scenarios were modeled using Flo-2D. In addition, we analyze the potential of recently proposed measures to provide protection for downstream communities, i.e., lowering the lake level by three meters (UNDP 2013). We also include a future scenario in which the lake will expand up-glacier to a point

where avalanches can reach the lake. We assume that the level of water in the lake will continue to be constant as it were during the last decade.

For this study we did not have geological information, such as sediment viscosity; however, the Flo-2D manual gives the most common values and combinations for these parameters. According to field observation and (ICIMOD 2009), the moraine dam's cohesion is small. The same situation is found in the lateral moraines downstream of the lake along the Imja Khola, which are a major potential source of sediment for GLOFs in the Himalaya and Peruvian Andes (Huggel et al. 2004).

GLOFs generally have average sediment concentrations by volume on the order of 50-60% (Huggel et al. 2004; Schneider et al. 2014). Julien and Leon (2000) recommend using a concentration of 50% by volume, which also coincides with the recommendation of Rickenmann (1999). Therefore, a sediment concentration of 50% has been used here and it represents an upper bound limit. Additionally, it is unlikely that the material will have low viscosity and high yield stress (Flo-2D, 2012); therefore, we use parameters recommended in the Flo-2D manual, $\alpha_1 = 0.0765$, $\beta_1 = 16.9$, $\alpha_2 = 0.0648$ and $\beta_2 = 6.2$, that provide lower dynamic viscosity and yield stress.

2.7.2 Imja Lake GLOF Modeling Results

2.7.2.1 Breach Model

Breach Parameters

Due to the absence of actual GLOF data for Imja Lake, empirical equations were used to compute the breaching parameters from a breach of the moraine at Imja Lake. To carry out the GLOF simulation, breach parameters were estimated and provided as inputs

to the HEC-RAS dam break model to produce the hydrographs needed as input to the Flo-2D flood routing simulation model. Table 20 shows the results of using the Froehlich equations and the moraine characteristics in Table 18 to calculate the predicted breaching parameters (breach width, failure time and peak flow) from Eqs. (1) – (3). Using the Froehlich equation prediction errors and uncertainty bands in Table 19, the ranges of the breaching parameters (upper and lower bounds) were calculated from Eqs. (4) - (5). The results show that lowering the lake by 3 m reduces the peak flow from 8274 m3/s to 7131 m3/s and lowering it by 20 m reduces it to 2163 m3/s. Under the current conditions scenario, the peak flow ranges from 4342 to 18954 m^3/s and the breaching time from 0.38 to 7.3 hours. Lowering the lake level by 3 m does not result in a significant change in the failure time or the peak flow; however, lowering the level by 10 m or 20 m does have a major impact on these parameters. Lowering the lake in 3 and 20 meters does decrease the peak flow to 12594 and 3821 m^3/s respectively.

Table 20: Breach Width, Failure Time and Peak Flow Values and Uncertainty Ranges Predicted by Froehlich's Equations for Five Scenarios: Current Conditions, Lake Lowering 3, 10, 20 m and Future Conditions.

Scenario	Value Type	Breach Width (m)	Failure Time (hr)	Peak Discharge (m^3/s)
Current Conditions	Lower	36	0.38	4342
	Predicted	**91**	**1.01**	**8274**
	Upper	217	7.30	18955
Lower 3 m	Lower	34	0.39	3745
	Predicted	**86**	**1.02**	**7131**
	Upper	205	7.40	16337
Lower 10 m	Lower	30	0.42	2539
	Predicted	**75**	**1.10**	**4838**
	Upper	179	7.98	11084
Lower 20 m	Lower	22	0.49	1135
	Predicted	**56**	**1.28**	**2163**
	Upper	135	9.28	4956
Future	Lower	42	0.50	5029
	Predicted	**106**	**1.31**	**9584**
	Upper	255	9.51	21955

Breach Hydrographs

The hydrographs generated using the HEC-RAS dam break module for the upper bound, predicted and lower bound peak discharge under the current conditions scenario are shown in Figure 22. The HEC-RAS hydrograph peak discharges were matched to the peak discharge values from the Froehlich equation values shown in Table 20 by adjusting the failure time within the range shown in the table. The hydrograph volumes agree with the volumes reported in Table 18. The GLOF peak discharge is 8394 m^3/s (see Table 20) compared to 8274 m^3/s predicted by Froehlich's equation, about a 1.4% difference. The range of peak discharge is 14728 m^3/s compared to 14613 m^3/s predicted by Froehlich's equation, about a 0.8% difference. These results illustrate good agreement between the HEC-RAS hydrograph values when fitted to the empirical Froehlich predicted values.

Figure 23 compares the resulting hydrographs for the Current Conditions Scenario and the Lake Lowering Scenarios (3, 10, 20 m of lowering). The peaks were matched to the predicted values shown in Table 20.

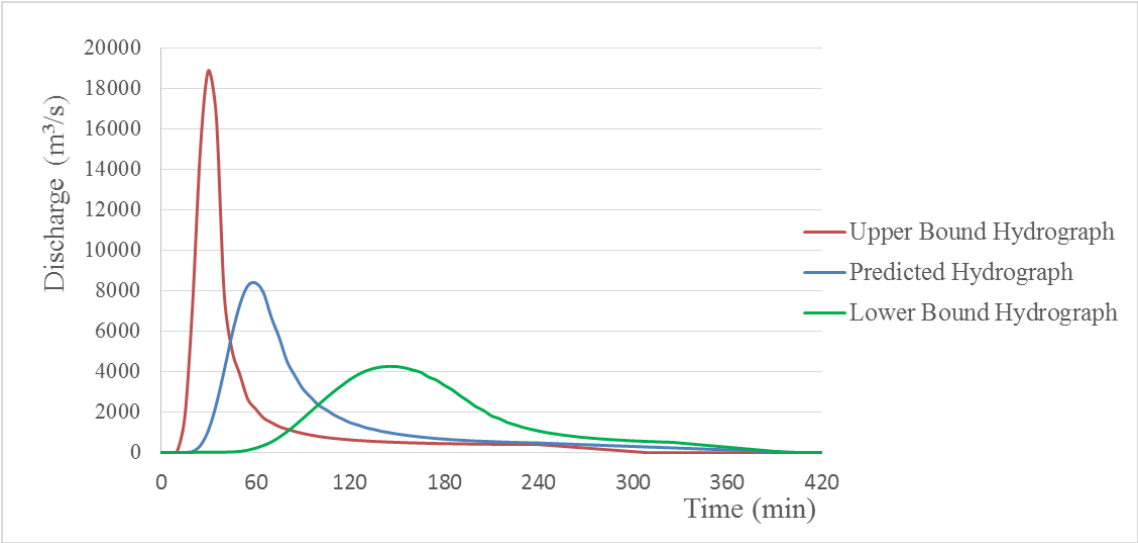

Figure 22: Imja Lake GLOF discharge hydrographs generated using the HEC-RAS dam break module for the upper bound, predicted and lower bound peak discharge under the Current Conditions Scenario.

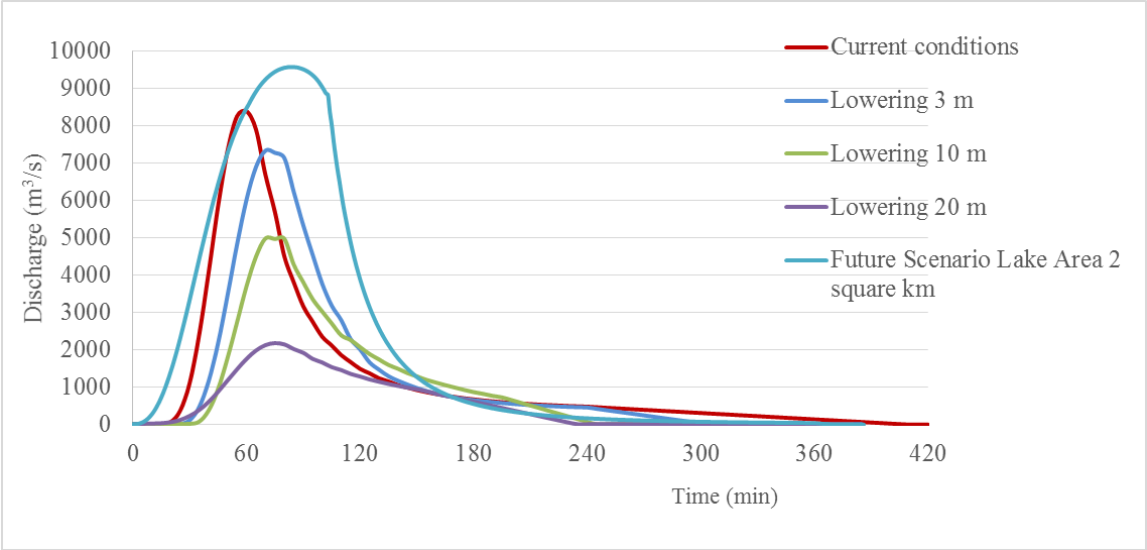

Figure 23: Imja Lake GLOF discharge hydrographs for five scenarios generated using HEC-RAS dam break module. Peaks were matched to the predicted values calculated using Froehlich equations.

2.7.2.2 Inundation Model Using Topography Derived from Contours Lines

Current Conditions Scenario

The results of modeling the Current Conditions Scenario of a potential GLOF from Imja Lake are shown in Table 21 and Figures 24 show the discharge at Dingboche and Phakding. At Dingboche, the flood arrives 1.25 hours after the breaching begins and peaks at 1.3 hours with the uncertainty ranging from 0.8-2.2 and 0.8-2.9 hours respectively. At Dingboche the peak water flow is 7515 m^3/s with the uncertainty ranging from 4142-14583 m^3/s respectively. The lag time between the peak flow at the breach and Dingboche is 20 minutes. At Phakding, the flood arrives 3.1 hours after the breaching begins and peaks at 3.2 hours with the uncertainty ranging from 2.4-4.4 and 2.6-4.7 hours. The lag time between the peak flow at Imja Lake and the peak at Phakding is 2.2 hours.

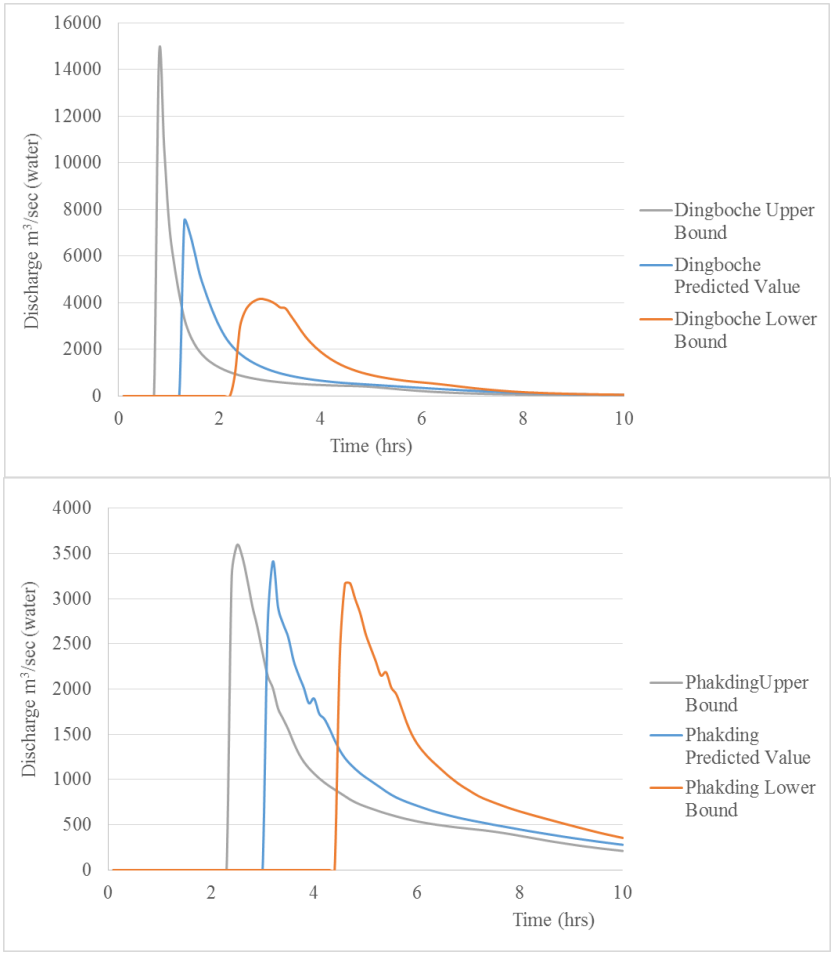

Figure 24: Flo-2D results (upper bound, predicted and lower bound) under Current Conditions Scenario at Dingboche and Phakding.

Table 21: Flo-2D Model Results for Current Conditions Scenario.

Station	**Value Type**	**Arrival Time** (hr)	**Peak Time** (hr)	**Peak Discharge** (m^3/s)	**Volume** (m^3*10^3)
Imja Lake	Lower	0.80	2.3	4272	Mean=31,155 Stdv=273.38
	Predicted	**0.33**	**1.0**	**8394**	
	Upper	0.16	0.5	19000	
Dingboche	Lower	2.2	2.9	4142	Mean=29,685 Stdv=218.48
	Predicted	**1.25**	**1.3**	**7515**	
	Upper	0.80	0.8	14583	
Phakding	Lower	4.4	4.7	3171	Mean=23,350 Stdv=327.37
	Predicted	**3.1**	**3.2**	**3412**	
	Upper	2.4	2.6	3473	

* a.m.s.l. = above mean sea level

Lake Lowering Scenarios

A proposed alternative for reducing risk from Imja Lake that is currently (2014) under design is deepening the outlet channel of the lake in order to lower the water level by 3 m (UNDP 2013). To examine the potential risk reduction for downstream communities if such a plan, or one of several variations, were to be implemented, the Imja Lake GLOF model was run with lake levels 3, 10, and 20 m lower than the baseline (5010 m). Table 22 shows the model results for each of the lake lowering scenarios.

Lowering the lake 3 m results in an 11.8 percent reduction in the peak flow at Dingboche and 43.2 percent at Phakding. In contrast, lowering the lake 10 m results in an almost 43.2% reduction at Dingboche and 17.29 % at Phakding, and lowering 20 m results in a 78.4 % reduction at Dingboche and 38.33 % at Phakding (Figure 25).

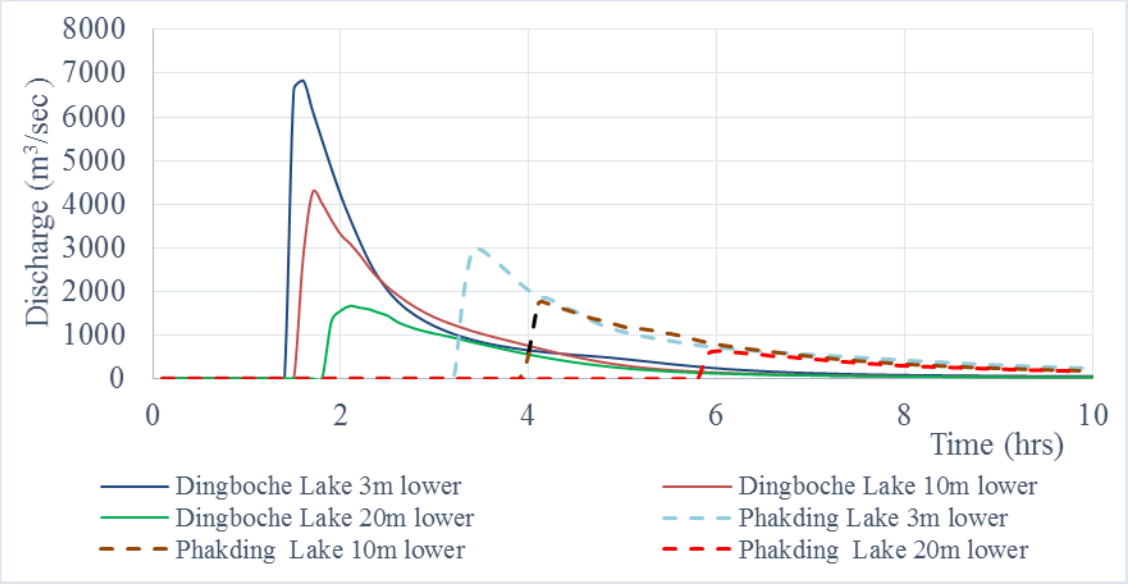

Figure 25: Flo-2D results at Dingboche and Phakding for 3, 10 and 20 m Lake Lowering Scenarios.

Table 22: Flo-2D Model Results under Lake Lowering Scenarios.

Scenario: Lower **Lake**	**Arrival Time** (hr)	**Peak Time** (hr)	**Peak Discharge** (m^3/s)	**Relative Peak Discharge Reduction*** (%)
Dingboche				
3 m	1.6	1.6	6625	11.8
10 m	1.6	1.7	4271	43.2
20 m	1.8	2.2	1624	78.4
Phakding				
3 m	3.2	3.5	2937	13.9
10 m	3.9	4.2	1730	49.3
20 m	5.8	6.1	629	81.8

* referenced to the peak value reported in Table 21 for Predicted Value.

2.7.2.3 Inundation Model Using 5 meters DEM

Lake Current Conditions Scenario

The results of modeling the Current Conditions Scenario of a potential GLOF from Imja Lake are shown in Table 24 and Figures 26, 27, 28, 29 and 30 show the flood depth and discharge at Dingboche. At Dingboche, the flood arrives 1.00 hours after the breaching begins and peaks at 1.3 hours with the uncertainty ranging from 0.6-1.9 and 0.8-2.8 hours respectively. At Dingboche the flood depth is 22.45 m and the peak water flow is 7544 m^3/s with the uncertainty ranging from 18.41-26.4 m and 4208-13248 m^3/s

respectively. The lag time between the peak flow at the breach and Dingboche is 20 minutes.

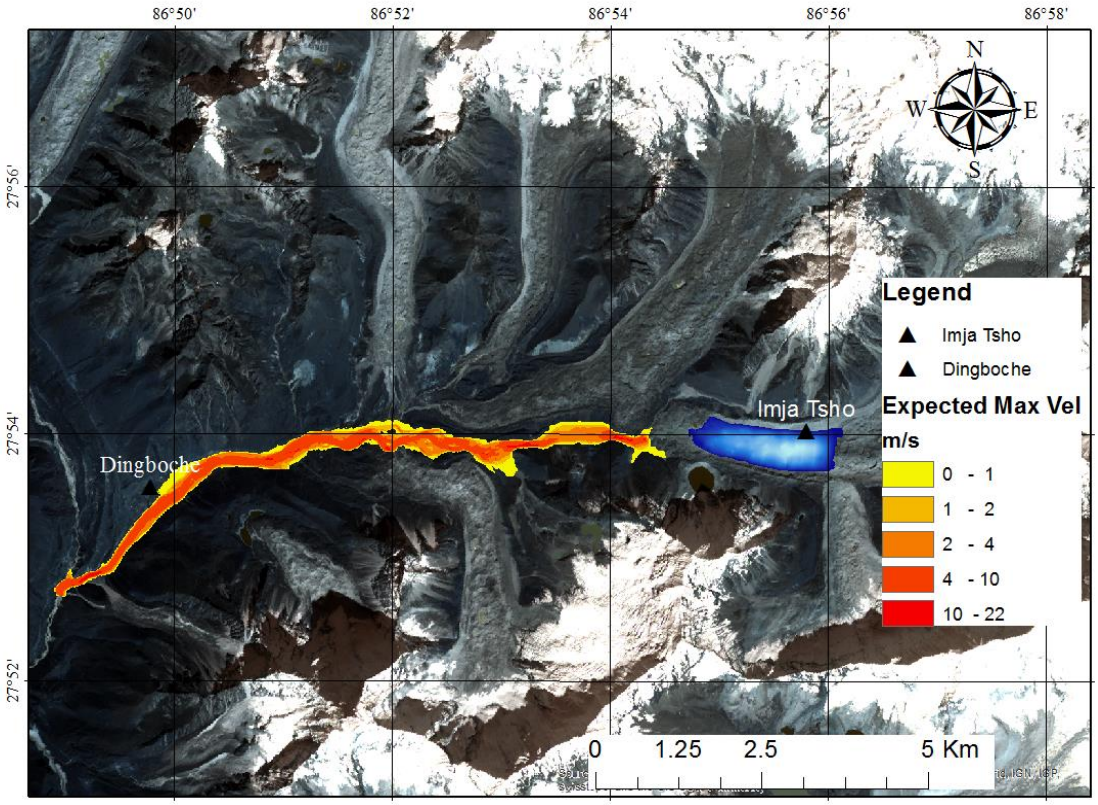

Figure 26: Inundation map from Imja Lake to Dingboche for the expected inundation with the lake current conditions.

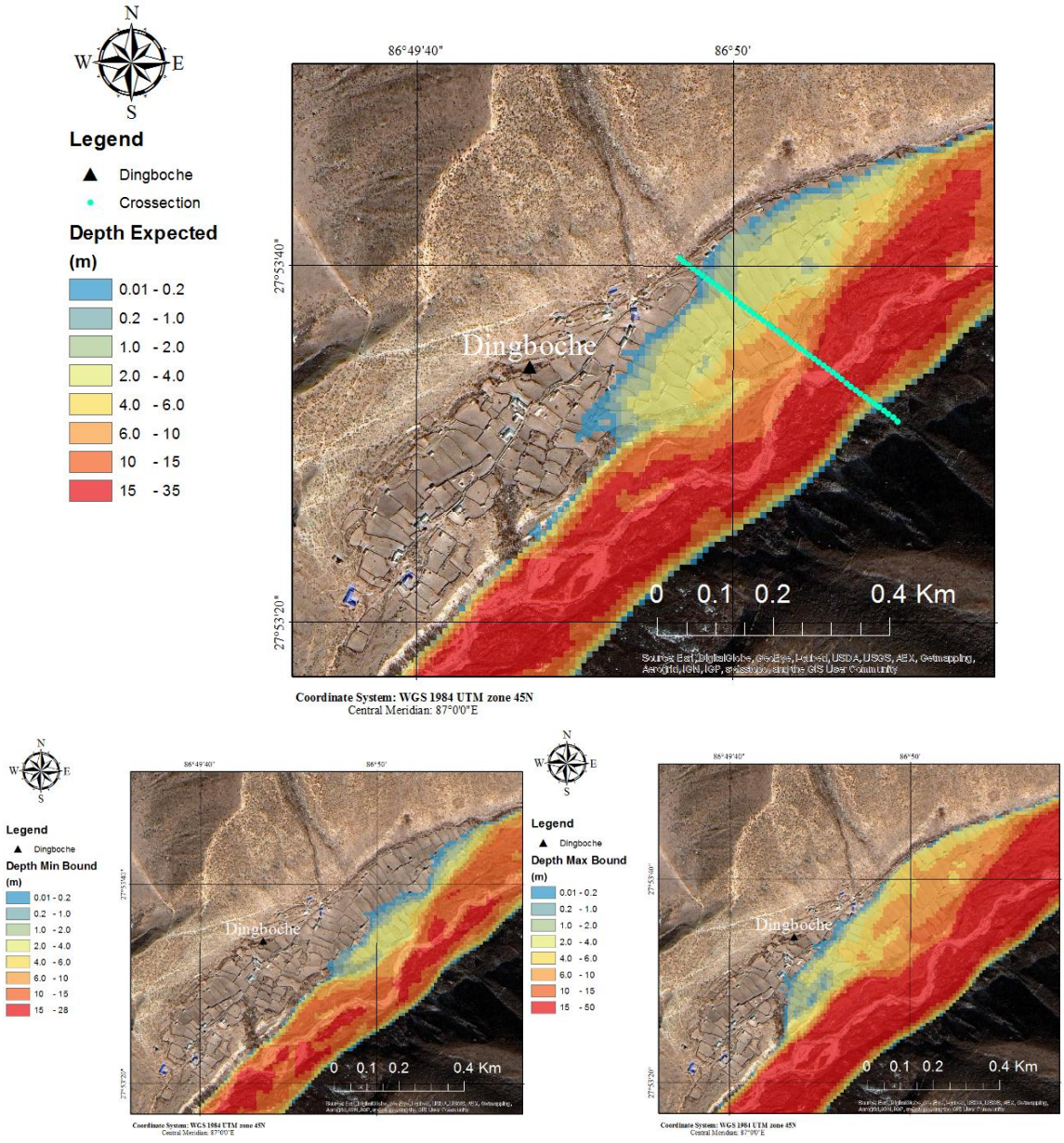

Figure 27: Inundation at Dingboche with the current Lake conditions. Upper figure shows the predicted inundation and the location of a cross section where the different scenarios are compared. Lower figures show the maximum and minimum extension of the inundation

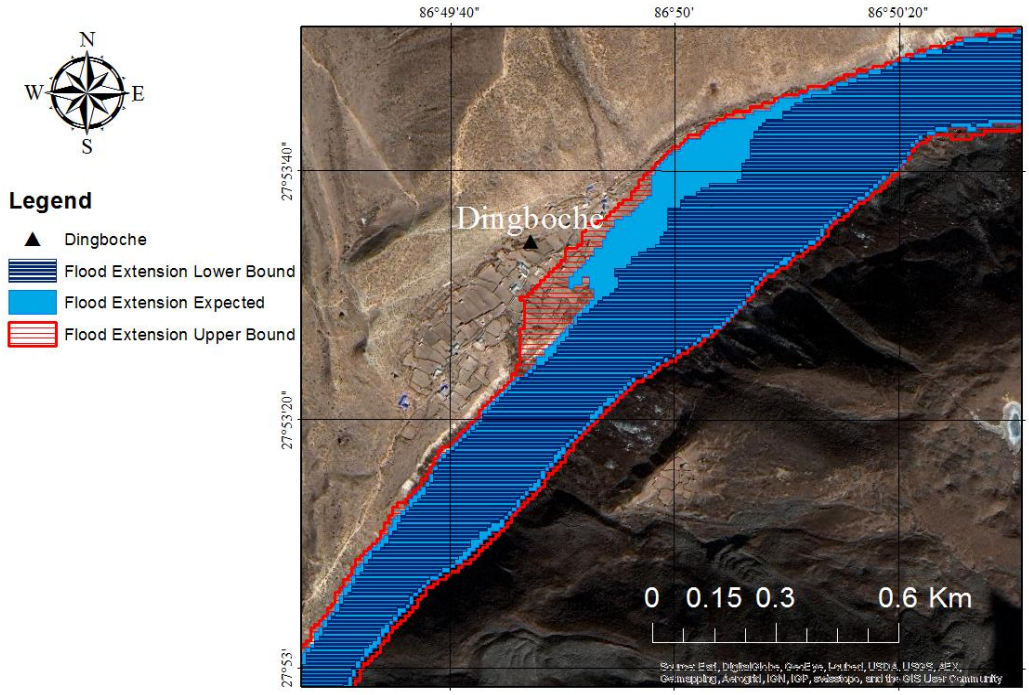

Figure 28: Superposition of the inundation extension for the Lake current conditions. Upper, Lower Bounds and Predicted scenarios.

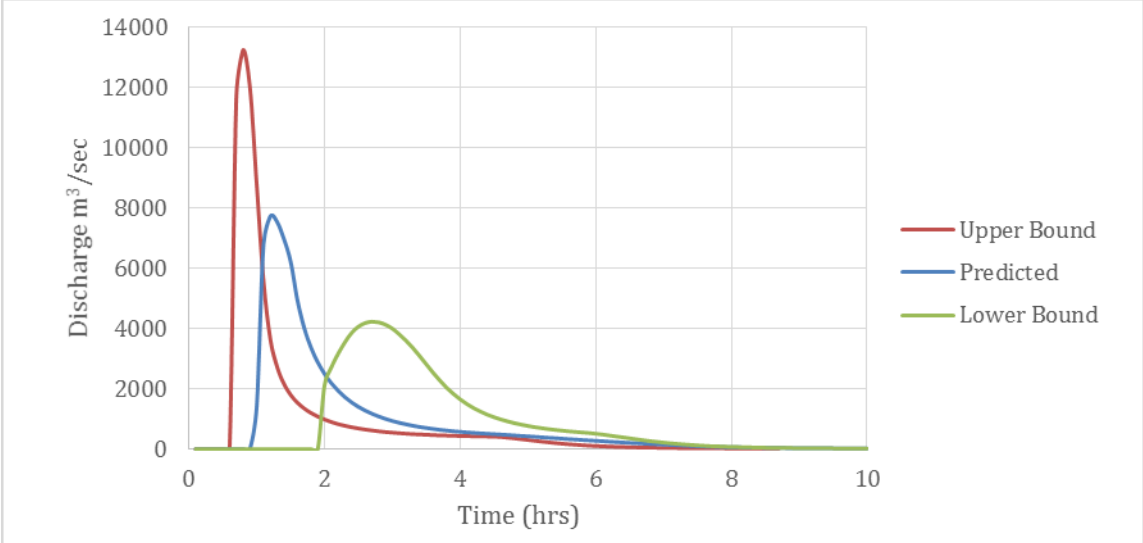

Figure 29: Flo-2D results (upper bound, predicted and lower bound) under Current Conditions Scenario at Dingboche

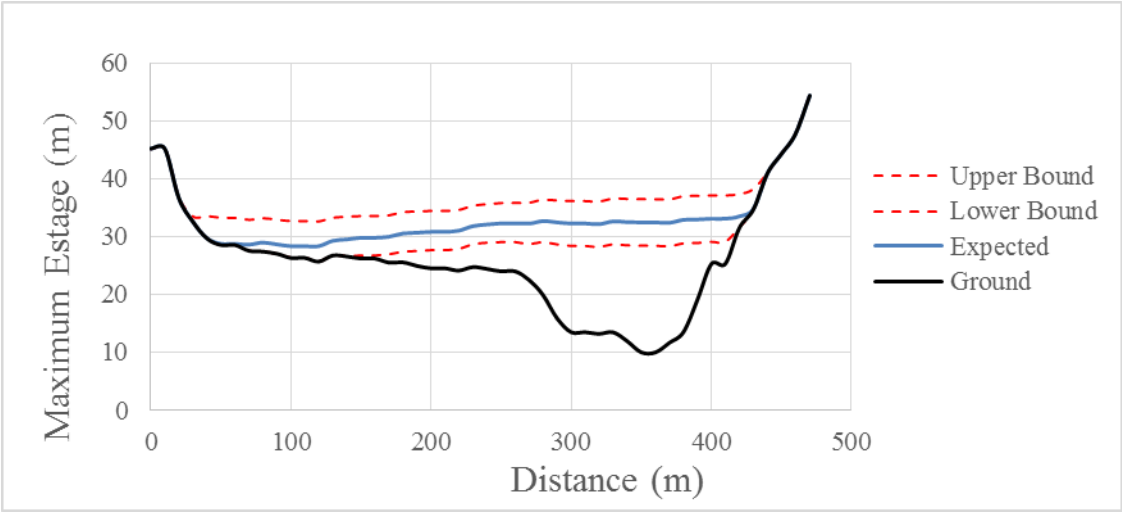

Figure 30: Water stage at the cross-section shown in Figure 1, for the expected, lower and upper bound scenario.

Table 23: Flo-2D Model Results for Current Conditions Scenario.

Station	**Pre-GLOF Stage** (m.a.s.l.*)	**Value Type**	**Arrival Time** (hr)	**Peak Time** (hr)	**Peak Depth** (m)	**Peak Discharge** (m^3/s)
Imja Lake	4970	Lower	0.80	2.3	12.1	4272
		Predicted	**0.33**	**1.0**	**16.6**	**8394**
		Upper	0.16	0.5	33.4	19000
Dingboche	4332	Lower	1.9	2.8	18.41	4208
		Predicted	**1.00**	**1.3**	**22.45**	**7544**
		Upper	0.60	0.8	26.4	13248

* a.s.l. = above sea level

Lake Lowering Scenarios

As it was done with the coarser data, the proposed alternative for reducing risk from Imja Lake (UNDP, 2013) is analyzed. The Imja Lake GLOF model was run with lake levels 3, 10, and 20 m lower than the baseline (5010 m). Table 24 and Figures 31, 32, 33 and 34 show the model results for each of the lake lowering scenarios. Lowering the lake 3 m results in a 2.76 percent reduction in the peak flood depth at Dingboche. In contrast, lowering the lake 10 m results in an almost 14.30% reduction, and lowering 20 m results in a 35.86 % reduction at Dingboche and 38.33 %. Additionally the peak discharge has a reduction of 6.51, 40.63 and 73.82 % as a result of lowering Imja Lake by 3, 10 or 20 meters.

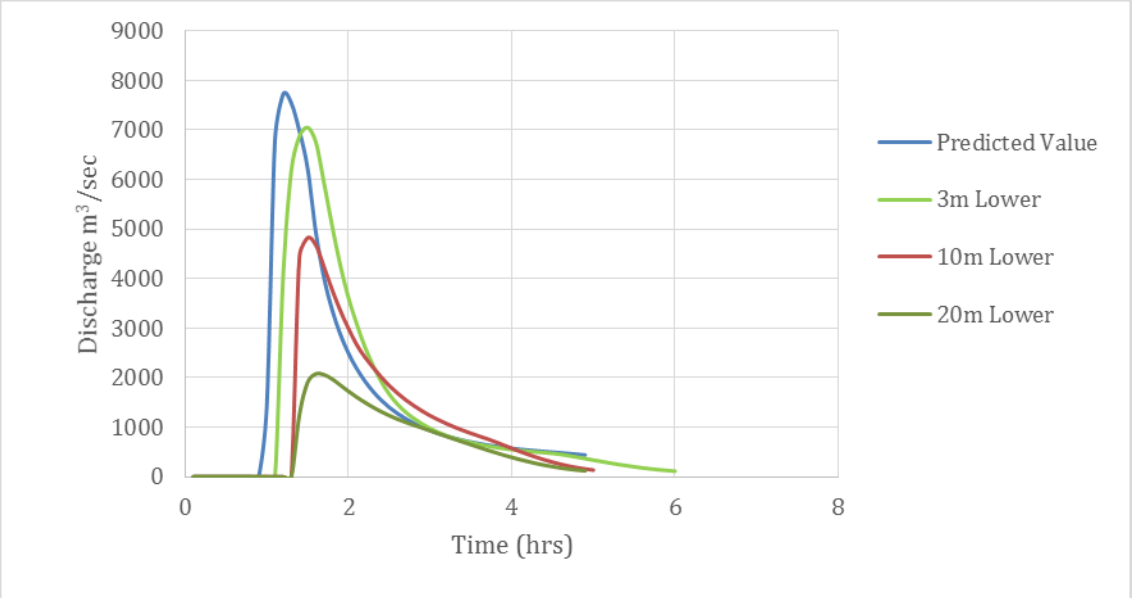

Figure 31: Flo-2D results at Dingboche and Phakding for 3, 10 and 20 m Lake Lowering Scenarios.

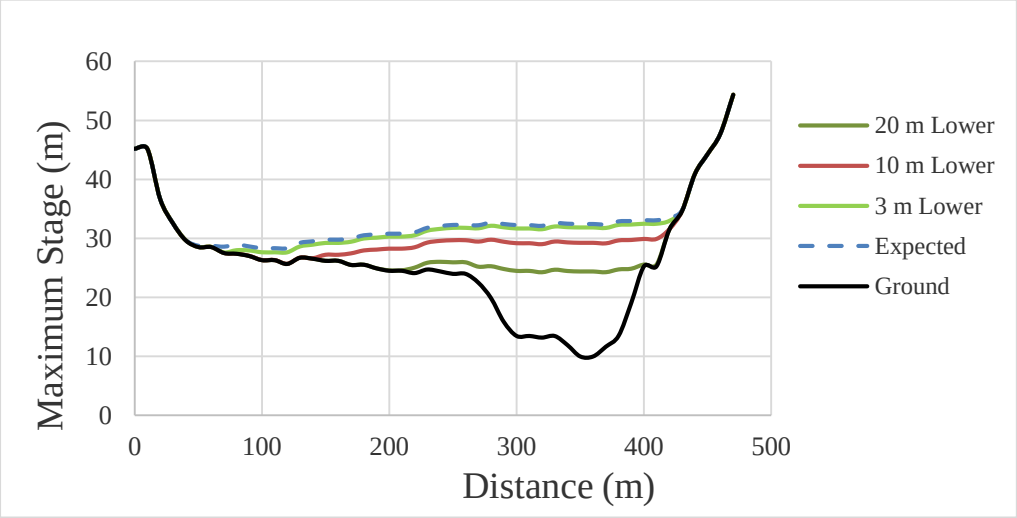

Figure 32: Expected water stage at the cross-section shown in figure 1, for the Lake lower by, 20, 10, 3 and 0 meters scenarios.

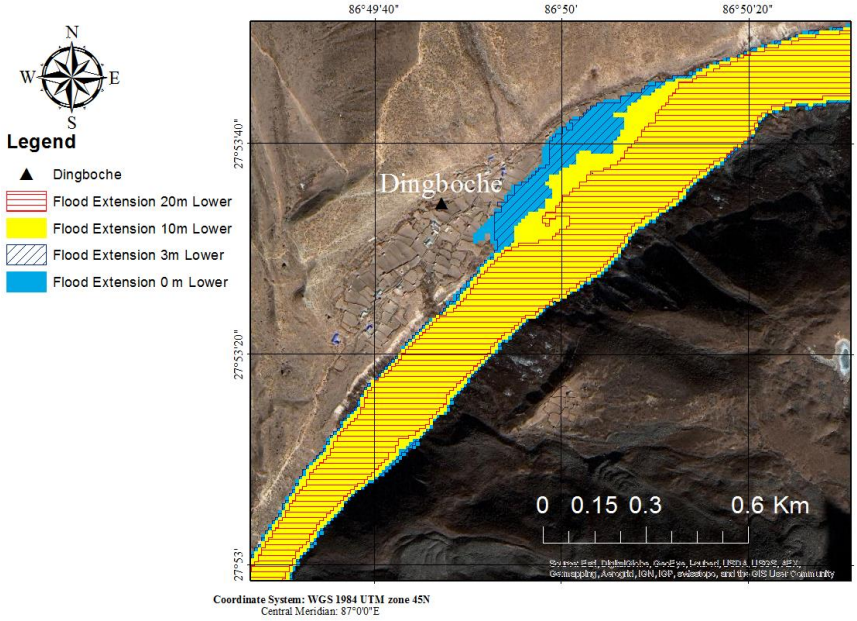

Figure 33: Superposition of the expected inundation extension for 4 scenarios. Lowering the lake by 20, 10, 3 and 0 meters.

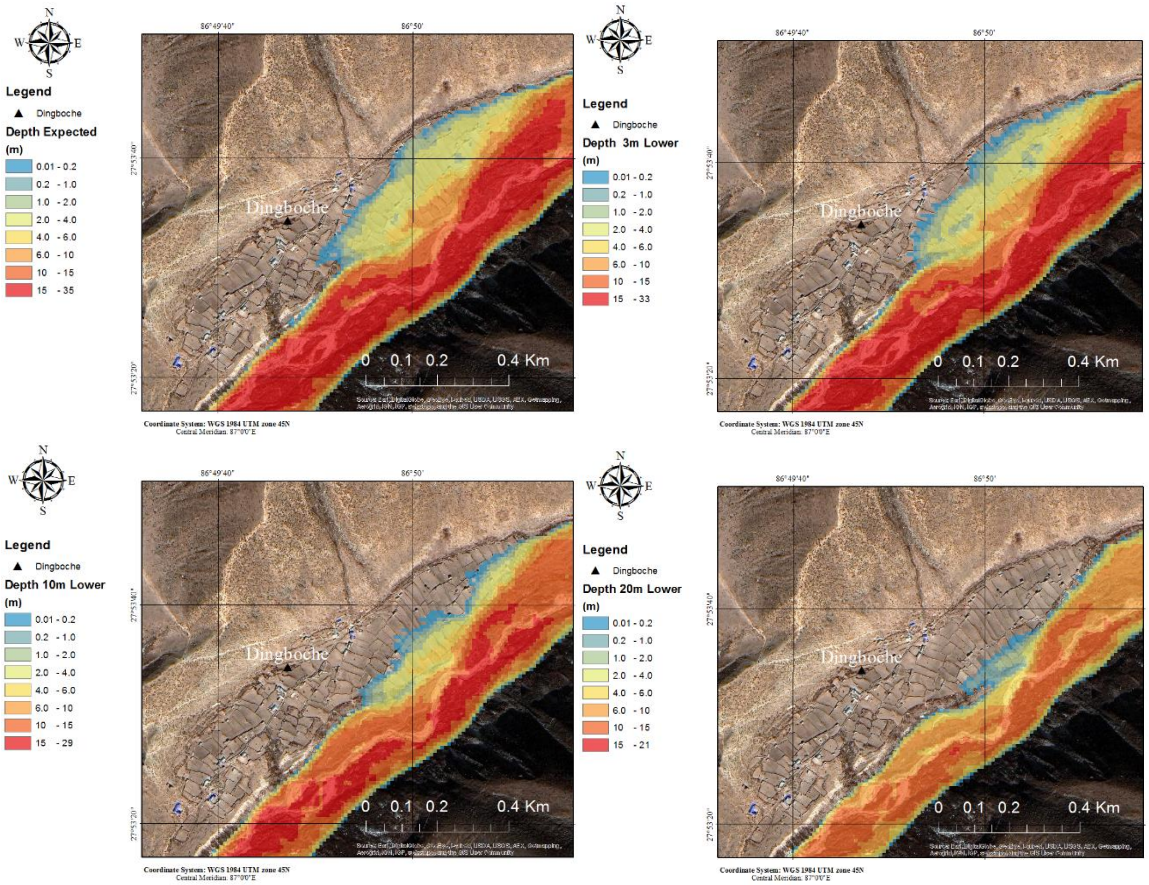

Figure 34: Expected inundations depth near Dingboche for 4 scenarios. Lowering the lake by 20, 10, 3 and 0 meters.

Table 24: Flo-2D Model Results under Lake Lowering Scenarios.

Scenario: Lower **Lake**	**Arrival Time** (hr)	**Peak Time** (hr)	**Peak Depth** (m)	**Peak Discharge** (m^3/s)	**Relative Peak Depth Reduction*** (%)	**Relative Peak Discharge Reduction*** (%)
3 m	1.1	1.5	21.83	7053	2.76	6.51
10 m	1.3	1.6	19.24	4479	14.30	40.63
20 m	1.3	1.8	14.40	1975	35.86	73.82

* referenced to the peak value reported in Table 23 for Predicted Value.

Future Conditions Scenario

There is no doubt that Imja Lake will keep growing toward the east. In this work we simulate the inundation downstream if a GLOF will occur when the lake reaches the rock/ice avalanche zone. The lake, as it has been mentioned, will have an area of at least 2 km^2. We calculated the peak discharge (Table 20) and calculate a discharge hydrograph for this future GLOF scenario (Figure 23). We simulate 2 cases; one that keeps the level of the lake as it currently is (5010m) and a second, which considers that the lake would have been lowered by 20 meters. A summary of the results is showed in Table 25. If the lake is not lowered the inundation depth will increase by 31.5 % and the peak discharge will increase in 23.77 % for the section analyzed at Dingboche. However if the lake is lowered by 20 meters, the inundation depths in the sections analyzed almost won't change even if the lake area increases (See Table 24 and 25 for Lake Lower 20 meters).

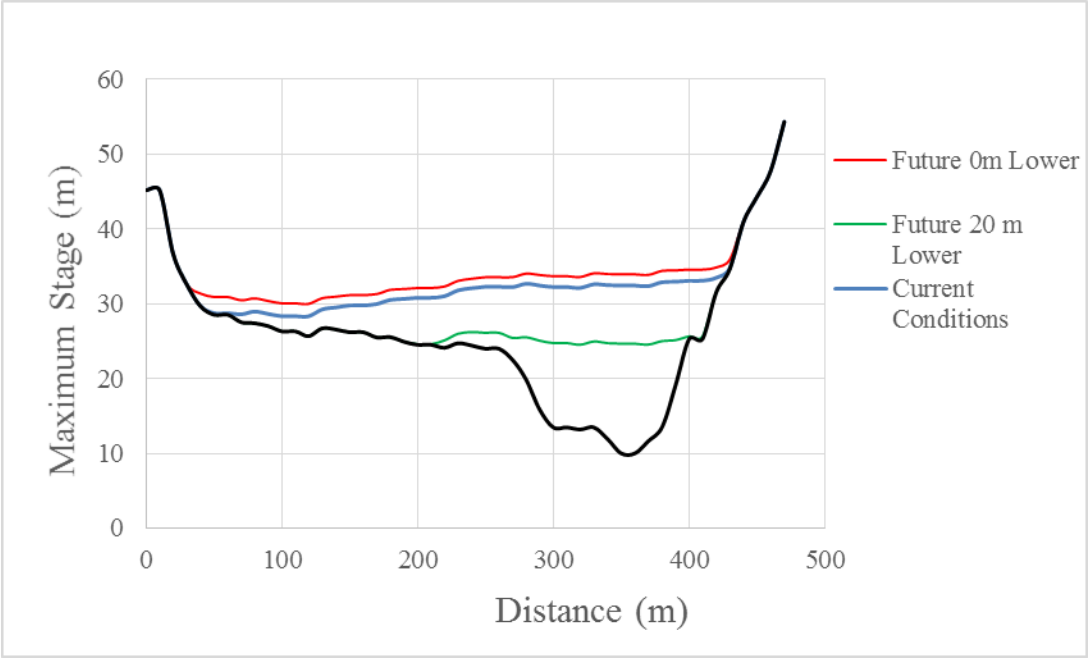

Figure 35: Water stage for the Future 0 and 20 m Lake lowering and current conditions scenarios.

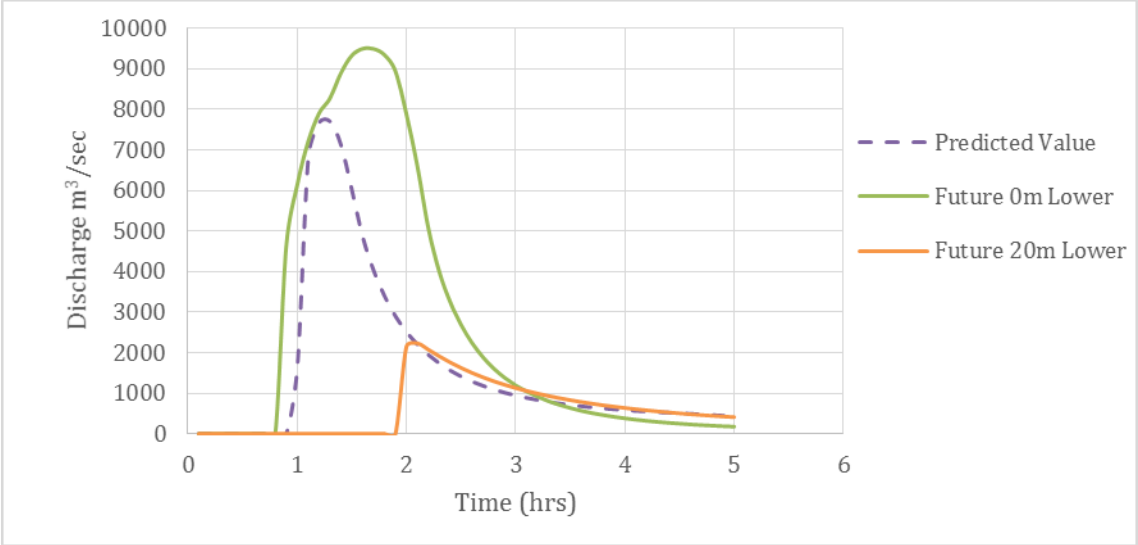

Figure 36: Expected hydrographs for the Future 0 and 20 m lowering and predicted value for current conditions scenarios.

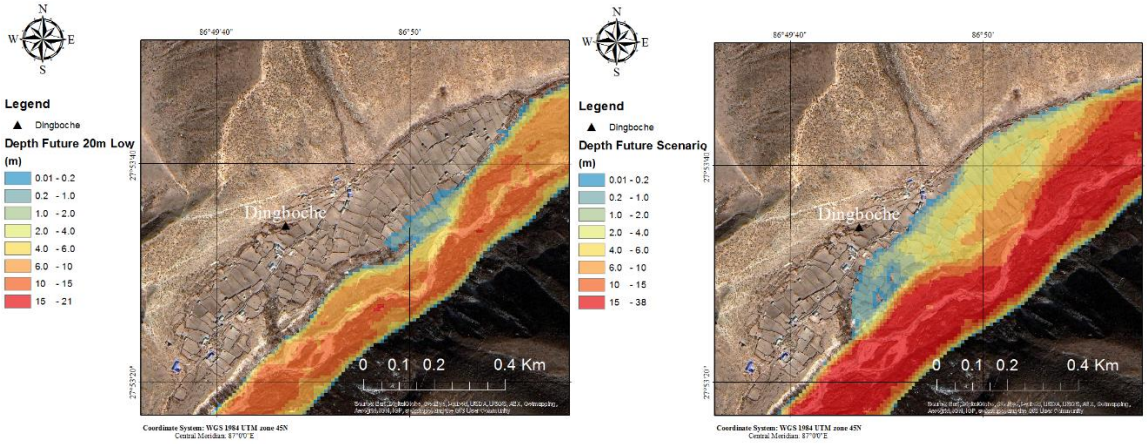

Figure 37: Expected depth for the Future 0 and 20 m Lake lowering scenarios.

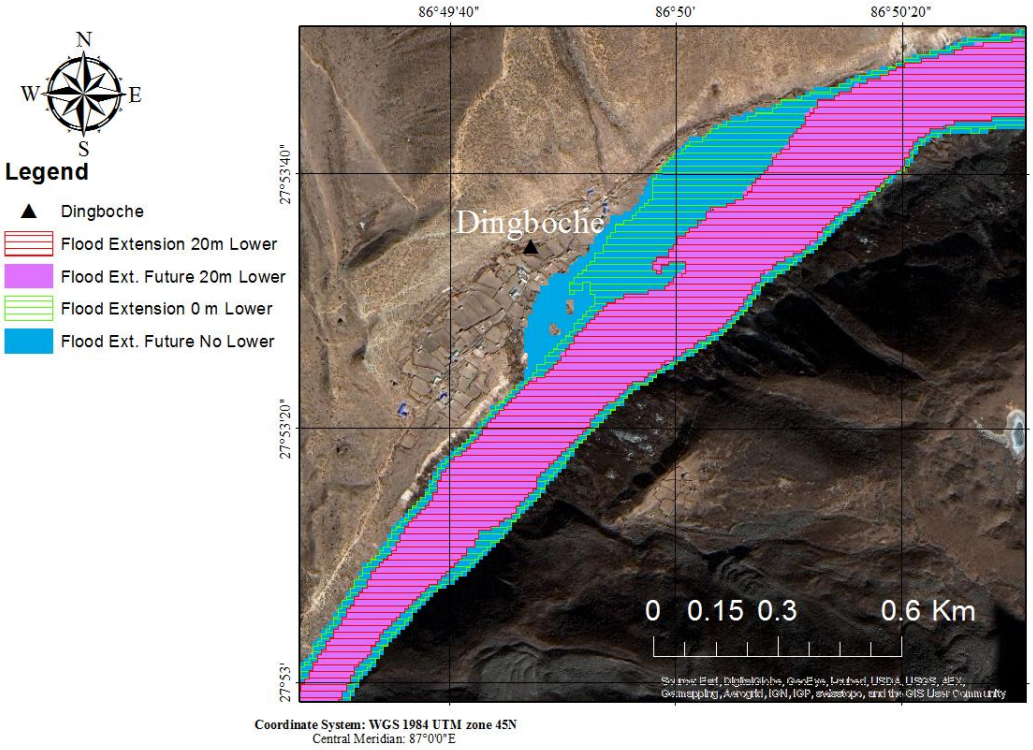

Figure 38: Superposition of the expected inundation extension for the Future 0 and 20 m Lake lowering and current conditions and 20 m Lake Lowering scenarios.

Table 25: GLOF Model Results at Dingboche Future scenario

Lake Lower (m)	Flood Arrival Time (hr)	Flood Peak Time (hr)	Flood Peak depth (m)	Water Peak Flow (m^3/s)	Relative Peak Depth Reduction* (%)	Relative Peak Discharge Reduction* (%)
	Dingboche					
0	1.1	1.7	23.95	9337	-6.68	-23.77
20	1.90	2.0	14.67	2076	11.62	72.48

* referenced to the peak flood depth reported in Table 23 for Predicted Value

2.7.2.4 Sensitivity Analysis

The sensitivity of the model was tested to perturbations in roughness coefficient values, and sediment concentration as indicated in Table 26. The peak flow at Dingboche decreases by as much as 13% when the roughness coefficient is increased from 0.05 to 0.60; whereas, the flow at Phakding is much more sensitive with the peak flow decreasing as much as 40% for the same variation in roughness coefficient. As the roughness coefficient is increased the flow slows down and the hydrograph peak decreases. Also the roughness coefficient values in the river range from 0.15 to 0.30 increasing as the distance from the river increases due to the vegetation available to around 0.40.

Table 26: Sensitivity Analysis Scenarios for Flo-2D Model.

Sensitivity Scenario	Roughness coefficients	Sediment concentration (by volume)	Peak Discharge	Dingboche Difference (%)	Phakding Difference (%)
1	0.05	50%	Predicted	0	0
2	0.15	50%	Predicted	-6.5	-6.3
3	0.30	50%	Predicted	-11.2	-21.5
4	0.45	50%	Predicted	-11.6	-29.2
5	0.60	50%	Predicted	-13.7	-39.6
6	Land Cover	40%	Predicted	-3.7	-37.2
7	Land Cover	30%	Predicted	-6.9	-51.4

Figure 39 illustrates the sensitivity of the result to the sediment concentration (C_v). In order to compare the different hydrographs, the water discharge with no sediment is shown in the Figure 39. The total volume (water plus sediments) is derived by dividing the water volume by (1-C_v). As we increase C_v, the velocity of the flow decreases; however, the mass carried by the water increases energy of the mixture balances. At Dingboche the water peak flow is almost unaffected by C_v; however, at Phakding the peak flow is delayed and decreased as C_v increases. The water peak flow at Phakding for C_v = 30% is 4462 m^3/s; therefore, the mixture peak flow is 6374 m^3/s. On the other hand, the water peak flow at Phakding for C_v = 50% is 2947 m^3/s; therefore the mixture peak flow is 5894 m^3/s. Consequently for the case C_v = 30%, it carries less mass, produces a higher peak and an earlier peak discharge time than C_v = 50%, which clearly

increases the hazard level of the inundation. If we compared the results for the variation in roughness coefficient and debris/sediment concentration with the uncertainties in the hydrograph generation we can conclude that the inundation is more sensitive to the volume release at the lake and the moraine breaching process.

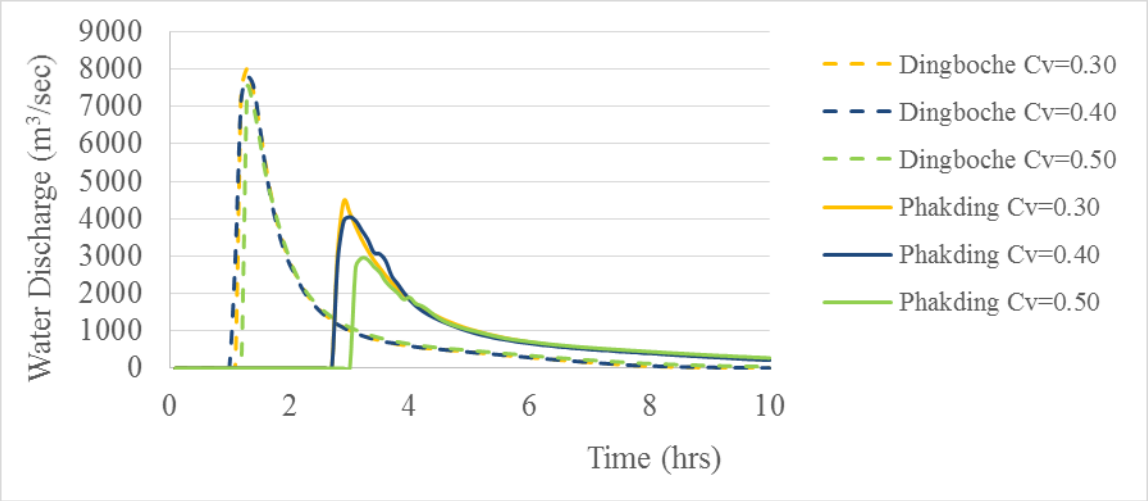

Figure 39: Influence of the sediment concentration by volume (Cv) on the water flow peak and time at Dingboche and Phakding. Cv values go from 30% to 50%.

2.8 DISCUSSION

Imja Lake is currently the focus of several groups in an effort to reduce the risk of a GLOF posed by the increasing lake level. While no agreed upon set of hazard indicators exists for Imja Lake, the definition of GLOF hazard was discussed in consultations with community members in Dingboche in September 2012. The hazard of a GLOF didn't exist 30 years ago, and their vulnerabilities stem from the location of their homes and farms relative to the flood plain. For them, hazard is having their farms or homes flooded, a prospect that they want either reduced or eliminated. To evaluate the

feasibility of proposed hazard reduction alternatives, scenarios that reduce the peak flood stage at Dingboche or Phakding to less than 10 m above the pre-GLOF water level will likely reduce the risk of overtopping terraces with agricultural fields. Based on the model results, lowering the lake 20 m is the only scenario that leads to this level of protection for the communities. Specially because the probability of outburst will be reduced considerably and the volume available would produce less damage than if a GLOF were to occur in the current lake conditions. This of course needs to be carefully studied in an economical assessment, which is not part of this work.

2.8.1 Previous Recommendations for Lowering Imja Lake

Kattelmann and Watanabe (1998) note that the methods of glacial lake control include the relocation of people and assets from the flood path, strengthening the outlet, reinforcing the outlet, and partially draining the lake. Of all the methods to increase glacial lake security, reducing lake volume appears to be the most reliable and successful, employed at over 40 dangerous lakes in Peru since the 1950s (Portocarrero 2014). Typically, the lake is lowered to a safe level using a drainage channel. A reinforced earthen dam is then constructed to replace the original unconsolidated moraine dam, such that if a surge wave does occur and the water level rises temporarily and overtops the dam, the dam will contain the excess water until the safe level is restored.

Siphons have been used on numerous lake lowering projects around the world as a way to stabilize lake water levels, e.g., Hualcán glacier lake (Lake 513) in Peru, where siphons were used to lower the lake by about 5 m with a capacity of about 0.5 m^3/s (Reynolds et al., 1998). Kattlemann and Watanabe (1998) note that siphons from Imja

Lake may be the most feasible alternative for lowering the lake. Grabs and Hanisch (1993) presented details of siphon methods for draining glacial lakes, showing that lowering glacier lakes at 5000 m by more than 5 m at a time is infeasible. Siphons were used to test the lowering of Lake Rolpa glacial lake in Nepal during 1995-97, demonstrating that siphons can be used successfully at high altitude in freezing winter conditions (Rana et al. 2000).

Regardless of the risk reduction alternative, the question of to how to safely lower the lake remains. For example, siphons may be used to lower the lake level progressively in conjunction with excavation along the outlet of Imja Lake. In this way, siphons would be used to lower the lake a few meters, then excavate the channel, and continue this sequence until the desired lake level is reached.

2.8.2 Strengthen the Outlet Channel

Strengthening and deepening the outlet of Imja Lake may be the best alternative for controlling the lake level. The lake lowering method proposed in the UNDP project is to excavate the existing outlet channel of the lake (near the end of the outlet lake complex) to increase its depth and thus discharge from the lake outlet, thereby lowering the lake level. The difficulties of employing this method, however, include: (1) the possibility of encountering ice during the excavation, significantly weakening the moraine and possibly inducing a GLOF; and (2) the existence of small ponds in the outlet complex that are separated with shallow necks (with as little as 1.5 m depth) through which the lake water flows, which would prevent the draining of the lake unless they were also excavated.

There is significant ice presents in the terminal moraine; however, since the Imja Lake natural channel spillway is relatively stable (Watanabe et al., 2009), it may be possible to excavate and reinforce the spillway and the pathway through the outlet to increase the outflow and lower the lake. Additional and more detailed surveys are needed to determine if ice extends close to the natural spillway. If it does not, then there should be little problem in reinforcing and expanding the natural spillway. However, if the core is close to the spillway, then stabilization may be impossible in that location.

The UNDP project has used the experience and design of the lake lowering system at Lake Rolpa as a model for Imja Lake. In that project, Lake Rolpa was successfully lowered 3 m and an outlet channel constructed, but the original recommendation of the designers was to lower the lake by 20 m. The final 17 m of lowering, however, was never attempted (Rana et al. 2000). As can be seen from the results presented here, following the Lake Rolpa experience and lowering the lake level of Imja Lake by 3 m would not lead to a significant reduction in GLOF hazard for downstream communities. The results shown above indicate that the lake should be lowered at least 20 m to ensure hazard reduction for the communities downstream of the lake. The process of lowering the lake by 20 m could be done in a synchronize process that allows to drain 3-4 meters using siphons, excavate and reinforce the walls, repeating the process until 20 meters is reached.

2.9 CONCLUSIONS

2.9.1 Field work

2.9.1.1 GPR Survey

The thickness of the glacier varies from 40-60 m thick near the lateral moraines to over 200 m thick in the center of the glacier, which indicates that the lake potentially can expanded his length many hundreds meters increasing his volume. This means that in the future the lake can release more water in a potential GLOF.

The presence or absence of ice in the core of the terminal moraine complex is of critical importance in designing a risk reduction program for the lake. This work has used Ground Penetrating Radar (GPR) to investigate the internal structure of the moraine complex in order to map out the ice thickness in critical areas.

The results of the GPR survey do not allow us to determine the thickness of the ice buried in the terminal moraine. The radar grams generated from the data collected don't show unequivocal prove that allow us to detect the top and bottom of the ice. The reasons for this lack of clarity in the GPR survey at the terminal moraine are not known by us. In consultation with experts in geophysics methods they think that other technics such as electric resistivity may have better outcomes than the GPR used; however, that was not part of the scope of this work.

2.9.1.2 Bathymetry Survey

The results of a 2012 bathymetric survey of Imja Tsho show that the lake has deepened from 98 m in 2002 to 116 m in 2012. Likewise, the volume has increased from

35.8 million m^3 to 61.6±1.8 million m^3 over the past decade as well, a 70 percent increase. The lake volume is increasing at a rate of 2.51 million m^3/yr, and the average depth is increasing by 0.86 m/yr. Our survey results also suggest that the lake bottom has continued to lower as the ice beneath it has melted. Most of the expansion of the lake in recent years has been due to the retreat of the glacier terminus (eastern end of the lake) through calving processes. The continued expansion of the lake has increased the volume of water that could be released from the lake in the event of a breach in the damming moraine to 34.08±0.54 million m^3, rather than 21 million m^3 estimated in 2002 if the lake surface elevation decreases from 5010 m to 4975 m (the elevation of the valley floor below the lake).

2.9.2 Hazard Level calculation

We used sixth qualitative, one semi quantitative and one quantitative methods to estimate the Imja Lake level of hazard for the current lake conditions and for a future scenario when the lake reach the avalanche zone. For the current condition there is an agreement in the methodologies that the lake has a medium to high level of risk which will increase as the lake grows to the east; where, it may be exposed to rock/ice avalanches.

2.9.3 Imja Lake GLOF Modeling

In this paper some possible GLOF hazard reduction measures were illustrated for Imja Lake in Nepal and analyzed their potential to reduce flood risk for downstream communities. The GLOF trigger mechanism considered here is a piping failure due to seepage in the face of the outlet dam. This could be a result of an increase of the

currently observed seepage rate due to further melting of the ice in the moraine, or an earthquake weakening the moraine and causing an increase in the seepage. It is expected than in the future surge waves that can overtop the moraine can be generated by avalanches of ice and rock at the east side of the lake. A model was developed to assess the magnitude of a potential GLOF from Imja Lake. The flooding impact on downstream communities due to the lake has been quantified, and several alternatives for reducing that impact have been illustrated along with their potential reduced flood levels. An alternative now under implementation by UNDP was considered, lowering the lake 3 m, and found not to provide significant flood reduction benefits to the downstream communities.

The results indicate that the lake needs to be lowered by 20 meters in order to reduce the impacts that a GLOF could have downstream. Also it has been proved that lowering the lake by 20 meters will be effective in a future scenario when the lake reaches the avalanche zone. All cases involving lowering the lake would require a coordinated sequence of siphoning to lower the water level in 3 m to 4 m increments, followed by outlet excavation to maintain the new level. The process would be repeated as needed to reach the desired lake level.

Chapter 3: Palcacocha Lake and Huaraz City in Peru

3.1 INTRODUCTION

Glaciers in the Andes of Peru provide fresh water to the arid western part of Peru during the dry season when little to no rainfall occurs (Vuille et al. 2008). The west coast of Peru uses the water coming from the high mountains for agricultural, domestic and industrial purposes. In Peru, the main source of electricity generation is hydropower, representing 80% of the electricity in the country (Vergara et al. 2009). Georges (2004) estimated that the glacier-covered area in the Cordillera Blanca of Peru had decreased from 800-850 km^2 in 1930 to 600 km^2 at the end to the 20^{th} century. Silverio and Jaquet (2005) estimated that Cordillera Blanca glaciers reduced from 643 ± 63 km^2 to 600 ± 61 km^2 between 1987 and 1996, and in another estimation the total area was reduced by 26% from 723 to 535 km2 between 1970 and 2003 (Tacsi et al. 2008). Tacsi et al. (2008) estimated that the reduction from 1970 to 1996 was 15.46% (0.6% per year) and from 1996 to 2003 was 10% (1.4% per year) (Racoviteanu et al. 2008). Racoviteanu et al., (2008) found 571 glaciers covering an area of 569 km2 and experiencing a decrease in glacier area of -0.68% per year over the thirty-three year period 1970–2003, representing a 22.4% decrease in area over that period. Current losses can, therefore, be estimated at about 1% per year.

Long-term slope destabilization due to warming and degrading permafrost in Peru concerns steep summits above about 5000 m a.s.l.. Related low-probability but high-magnitude ice/rock avalanches are especially dangerous in connection with lakes forming at the foot of steep mountain walls (for instance Artesonraju and the new lake probably

forming soon at the flat tongue of Glacier Artesonraju), because they can trigger large impact waves permafrost (Carey et al. 2011; Haeberli 2013). A detailed study carried out on the large Monte Rosa east face in the European Alps by Fischer et al. (2013) documents that rates of rock and ice losses in such mountain flanks are not only increasing but can also have self-reinforcing effects. Concerning such slope instabilities it is important to understand the concepts of long-term disposition, short-term disposition and trigger effects. Primary long-term disposition refers to the factors geology (lithology, layering, fracturing), topography (vertical extent, slope) and ice conditions (ice cover, hanging glaciers, permafrost) - i.e. always to a combination of factors. Short-term disposition refers to changes in these factors: With ongoing climate change, ice conditions are critical because among the primary long-term disposition factors they are changing by far most rapidly and fundamentally. Trigger effects leading to discrete events mainly include earthquakes, extreme snow melt, heat waves, heavy precipitation (Huggel et al. 2010; Haeberli 2013).

Evaluation of hazard posed by glacial lakes must be based on systematic information about lake types, dam characteristics, outburst mechanisms, down-valley processes and possible cascades of processes. In addition changes in climate patterns are likely to increase the frequency of rock/ice avalanches as a consequence of the reducing in the stability of permafrost bedrock and steep glaciers in cold mountain regions such Cordillera Blanca (Fischer et al. 2012a; Fischer et al. 2013).

3.1.1 Glacier lake protection system examples in Peru

Some examples of glacier lake protection systems that were successfully installed in Peru but now due to changes in landscape were extracted from Haeberli et al. (2013).

As a consequence of glacier vanishing, many new lakes formed in the Cordillera Blanca, fundamentally changing hazard potentials for the population. Examples in Peru of corresponding historical to recent incidents and catastrophes are listed in Table 25. Due to the historical relationship between people in Cordillera Blanca and dangerous event related to High Mountain. Because of this the Peruvian has a vast experience dealing with this event. They have cumulated more than 50 years of successful lake interventions, lowering lakes level and reducing the risk. Although these works have been successful experiences they need a revision because in the last years the dangers to which they were designed have evolved. In this work we list some examples that have been personally visited during our 2012-2013 visits to Cordillera Blanca.

Table 27: Main catastrophic events in Ancash (Haeberli et al. 2013).

Year	Event	Year	Event
1702	Huaraz City Inundation	1953 1959	2 Debris flow from Tulparaju lake
1725	GLOF that washed out Ancash town	1962	Debris flow in Mount Huascaran above Ranrahirca
1725	Avalanches and debris flow in Huaraz	1965	Debris flow from Tumarina lake-Carhuascancha
1869	Debris flow in Monterrey-Huaraz	1970	Debris flow in Yungay and Ranrahirca
1883	Debris flowing Macashca near Huaraz	2001	Avalanche produced an overflow in Mullaca lake
1917	Debris flow in Mount Huascaran above Ranrahirca	2002	Rock avalanche produced an overflow in Lake Safuna Alta
1938	Debris flow in Quebrada Ulta-Carhuaz	2003	Landslide from a lateral moraine in Palcacocha lake overtopping the security dike. This event left Huaraz without potable water for 6 days
1941	Debris flow in Pativilca river basin	2003	Avalanche from Huandoy peak, killing 9 people
1941	Debris flow in Huaraz (~5000 people died)	2006	Overtopping of Matara Lake producing several damage to infrastructure
1945	Debris flow inundated the Chavin Huantar ruins	2008	Overtopping of a lake in formation in Quebrada Cojup
1950	Debris flow in lake Jancarurish destroying an hydroelectric facilities	2009	Landslide in Rampac Grande peak killing 9 people
1951	2 debris flow from Artesoncocha Lake	2010	Ice/rock avalanche in Laguna 513 producing waves that overtopped the 20 m freeboard producing damage to infrastructure
1952	Debris flow from Millhuacocha lake-Quebrada Ishinca	2012	Moraine breach in Artison Baja dike

3.1.1.1 Lagunas Arhuaycocha y Artison

In the 1960s already, a dam of loose material 6 m high and with two outlets in its base was built at the lower end of Laguna Jatuncocha (8°55’45’’S/77°39’30’’; Figure 26). This dam worked as a retention structure when in February 2012 the Laguna Arteson

Baja higher up in the same catchment overtopped and breached its dam consisting of loose moraine material and debris-flow deposits, lowering abruptly the level of the lake and causing debris flow, the traces of which can easily be recognized in Figure 40. The artificial dam structure at Laguna Jatuncocha certainly helped to considerably reduce the effects of the sudden drainage of Arteson Baja.

Figure 40: Arhuaycocha, Arteson and Jatuncocha lakes. From Artison to Jatuncocha is possible to observe the material deposited from 2012 breach at Arteson Baja (Source: Google Earth)

Within the same complex of lakes in the catchment above Laguna Jatuncocha, there is also Laguna Artison Alta, with a volume of 1.4 million cubic meter of water. This lake has a solid rock dike. However, it is exposed to potential avalanches of ice, which

can create huge impact waves, overtopping the rock dam and initiating a cascade of effects downstream, affecting Artison Baja and Jatuncocha.

In addition there is Laguna Arhuaycocha with a volume of 19 million cubic meter of water in another part of the catchment. This lake is also exposed to ice avalanches which can release a large amount of water downstream, affecting Laguna Jatuncocha. Although the structure built 50 years ago in Laguna Jatuncocha reduced the risk during the Laguna Artison Baja GLOF, it may not sufficient to prevent future and more extreme events. Therefore more detailed investigation and additional constructions are needed in order to increase the protection of downstream communities. Such projects could possibly be combined with tourist development and/or hydropower production.

3.1.1.2 Lagunas Artesonraju/Parón

Laguna Parón has been regulated for combined flood protection, hydropower production and regular water supply since 1970 by a high-technology tunnel that controls the level of the lake. However, new lakes are forming in the catchment above Laguna Parón (Figure 41). The retreat of the flat tongue of Glacier Artesonraju will soon enable the formation of a lake, which could end up with a volume of millions of cubic meters of water. This new lake is exposed to potential rock/ice avalanches of considerable volume, which can produce impact waves overtopping the reservoir and affecting Laguna Parón. Corresponding flood waves can be kept under control as long as an adequate free-board is guaranteed for Laguna Parón. Laguna Parón is indeed an early and successful pioneer example of a multipurpose structure related to lake management in high mountains subject to effects from climate change.

Figure 41: Lakes Paron and Artesonraju and the location of a lake forming on Artison Glacier.

3.1.1.3 Laguna 513/ Pampa de Shonquil

Lake 513 started forming in the 1980s in the Hualcán Mount mountains (9°12'45''S/77°33'00''W) near Carhuaz, Ancash (Figure 42).The massive bedrock dam is mainly granodiorite. Three artificial tunnels were installed already in the 1980s to lower the lake level and create a free-board of 20 m as a protection against impact waves from expected ice avalanches. This system was tested by an ice/rock avalanche event on April 11, 2010. The wave generated by the avalanche overtopped the lake threshold by about 5 m. Due to the safety system, the resulting flood event can be judged to have been "minor" in comparison with what would most likely have happened without the artificial

tunnels. The event nevertheless affected the population and infrastructure, among others, by destroying the fresh-water intake system and cutting the fresh-water supply for the town of Carhuaz during one week (Schneider et al. 2014).

Figure 42: In Pampa Shonquil we can appreciated the material deposited from 2010 Lake 513's GLOF.

Even larger events cannot be excluded for the future. An early warning system was installed and is now being tested/calibrated. Extensive modeling exercises concerning the involved process chains were carried out in order to define hazard zones and escape possibilities. Installing a flood retention structure in the flat Pampa Shonquil could be a long-term option.

3.2 STUDY AREA: PALCACOCHA LAKE AND HUARAZ

Another example of evolving hazards related to new lakes is Lake Palcacocha. This lake was declared in an emergency state since its level is considered higher than the safe level (Diario la Republica 2010). The moraine dam is assumed to be able to fail abruptly releasing a huge volume of water from the lake and to create a flood wave and/or debris flow (Instituto Nacional de Defensa Civil 2011).

Lake Palcacocha is located at 9°23′ S, 77°22′ W at an elevation of 4,562 m in the Ancash Region of Peru and is part of the Quillcay watershed in the Cordillera Blanca (Figures 43 and 44). The lake has a maximum depth of 73 m and an average water surface elevation of 4562 m. The outlet of the lake flows into the Paria River, a tributary of the Quillcay River that passes through the City of Huaraz to the Santa River, the main river of the region.

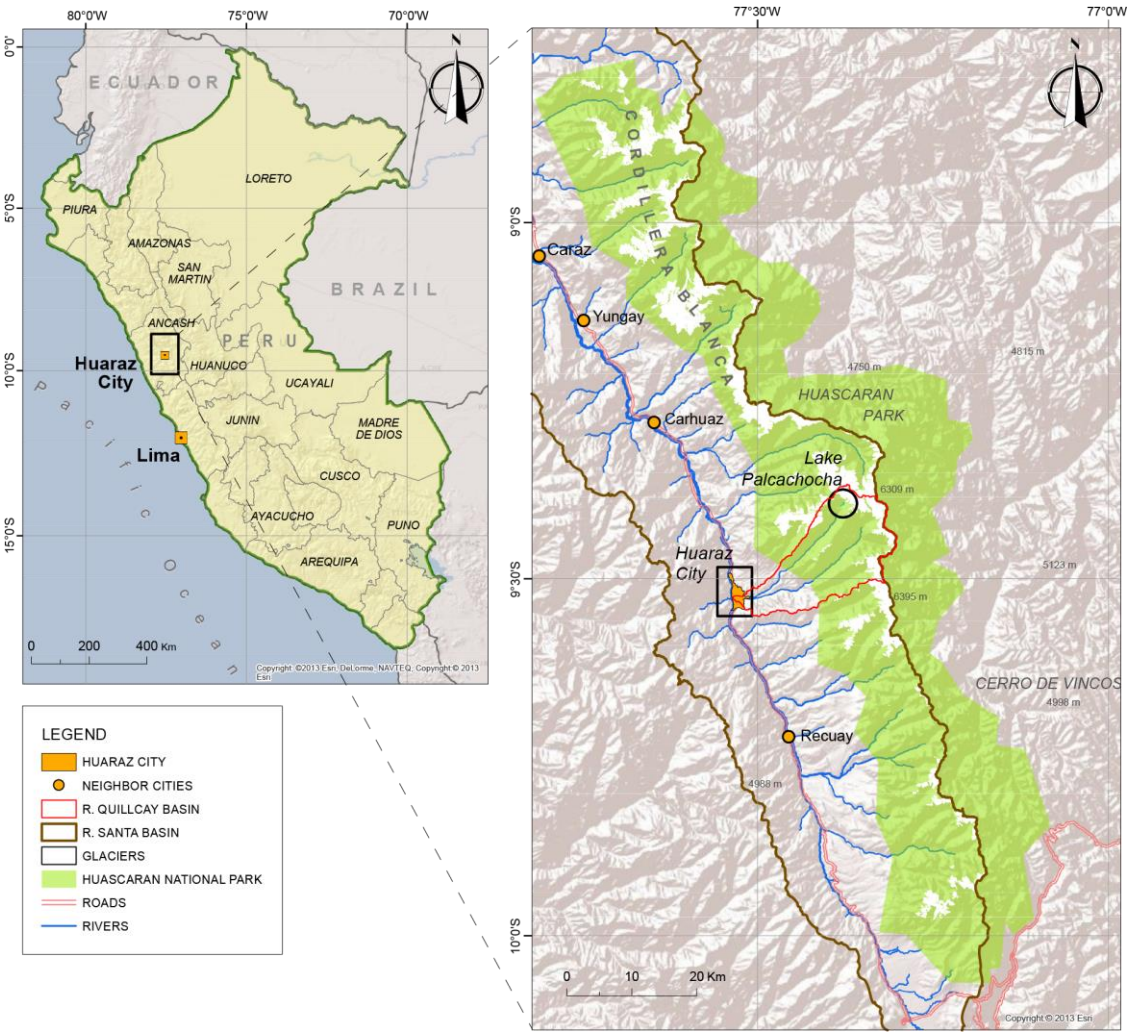

Figure 43: Map of the study area showing Lake Palcacocha and the city of Huaraz in the Quilcay watershed (From: Somos-Valenzuela et al. 2014a).

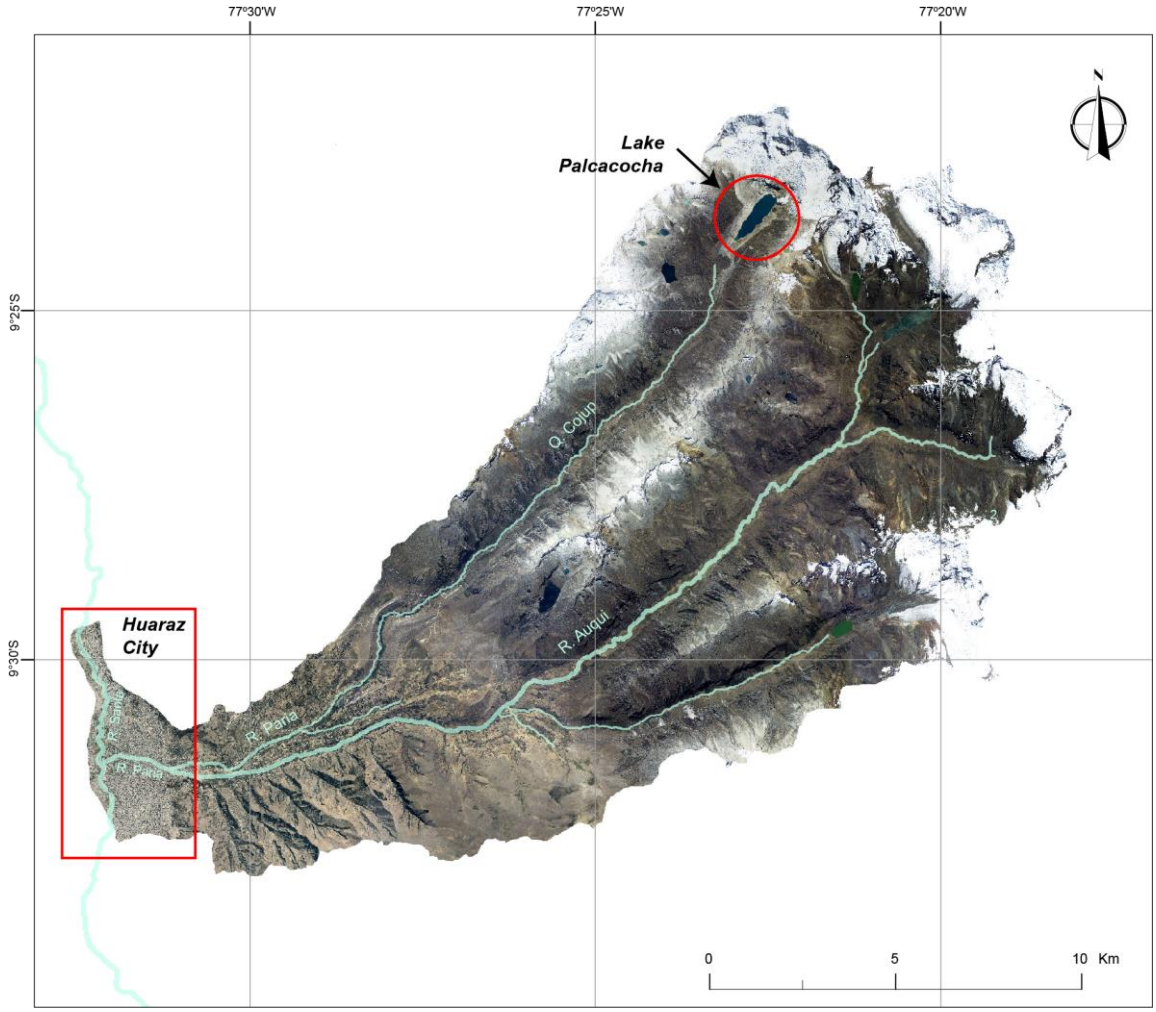

Figure 44: Aerial photograph of the Quilcay watershed showing Lake Palcacocha, the Paria River and the City of Huaraz (From: Somos-Valenzuela et al. 2014a). Data source: Horizons (2013)

3.3 JUSTIFICATION AND AIMS OF OUR WORK IN LAKE PALCACOCHA

Palcacocha Lake is of a special interest because the city of Huaraz, which is located at the bottom of the Quillcay sub-basin, was already devastated by a flood

released from Laguna Palcacocha on December 13, 1941 (Figure 45). In that opportunity, 4000-5000 people lost their lives (Vilimek et al. 2005, Carey, 2010) (Figure 46). Safety system were put in place in the early 70s; however due to the expansion of the lake the danger raises again to a level that the GLOF of 1941 could be repeated. Additionally the city has growth and the population exposed to this danger increased from 30 to 100 thousands from 1941 to 2007; therefore the life toll can be even higher in the current conditions.

Figure 45: Aerial photograph of the city of Huaraz taken 2 years after the GLOF event (Gov. Pro. Huaraz 2005)

Figure 46: Example of the impacts that the 1941 GLOF left in Huaraz. People killed by the GLOF were found 2-3 meters below the sediments. (Gov. Pro. Huaraz 2005)

According to the Report of Hazard 003-12/05/2011 from the National Institute of Civil Defense of Peru, in 1941 the Lake had an estimated pre-event volume of 10 to 12 million m^3 of water. In 1974, some structures were built in order to keep a safe (low) water level in the Lake (Figure 47). The volume in 1970 was 500,000 m^3 but with the retreating glacier tongue increased to about 17 million m^3 of water in 2011. Ice/rock avalanches from the steep surrounding slopes can now directly reach the lake (Haeberli et al. 2013).

a) b)

Figure 47: a) Hydraulic structures for draining water from Lake Palcacocha. b) Front view of the Lake in September 2004 showing the two artificial concrete dams (photo by Z. Patzelt 2004)

Hegglin and Huggel (2008) emphasized that a process chain of debris flows and hyper concentrated flow from Laguna Palcacocha already had a high probability of reaching the town of Huaraz with a Palcacocha Lake's volume of 3 million m^3 at the time of their study. Also in an evaluation of several lakes in Cordillera Blanca Emmer and Vilímek (2013) concluded that Palcacocha Lake represents the highest risk of outburst in Cordillera Blanca. Currently there are some actions toward reducing the level of the Lake using siphons. However a more definitive structure needs to be put in place, for example the relatively flat/stepped topography (long profile) of the Quebrada Cojup (Figure 48) offers possibilities to install retention structures at several points along the river. Such structures would/could protect the city of Huaraz from potential outbursts of Laguna Palcacocha as well as from other (smaller) lakes in the same catchment, although the most general solution in Peru is the reinforcement of the moraine dike and lowering of

the water level. Additionally there is one example of early warning system in Lake 513, which experience may be repeated at Palcacocha Lake.

Figure 48: Paria River canyon (Quebrada Cojup) looking downstream (Photo: Daene McKinney).

Consequently the aims of this work in Peru are to: simulate the inundation flood due to a moraine breach at Palcacocha Lake considering the uncertainty associated to the breaching process; estimate the number of people that may lost their life due to this event; and calculate the effectiveness in life loss reduction if an early warning system (EWS) were to be installed.

3.4 PALCACOCHA LAKE GLOF MODELING

3.4.1 Data and Methodology

3.4.1.1 Digital Elevation Model and Bathymetry Data

A 5m *x* 5m horizontal resolution digital elevation model (DEM) generated exclusively for this work was used (Horizons 2013) (Figure 49) using high-resolution Laser Imaging, Detection and Ranging (LIDAR) techniques, which provide vertical accuracies of up to 7 cm. A set of ten Ground Control Points (GCP), temporarily established to support the LIDAR flights, allowed control, calibration and adjustment of the LIDAR data, and orthocorrection of high-resolution aerial images. A drainage line dataset created by the Geographic-Military Institute of Peru was used to verify the DEM information and provide the streamline of the Paria River, which drains from Lake Palcacocha as well the Quillcay, and Rio Santa streamlines.

The Glaciology Unit and Water Resources of Peru's National Water Authority (UGRH) carried out a bathymetric survey of Lake Palcacocha in 2009 that was used to represent the elevation of the lake bottom in the DEM (Figure 50 and 51). At 2009 Lake Palcacocha hold a volume of 17.2 million cubic meters of water. The volume may have increase after 2009 since the lakes has expanded toward the glacier tongue; however there is not a more updated bathymetry. Therefore we don't include that probable increase volume in this work.

The distance from the moraine damming Lake Palcacocha to the Rio Santa is 22 km. However, besides the urban center of the City of Huaraz, other isolated

infrastructures are spread between the lake and the city, including small houses, a primary school, fish farms, and water supply facilities

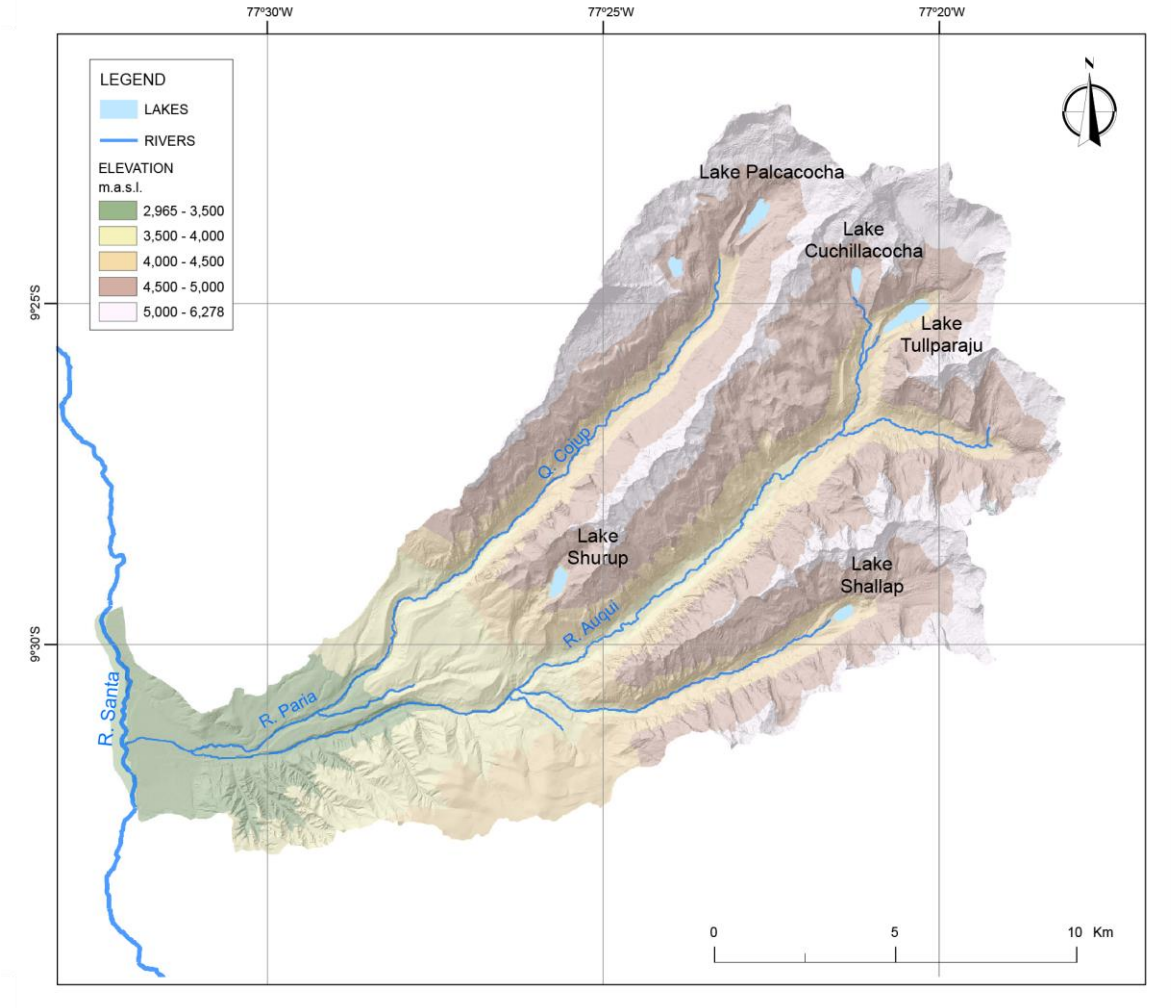

Figure 49: Digital Elevation Model (DEM) of Quillcay watershed (From Somos-Valenzuela et al. 2014a).

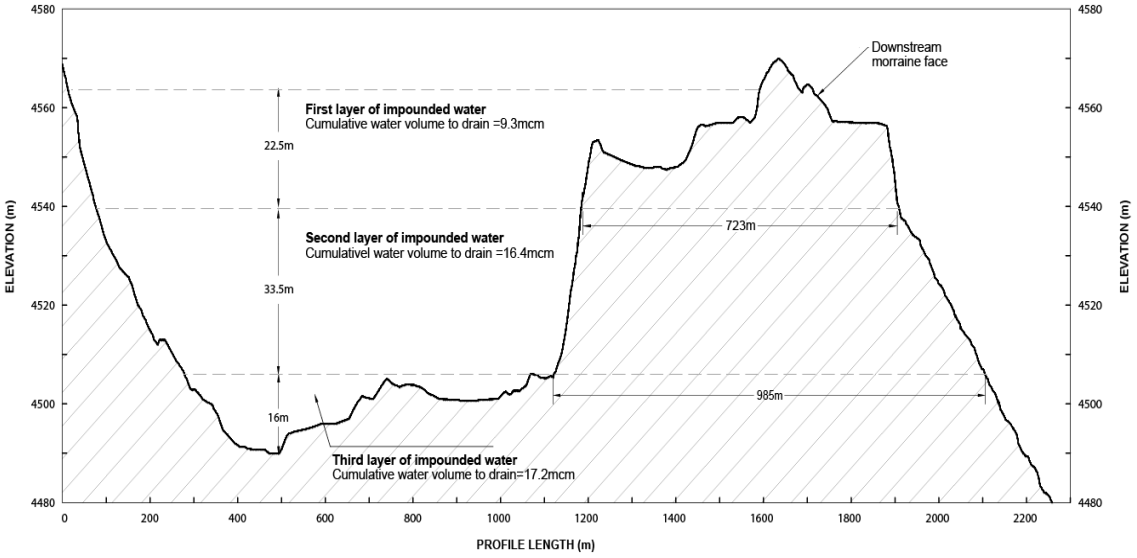

Figure 50: Partial longitudinal profile of Lake Palcacocha and the terminal moraine (Somos-Valenzuela et al. 2014a).

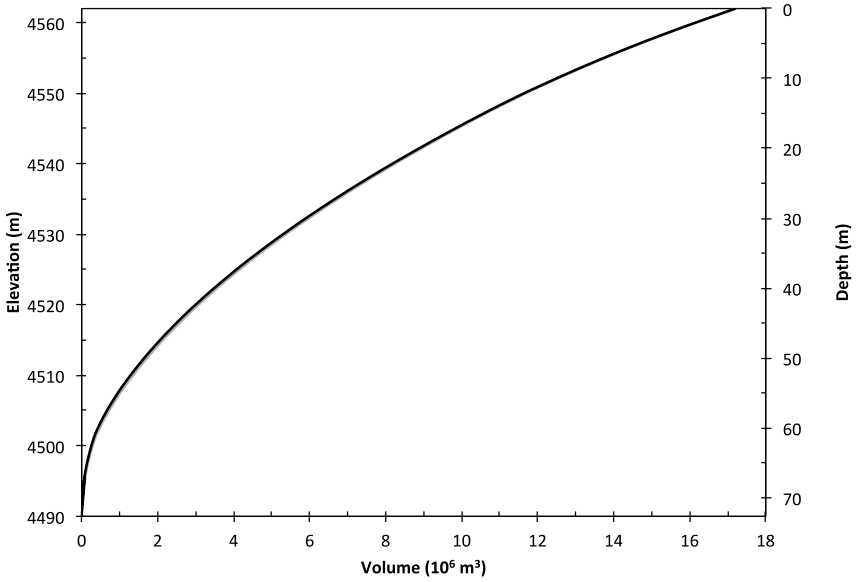

Figure 51: Palcacocha Lake volume vs depth curve. Volume is mainly concentrated above 4500 m (60 m depth measured from the surface) (Somos-Valenzuela et al. 2014a).

3.4.1.2 Roughness Coefficient Values

As we did at Imja Lake we use land cover map to assign manning roughness values. For this work we did not have access to a land cover map. As an alternative, automatic classification of vegetation indices (VIs) (Rouse et al. 1973) derived from spectral images was used. The VI is used to classify the different land cover classes present in the river basin and the elevation map is used to estimate cover texture, which is used to estimate roughness values. Roughness values can be assigned to different land covers either manually or automatically (Forzieri *et al*. 2011, 2010). We have used a combination of the two procedures mentioned above and the scheme developed by Hossain *et al.* (2009) (Hossain et al. 2009), which is an adaptation of Hamandawana *et al.* (2006). The procedure calculates the normalized differential vegetation index (NDVI) from a multispectral image; then, an Iterative Self-Organizing Data Analysis Technique (ISODATA) is used to determine the number of classes into which the pixels in an image can be classified (Ball and Hall 1965). Finally, sliding representation is used to assign roughness coefficient values to the classes.

Landsat 7 Band 3 (near infrared 0.77-0.90 μm) and Band 4 (red 0.63-0.69 μm) from an October 22, 2013 image (WRS_PATH 8, WRS_ROW 67)[2] were used to calculate NDVI values to assess the presence of live green vegetation (Rouse *et al*. 1973).

$$NDVI = \frac{(Band_4 - Band_3)}{(Band_4 + Band_3)} \tag{6}$$

[2] U.S. Geological Survey–EROS Data Center, http://landsat.usgs.gov/

NDVI values range from -1 to 1, and higher values indicate the presence of more live green vegetation. The raw digital number (DN) from the image was adjusted by converting it to irradiance for both bands and then to reflectance (Chander and Markham 2003; Chander et al. 2009). The adjustments produce more consistent NDVI values since they consider sun elevation, acquisition date, and gain/bias settings of the sensors for each band.

The ISODATA scheme (Ball and Hall 1965) minimizes the variability within clusters and categorizes pixels into a number of classes based on minimizing the sum of squared distances between each pixel and its assigned cluster center, equivalent to minimizing the Mean Squared Error (MSE) (Hossain *et al.* 2009)

$$MSE = \frac{\sum_{\forall x}[x - C(x)]^2}{(N-c)b} \tag{7}$$

Where $C(x)$ is the mean of the cluster that contains pixel x, N is the number of pixels, c is the number of clusters, and b is the number of spectral bands. Finally, density sliding was implemented based on the threshold values generated using the NDVI raster.

We inspected Paria River from Lake Palcacocha to the Rio Santa in June-July 2013, and we have combined our field observations with the automatic classification results. Although there are a considerable number of land cover types, we use 5 main classes that are most representative of the system. In addition, the variation of the roughness coefficient values for the different land cover types present in the area, based in our observations, is minimal. Table 26 shows the roughness coefficient values assigned according to the land cover observed in the field.

Table 28: Roughness Coefficient Values for the Paria River (FLO-2D, 2012)

Class Type	Class Description	Min.	Max
Urban	Uneven concrete, street with holes as well as different features increasing the roughness of the concrete.	0.10	0.15
Bare Soil	Earth, Rock, Gravel	0.05	0.013
Cultivated Areas or grass	No Crop or short grass	0.06	0.22
Tree	Cleared land with tree stumps, no sprouts	0.30	0.40
Natural Streams	Mountains Streams, no vegetation in channel, banks usually steep, trees and brush along banks submerged at high stages. Bottom: Cobbles with large boulders	0.04	0.07

3.4.1.3 Hydrograph Calculation

Trigger effects leading to avalanches include earthquakes, snowmelt, heat waves, and heavy precipitation (Huggel et al. 2010; Haeberli 2013). (Emmer and Vilímek 2013; Emmer and Vilímek 2014) and Haeberli *et al.* (2010) recommend that the evaluation of hazards posed by glacial lakes be based on systematic and scientific analysis of lake types, moraine dam characteristics, outburst mechanisms, down-valley processes and possible cascades of processes. In addition, changes in climate patterns are likely to increase the frequency of avalanches as a consequence of reduced stability of permafrost, bedrock and steep glaciers in the Cordillera Blanca (Fischer *et al.* 2012).

For the calculation of the hydrograph at the lake we are going to consider two processes. The first one is the instantaneous wave that an ice rock avalanche could

produce overtopping and eroding the moraine complex. The avalanche and the wave calculations are not part of this work; however is necessary to include the overtopping hydrograph at the moraine complex calculated as a consequence of an avalanche falling into the lake in order to consider its effects in the risk analysis that we are performing here (Figure 52). That work belongs and is explained in details in Somos-Valenzuela et al. (2014a).

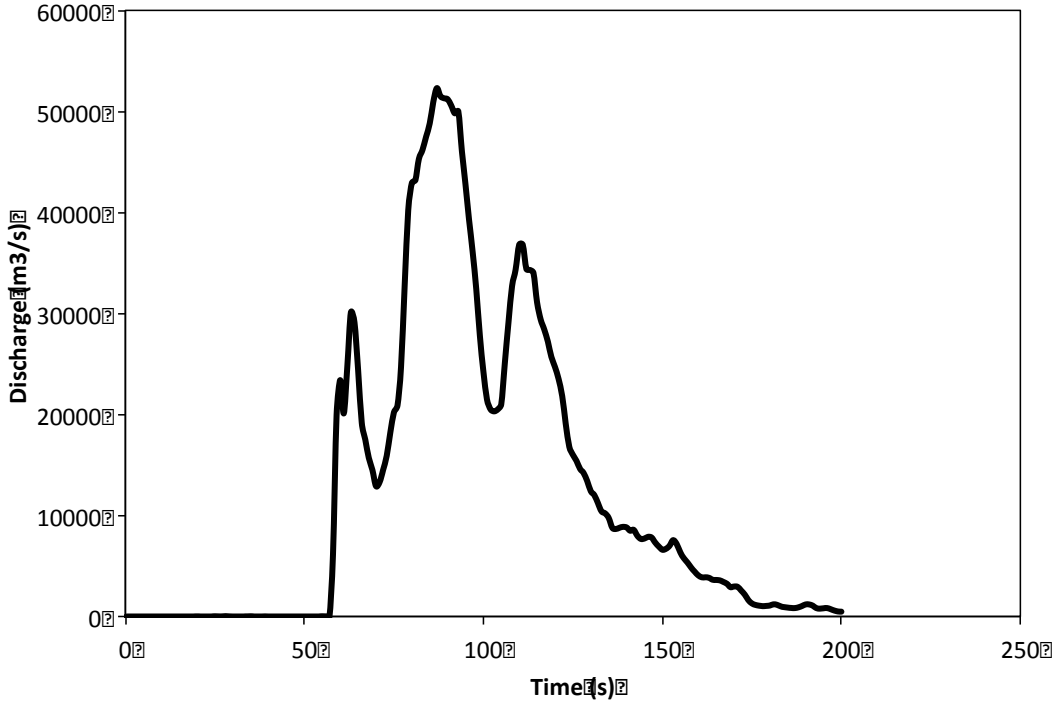

Figure 52: Hydrograph of discharge at the lake outlet due to wave overtopping for the large avalanche scenario (Somos-Valenzuela et al. 2014a)

For the moraine breaching process at Palcacocha Lake we are going to use the same process described in Imja Lake work. The relevant moraine characteristics for a potential Palcacocha Lake GLOF simulation calculation are given in Table 29.

Table 29: Moraine Characteristics used in Palcacocha GLOF Simulation.

Description	Lake Conditions
Moraine Height (h_d, m)	56
Breach height (h_b, m)	56
Water height (h_w, m)	48
GLOF Volume (V_w, m^3)	$16.9x10^{06}$

Similarly, as it was done with Imja Lake simulations, we are using empirical equations to calculate the peak discharge during the moraine breach process, for the calculation of the breaching time and the breach average width estimation. Similarly, Froehlich equations provide the lowest uncertainty in the calculation and offer a simple method to estimate breach parameter at Palcacocha Lake (Rivas et al. 2014). For more details of the moraine, breach calculation refers to section 3.4.1.4 Breach Model at Imja Lake.

For this work we are evaluating the worse scenario, which means that given the fact that there is not study of the moraine composition we assume that beneath the outlet the material is similar to the moraine core exposed by the GLOF in 1941 (Figure 46). The expose wall has low cohesion materials and it is easily erodible. Consequently the breach cut can go as depth as the bottom of the lake (56 m), see Figure 53.

Figure 53: Lake Palcacocha moraine showing the breach cut left by the 1941 GLOF event (by Daene McKinney)

3.4.1.4 Inundation Simulation

FLO-2D is also used to calculate the flooding downstream of Lake Palcacocha. The same assumptions than the ones at Imja Lake were used here; therefore, for more details refer to Section 2.7.1.4 and Appendix A.

3.4.2 Palcacocha Lake GLOF modeling results

3.4.2.1 Roughness Coefficient Values

Figure 54 shows the NDVI values resulting from the combination of Band 3 and Band 4 from the Landsat 7 image after the reflection correction according to the procedure described. For the higher NDVI values, more intense vegetation is present. Along the Quebrada Cojup we can see the presence of more green vegetation, which is corroborated from the field observations, there is considerable vegetation along the banks of the Quebrada. The opposite happens in areas with low values of NDVI such the city (bottom left of Figure 54) in which the percent green area decreases considerably.

The results from the classification are presented in Table 30 and Figure 55.

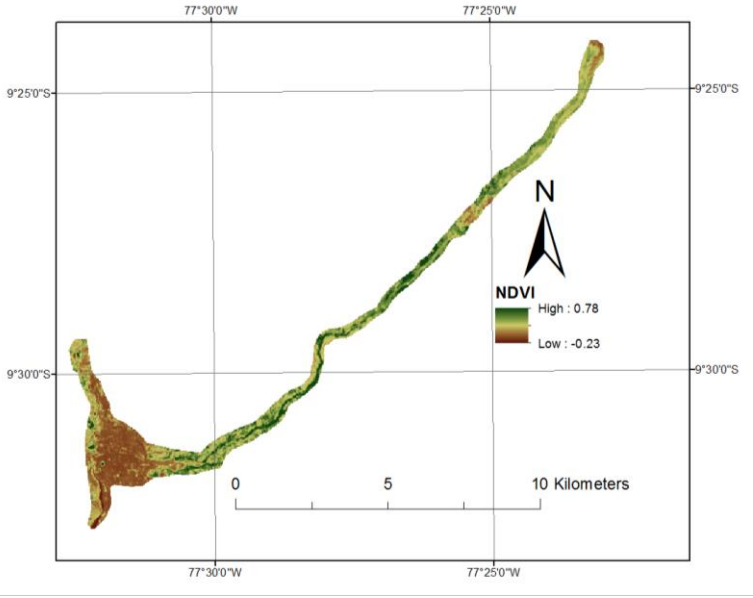

Figure 54: NDVI results using reflection corrected Landsat 7 image values. The second step was to run the ISODATA non-supervised classification in GIS using the NDVI raster data with a sample interval of 1 to include all the cells available.

Table 30: Results from the NDVI non-supervised ISODATA classification in 5 classes with a sample interval of 1.

Class ID	Mean NDVI Values	Covariance	Number of Cells
1	0.07138	0.00118	5021
2	0.19910	0.00119	3413
3	0.31165	0.00100	4286
4	0.41787	0.00134	3992
5	0.57879	0.00367	1636

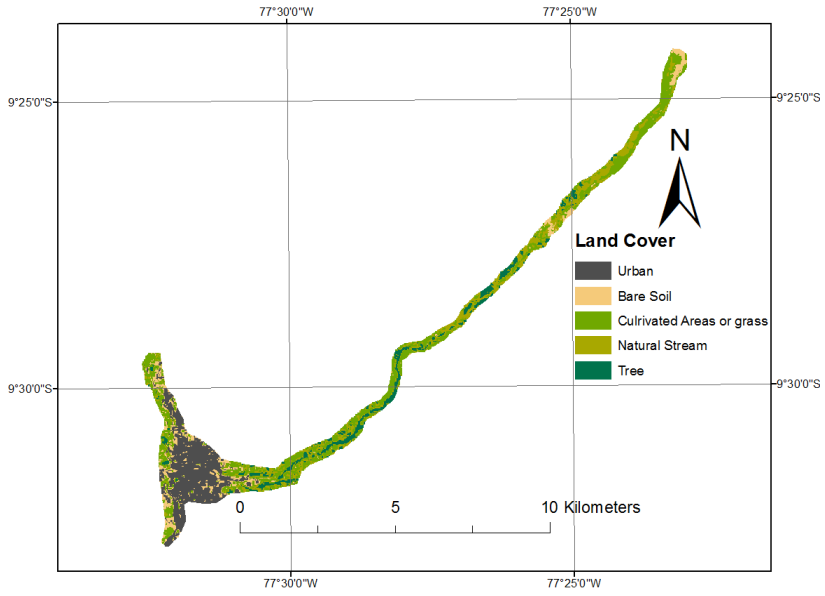

Figure 55: Land Cover according to the ISODATA classification.

Finally, using the ISODATA raster, we assigned the maximum, minimum manning value from Table 28.

3.4.2.2 Hydrograph Calculation

Due to the absence of actual GLOF data for Palcacocha Lake, empirical equations were used to compute the breaching parameters from a breach, imitating the work we did at Imja Lake. Table 29 shows the results of using the Froehlich equations and the moraine characteristics in Table 27 to calculate the predicted breaching parameters (breach width, failure time and peak discharge) from Eqs. (1) – (3).

Table 31: Breach Width, Failure Time and Peak Flow Values and Uncertainty Ranges Predicted by Froehlich's Equations for Palcacocha Lake conditions.

Scenario	**Breach Width (m)**	**Failure Time (hr)**	**Peak Discharge (m^3/s)**
Lower	30.8	0.2	5250
Predicted	**77.3**	**0.53**	**10003**
Upper	185.5	3.8	22917

Discharge hydrographs from Lake Palcacocha were generated for the breaching of the moraine using Hec-RAS. Figure 56 shows the outflow hydrographs corresponding to the peaks predicted using Froehlich equations, the error in the peak flow calculated in Hec-RAS is less than 1%. In Figure 56 we also include the overtopping wave due to an avalanche, which may trigger the moraine breaching process (Somos-Valenzuela et al. 2014a)

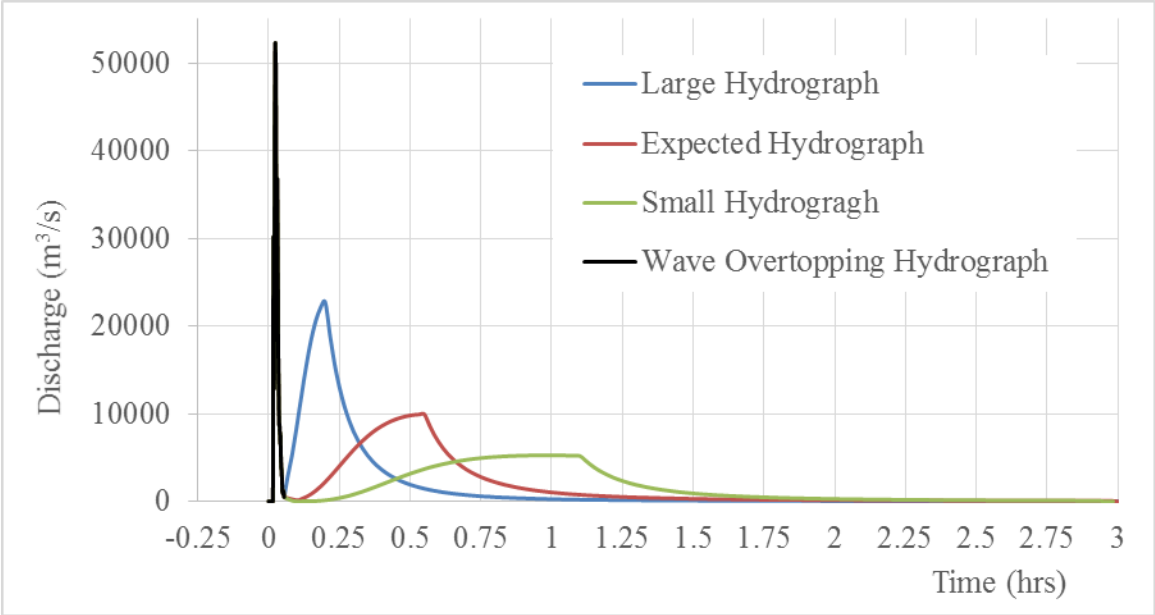

Figure 56: Potential outflow hydrographs from Lake Palcacocha due to a moraine breach scenarios combined with the wave overtopping hydrograph.

3.4.2.3 Inundation Simulation

Figure 57 shows the locations of the five cross-sections downstream of Lake Palcacocha where flood hydrographs from the Flo-2D simulations are reported. Table 32 provides details of the locations of the cross-sections. Table 33 provides details of the results at the cross-sections. At cross-section 1 the hydrograph is still similar to the original hydrograph at the lake with the overtopping-wave hydrograph preceding the moraine erosion hydrograph. The hydrograph at cross-section 2, located just upstream of the point where the Paria River canyon (Quebrada Cojup) narrows and becomes steeper, shows that the flow from the moraine erosion and lake discharge catches up to the overtopping flood wave; at this point the volumes from the two events mix and continue downstream as one event. This is expected because the river is relatively wide with gentle

slopes between the lake and the second cross-section, and in this reach the maximum velocity is only 2-4 m/s. Sediments eroded from the moraine would be deposited in this section before the flood continues downstream. Cross-section 3 is located at the entrance to the Huascaran National Park where the large moraines will supply sediment to the inundation starting at this point. In addition, villages start appearing below this point increasing people's exposure to the GLOF. Cross-section 4 is located at the entrance to the city. The biggest changes in slope occur between cross-sections 3 and 4, when the flow accelerates; as a consequence the flow is able to scour the large lateral moraines in this reach adding to the volume of sediments in the flood. The hydrograph at cross-section 5 shows the peak discharge in the Rio Santa exiting the city. The peak has attenuated considerably at this point.

The peak flow arrives at this cross-section after about 0.28, 1.3, 1.6 hours for the upper, expected and lower breach events, respectively. The peak flow takes about 30 minutes to cross the city.

Table 32: Location of Flood Hydrograph Cross-sections Downstream of Lake Palcacocha

Section	Latitude (deg)	Longitude (deg)	Elevation (m)	Distance to Lake Outlet (m)
1	-9.4200	-77.3900	4,313	1,912
2	-9.4605	-77.4292	4,052	8,319
3	-9.4831	-77.4516	3,774	11,886
4	-9.5264	-77.5040	3,165	20,177
5	-9.5039	-77.5373	2,965	26,517

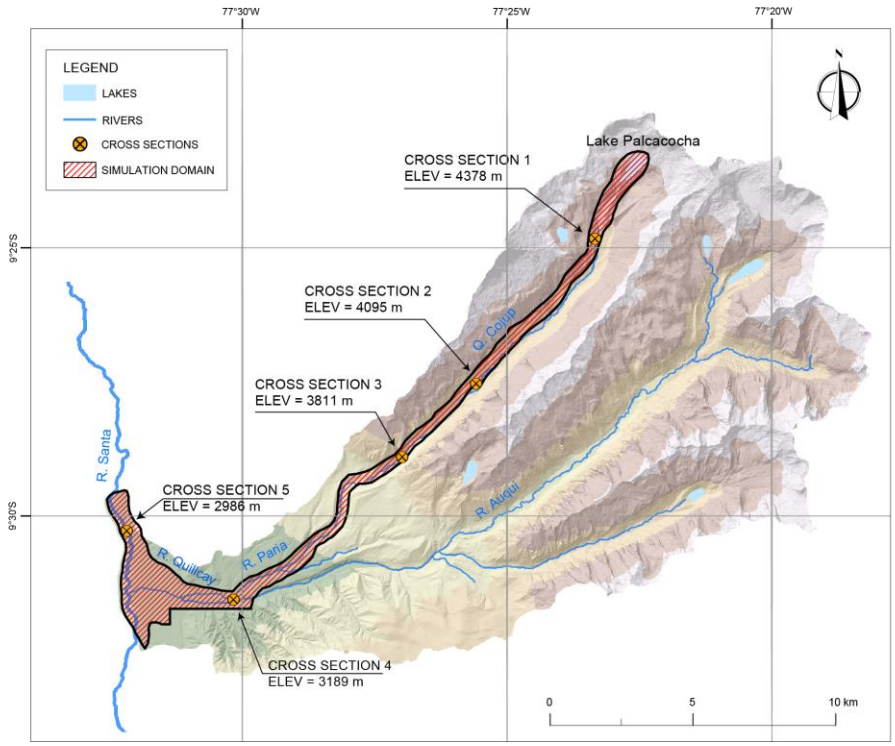

Figure 57: Cross-sections (XS) for FLO-2D Simulation Results (Somos-Valenzuela et al. 2014a).

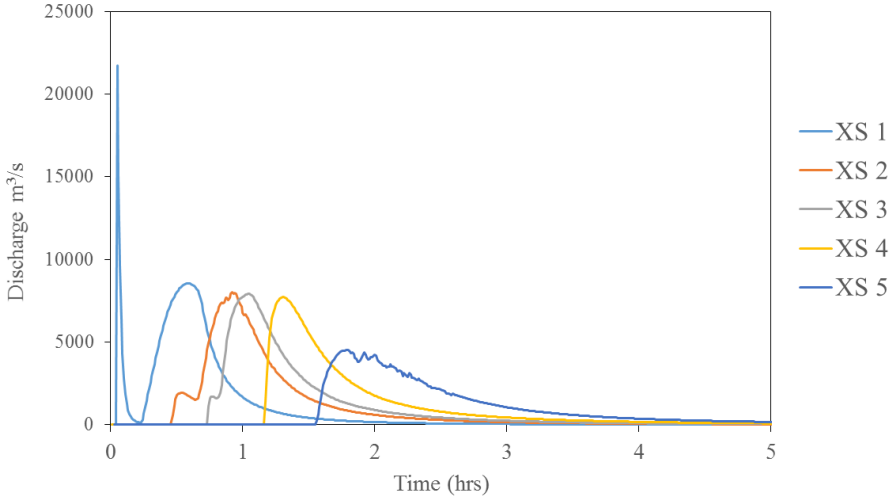

Figure 58: Hydrographs at the cross-sections for the Lake hydrograph that matches the expected peak.

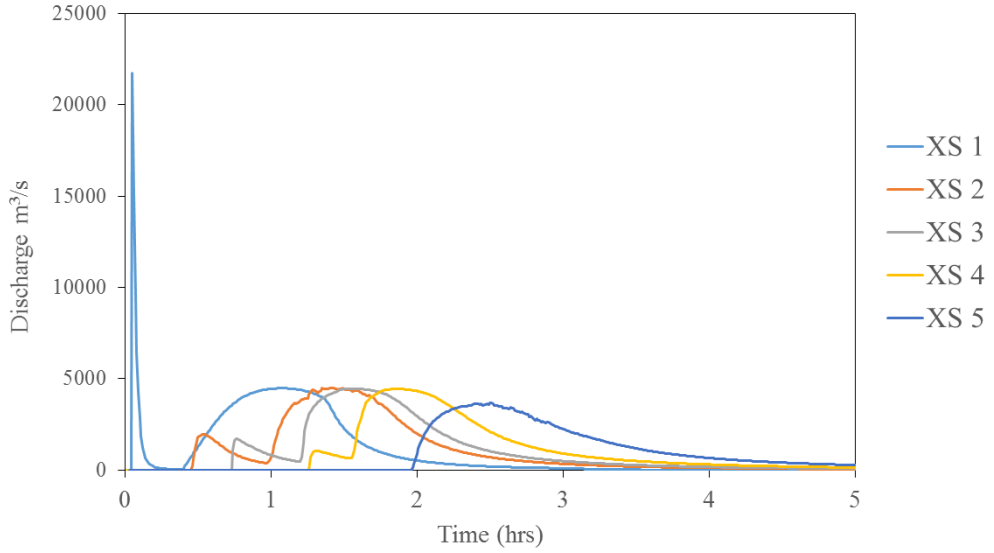

Figure 59: Hydrographs at cross-sections for the hydrograph matching the lower peak.

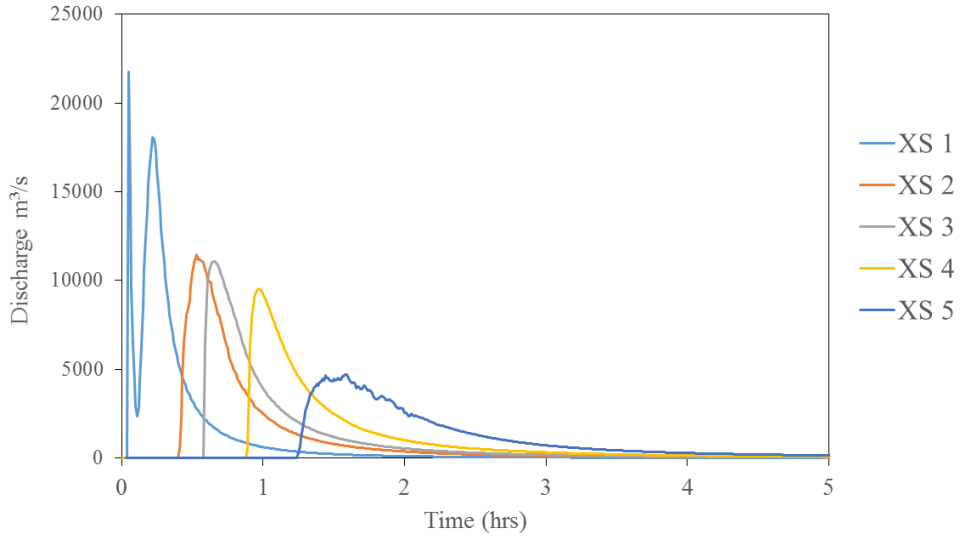

Figure 60: Hydrographs at cross-sections for the hydrograph matching the upper peak.

Table 33: Flo-2D Simulation results at cross-sections downstream Lake Palcacocha.

Cross Section	Scenario	Arrival Time (hr)	Peak Time (hr)	Peak Discharge (m^3/s)
XS 1	Overtopping wave	0.05	0.05	21,730
XS 1	Upper	0.11	0.24	17,357
	Expected	0.26	0.62	8,474
	Lower	0.43	1.11	4,463
XS 2	Upper	0.42	0.56	11,130
	Expected	0.47	0.9	7,674
	Lower	0.49	1.43	4203
XS 3	Upper	0.62	0.68	10,856
	Expected	0.74	1.09	7,599
	Lower	0.77	1.55	4,443
XS 4	Upper	0.91	1	9,238
	Expected	1.21	1.33	7,628
	Lower	1.31	1.86	4,432
XS 5	Upper	1.24	1.61	4434
	Expected	1.55	1.88	4406
	Lower	1.96	2.53	3540

3.4.2.4 Inundation in Huaraz

The resulting maximum flood depths within Huaraz for the expected, lower and upper scenarios are shown in Figure 61 from left to right respectively. The deepest areas are near the existing channels of the Quillcay River and the Rio Santa. The highest inundation depths occur at the south side of the river, where most of the commerce is located in Huaraz. Considering the expected scenario, within the city, the area where the depths are small (<1 m) is limited to 0.13 km^2 in a narrow band ranging from 20 to 60

meters in width along the outskirts of the flooded area. The area flooded to a depth between 0.2-1 m covers an area of 0.51 km^2, and the area flooded to depths greater than 1 m covers an area of 4.5 km^2. The area near the channel of the Quillcay River shows depths of 5-10 m in a band approximately 350 m wide in the east side of the city and up to 500 m wide in the west side of the city near the Santa River. In comparing the three events, one can see that areas that had inundation depths of 1-2 m in the upper scenario have depths of 0.2-1 m in a small event, and a mixed of values from 0.2 -1 and 1-2 in the expected scenario.

The maximum velocities within the city are shown in Figures 62 for the expected, lower and upper scenarios from left to right respectively. Similar to the inundation depths, the maximum velocities occur along the channels of the Quillcay River and the Rio Santa. Considering the expected scenario, within the city, velocities in excess of 5 m/s occur only in the narrow river channel in the canyon and in small isolated areas in the city. Velocities between 2-5 m/s occur in the areas where the inundation depths are between 2-5 m. In the outer area velocities of 0–2 m/s occur in areas with depths lower than 2 m. Velocity reductions or increases for the lower or upper scenarios, compared to the expected scenario, follow the same pattern as the inundation depths discussed above. Additionally as it is expected the shortest travel time corresponds to the largest scenario reaching the Santa River in less than 1 hour and 15 minutes. In the expected scenario the inundation reaches the Santa River between 1 hour and 30 minutes and 1 hours and 45 minutes. Finally in the lower scenario the inundation reaches the Santa River after 2 hours (Figure 63).

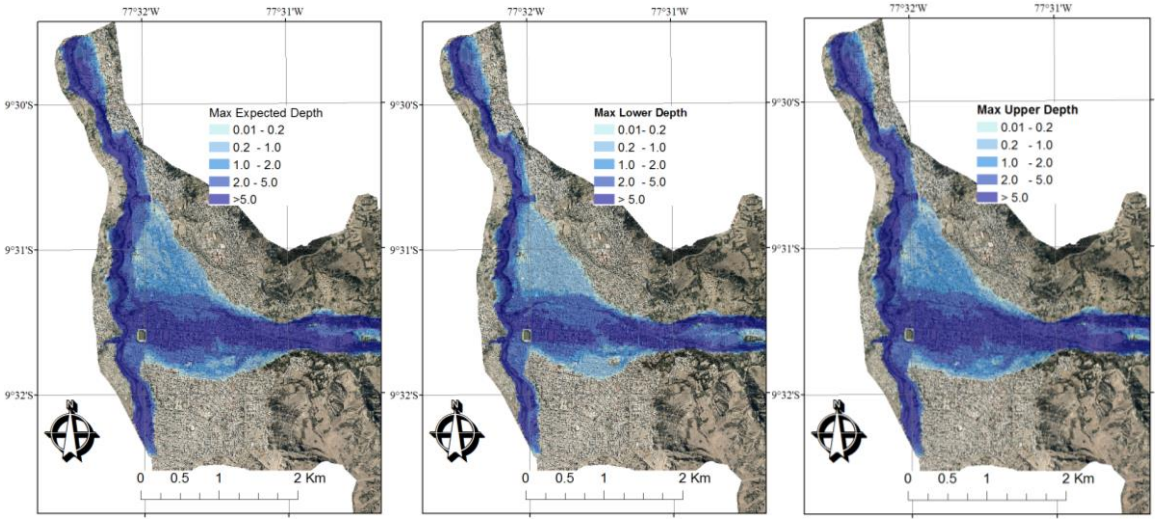

Figure 61: Peak depth in meters for the three scenarios (expected, lower, upper).

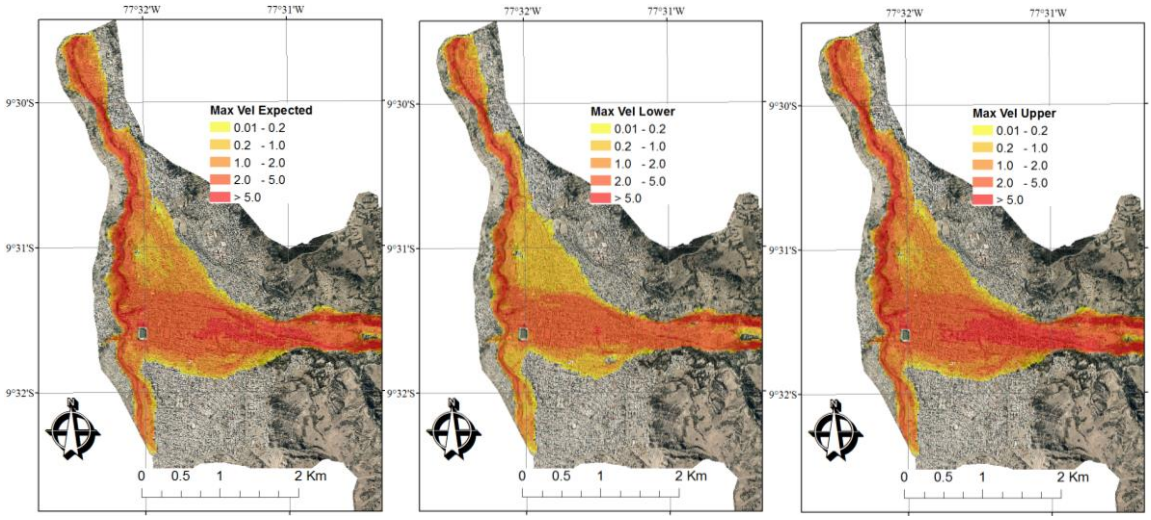

Figure 62: Peak velocity for the three scenarios (expected, lower, upper) in meter per seconds

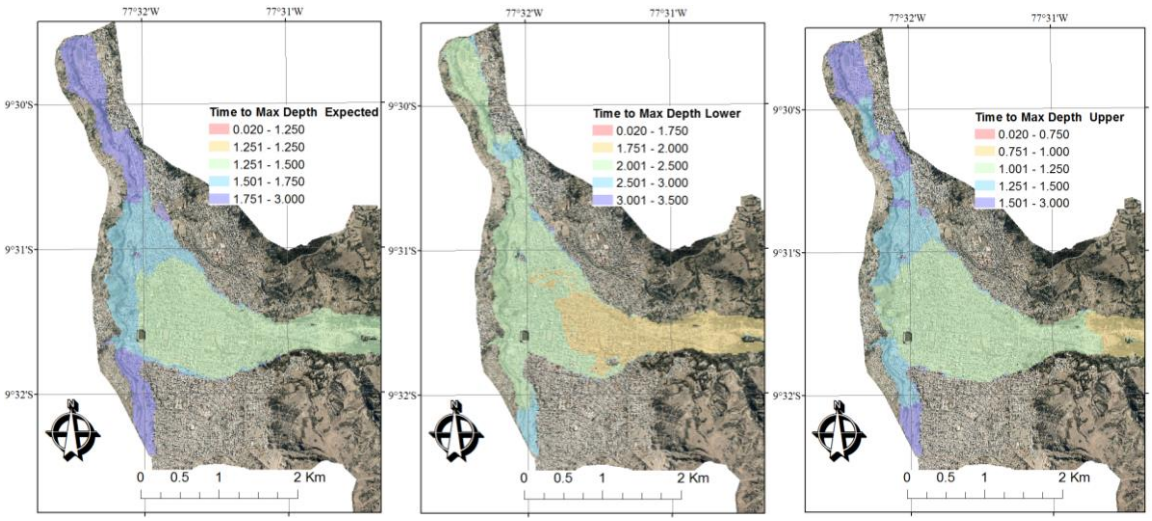

Figure 63: Time in hours that the peak flow takes to reach the inundation area for the three scenarios (expected, lower, upper)

3.4.3 Inundation model sensitivity analysis

A sensitivity analysis for the inundation was made for the roughness coefficient and the sediment concentration. Starting from the sediment concentration we simulated 5 scenarios with concentration by volume of 0, 20, 30, 40 and 50 % in order to know the effects that the sediments concentration has in the velocity and the elevation of the flood. The water discharge hydrograph for cross sections 4 and 5, before and at the city, were plot in Figures 64 and 65. The arrival time and the peak time differences are lower than 30 minutes, which is half of the difference between the arrival time for the lower and upper scenario from the moraine breach uncertainty calculation (see Table 33). Since the inundation travel times are very similar for all the concentration, it was expected that the inundation were deeper in the scenario with a concentration of 50% since the flow volume was double than the scenario with no sediments (Figure 66 and 67). This

difference can clearly be seen in cross section 4 where the inundation depth is more affected by the river that is narrowest at that point compared to cross section 5 where the river is less narrow, and step and the inundation can spread through the city. For this work are more important the results at the city, since there it is where we are focusing our risk analysis. Cross section 5 is more representative of the city topography. At XS 5, the inundation with CV of 50% is 6 meters deeper than the inundation with no sediments and 3 meters deeper than the inundation with 30 %. The inundation that considers 30 % of concentration by volume is a good lower limit for the sediment concentration by volume (FLO-2D 2012).

Additionally the higher concentration, which was considered in the final results, provides a good upper limit for the risk calculation.

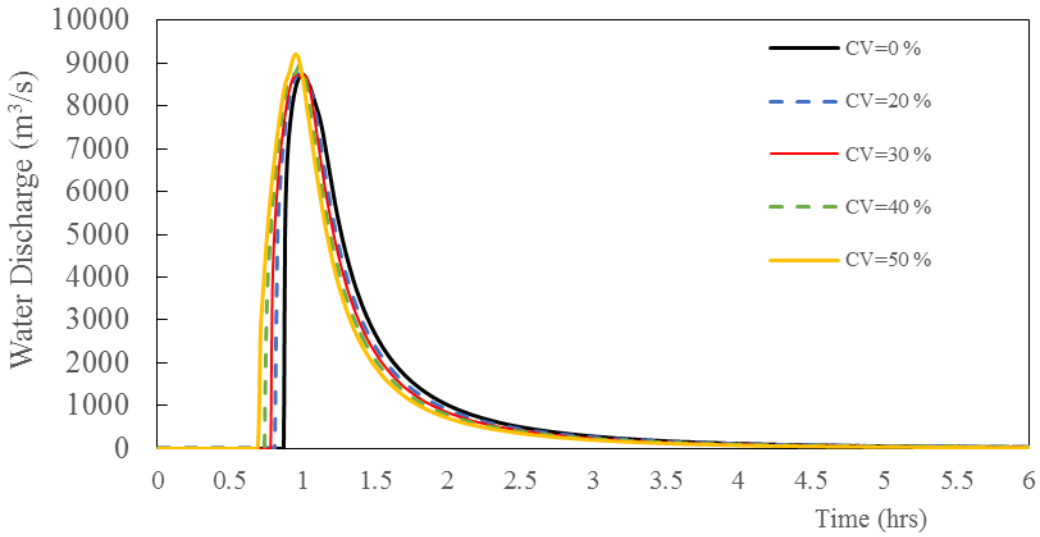

Figure 64: Hydrograph at XS4 for different sediment concentration by volume %

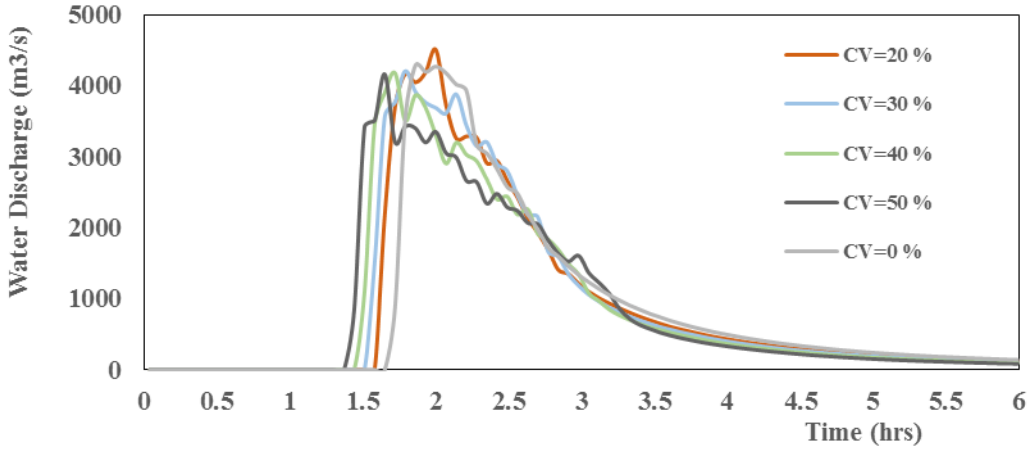

Figure 65: Hydrograph at XS5 for different sediment concentration by volume %

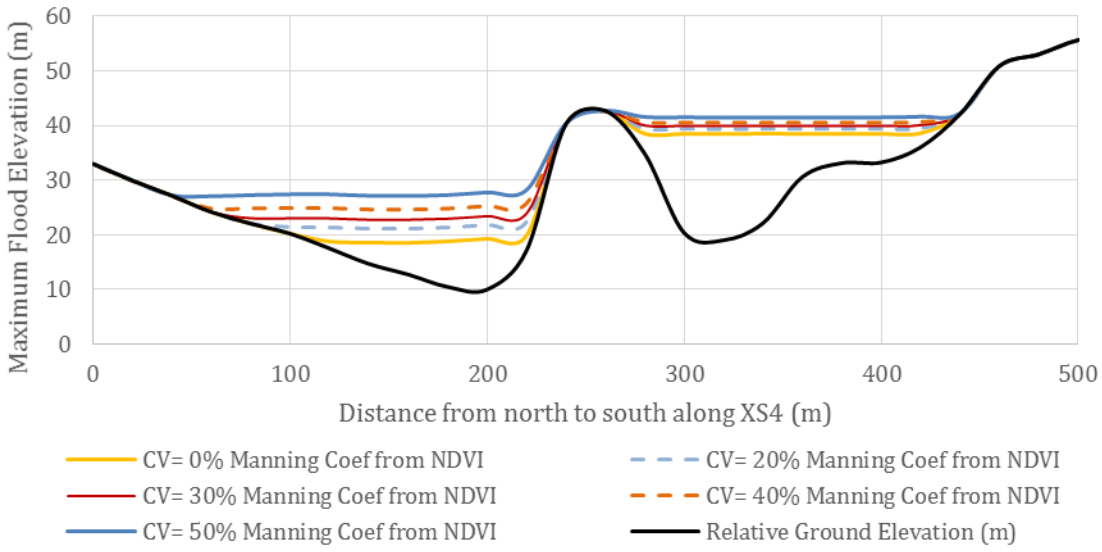

Figure 66: Cross section 4 showing the elevation stage for different % of sediment concentration.

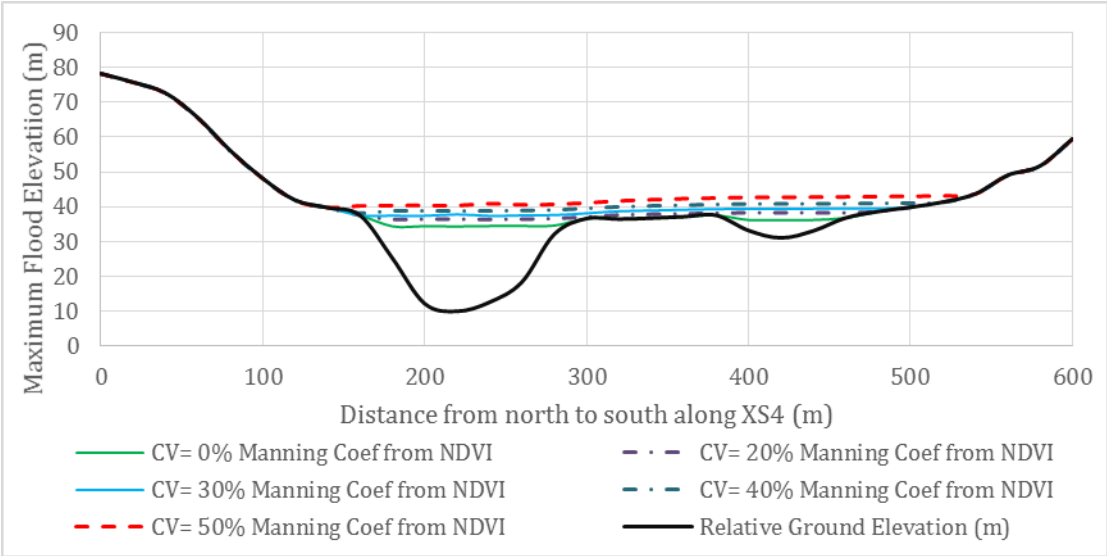

Figure 67: Cross section 4 showing the elevation stage for different % of sediment concentration.

For the Manning roughness coefficient we assumed that all the cells in the model have a constant value of 0.10, 0.20, 0.30 or 0.40. As the roughness coefficient increases the bed exerts a bigger opposition to the inundation slowing down the inundation (Figure 68, 69). However, the differences in travel time are within the results obtained from the uncertainty in the hydrograph discharge calculations. On the other hand, the inundated areas do not change considerably especially in cross section 5 which is located before the inundation leaves the city (Figure 70, 71)

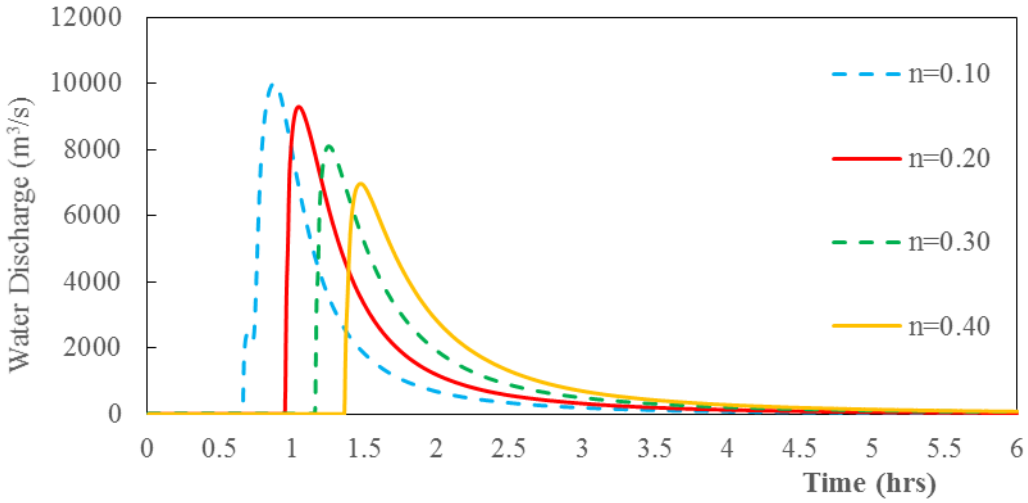

Figure 68: Hydrograph at XS4 for different manning roughness coefficients

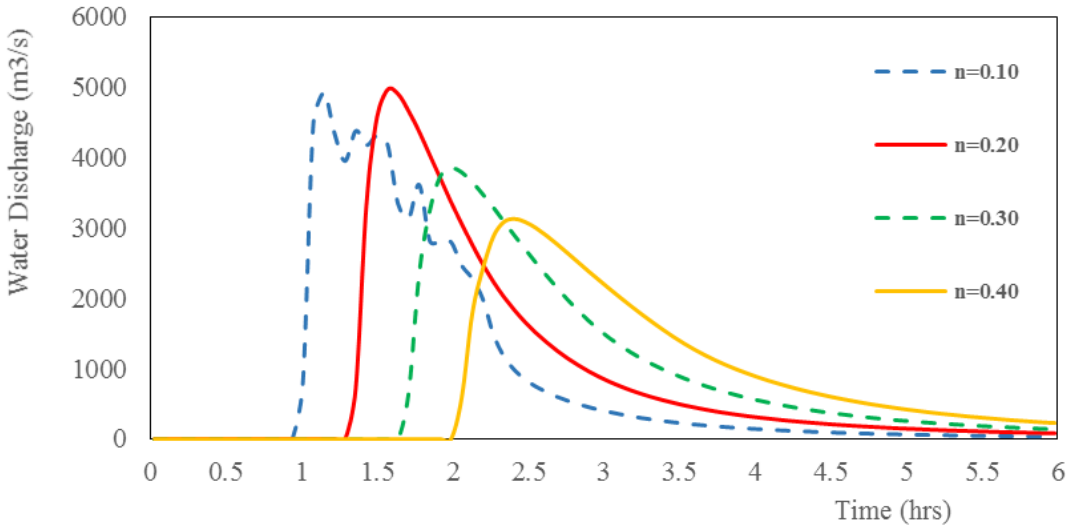

Figure 69: Hydrograph at XS5 for different manning roughness coefficients

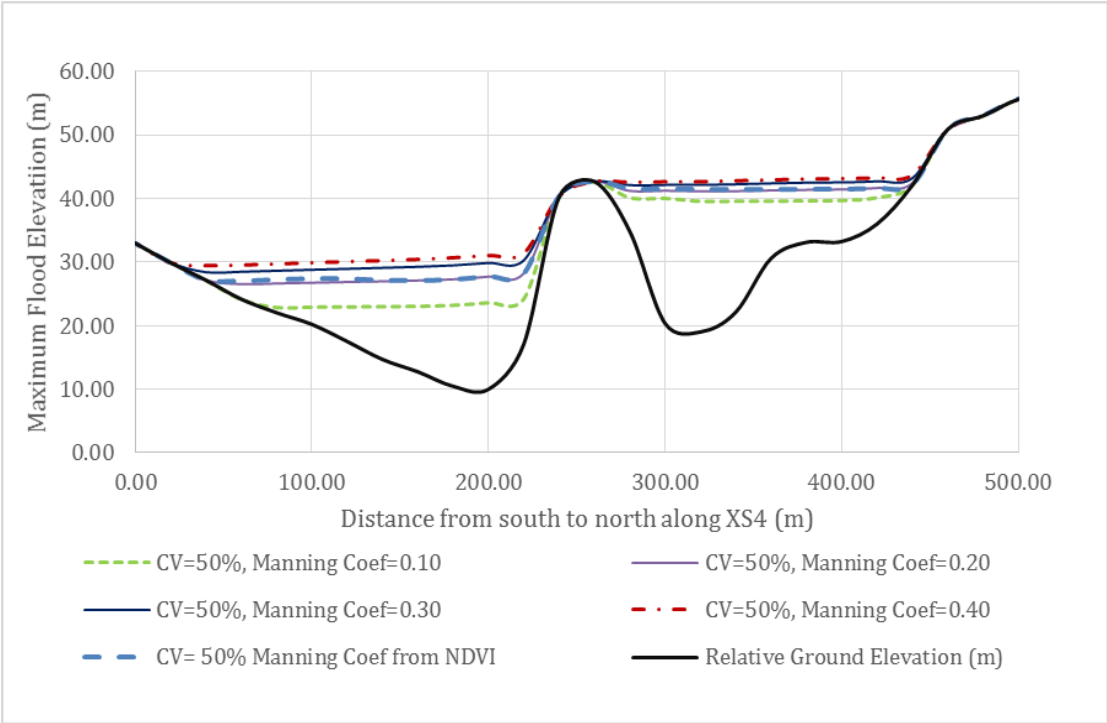

Figure 70: XS 4 showing the elevation stage for manning roughness coefficients.

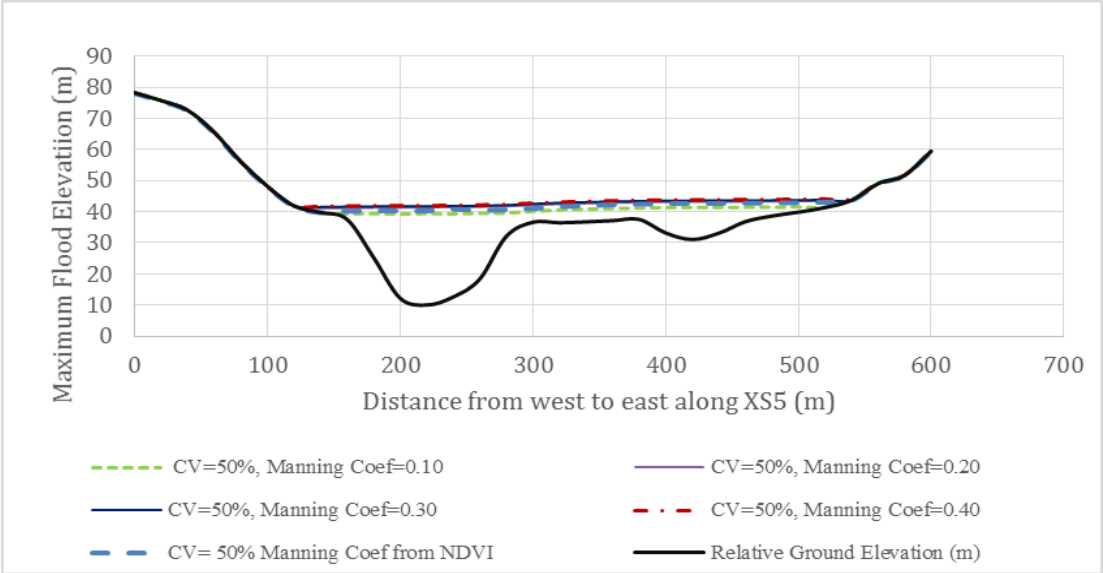

Figure 71: Cross section 5 showing the elevation stage for manning roughness coefficients.

Although the inundation is sensitive to the concentration by volume by changing the area inundated and to the changes in manning roughness coefficient by changing the travel time, these variations are lower than the variations related to the uncertainty in the hydrograph generation. These results agree with the literature that indicates that the main drivers for this type of inundation are the time that it takes for the breach to form and the water volume release from the lake.

By comparing the simulations report in Table 33 with the simulations for different roughness coefficient it is possible to see that a coefficient lower than 0.20 could affect our results giving a shorter time for the inundation to reach the city. However, if we check the type of land cover present in the area studied, we can see that the roughness coefficient should be above 0.20. Additionally as it was mention a lower limit for the concentration by volume should be in the order of 30% and a maximum and safe limit of 50%, which was used in our work. Finally, we concluded that for this work we are using a realistic upper limit which is the scenario recommended for the problem analyze.

3.5 RISK ANALYSIS

Risk has two domains; one is related with the probability of occurrence of an event and a second domain related with the ability to produce harm to the environment affected by an event (Cutter 1996; Cutter et al. 2003).

Lack of data available related to avalanche frequency that can trigger a GLOF at Lake Palcacocha makes difficult or impossible, to come out with consistent probability of occurrence of a GLOF. This situation was pointed out by Schneider et al. (2014) in their risk analysis at Lake 513. Additionally, in this work it is assumed that a wave generated

by an avalanche falling into the lake will overtop the moraine initiating an erosive process that would lead the moraine collapse and initiate a GLOF. But then again, there is not enough information that allows calculating the probability of moraine breaching given that an avalanche occurs. Therefore, this work will assume that there is an avalanche that will trigger a chain of processes in which the moraine will breach generating a GLOF, ignoring the first component of the risk due to the lack of data and understanding of the processes involved.

Consequently, this work is going to be center in the second component of the risk associated to a GLOF in Huaraz. Although incomplete it allows analyzing how the city would be affected by a GLOF, allowing generating results that inform decision makers and the population of the potential impacts of a GLOF event.

Recalling the definition of risk given at the beginning of this section, the second component of risk is the ability that an event has to produce harm, which is related to the vulnerability. Vulnerability is used in risk, hazards and disasters and lately in environmental and development studies The term vulnerability is related with potential loss (Cutter 1996).. The term Vulnerability means different things to different people depending on the research orientation and perspective (Cutter et al. 2003). O'Brien *et al.* (2004) suggested that in order to solve this confusion is necessary to make more explicit interpretations of vulnerability in future assessments. Cutter (1996) gives 18 different definitions, highlighting the definition given by Timmerman (1981) "Vulnerability is the degree to which a system acts adversely to the occurrence of a hazardous event. The degree and quality of the adverse reaction are conditioned by a system's resilience (a measure of the system's capacity to absorb and recover from the event)".

For this work, the term vulnerability is defined as the potential to produce harm that an event has to a system. The potential to produce harm has two components: one is related to the event itself since it does not affect all the members of a system with the same intensity. Therefore, if we have a system with a homogeneous population a given event could produce different level of harm to the individuals in that system. On the other hand, the second component is related to the system affected by an event. If a population is affected by the same event its level of harm could also be different. The previous is related to the heterogeneity of the members of the population. For example, the same inundation intensity will affect differently to people living in above houses than concrete buildings.

In this study, two methodologies are used to estimate vulnerability. The first one is a qualitative analysis that divided the population into levels of vulnerability. The importance of this approach is that allow identifying areas within a population in which potentially the population could be more affected by a GLOF without knowing the real consequences of such event. The methodology selected is the methodology proposed for The Civil Defense Institute (INDECI) (INDECI 2006). The second methodology used here is an adaptation of the LifeSIM model by Aboelata and Bowles (2005), which is also used in the Corp of Engineering model FIA (USACE 2012). This methodology gives a quantitative approach, and it is used to calculate the expected number of people that can loss their life if a GLOF were to happen, including the uncertainty in the breach process at the moraine. Also, we include a second scenario to calculate the reduction in life losses if an early warning system were installed

3.5.1 Risk analysis INDECI Approach

The Civil Defense Institute (INDECI) defines risk as the intersection between the magnitude of and event in a specific area with the characteristic of the population being affected and the quality of the infrastructure in which people live. The INDECI approach intersects physical vulnerability and social vulnerability. Physical vulnerability or biophysical vulnerability is related with the exposure of people or places to hazard. While social vulnerability is related with the measure of resilience to hazards (Cutter 1996; Cutter et al. 2003; Hegglin and Huggel 2008).

3.5.1.1 Physical Vulnerability

In this work, following INDECI methodology, we are going to use the flood hazard, population density and infrastructure material as indicators of the physical vulnerability. Flood hazard is a function of the flood intensity, which is also a function of the maximum velocity and depth of the flood (Table 34) (García et al. 2002; Garcia et al. 2003; Garcia and Lopez 2005). The criteria listed in Table 34 were first proposed in the Venezuelan project PREVENE (2001) for the evaluation of the impacts of debris flow in two alluvial fans. Later this was adapted and applied to other alluvial fans in Venezuela (García et al. 2002). The methodology is an adaptation of the Austrian (Fiebiger 1997), and Swiss (OFEE et al. 1997) methodologies, in which García et al. (2002) assumed that the infrastructure in Venezuela is less resistant than the infrastructure in Austria or Switzerland. This is important since the city of Huaraz is more similar to a city in Venezuela than a city in Europe in terms of building resistance. This methodology consists of the classification of areas inundated with water or mudflow into three hazard

levels (low, medium, and high). The classification criteria are shown in Table 34 for mud flows since that is the most probable case for a GLOF from Lake Palcacocha. Note that we also consider a very low hazard level for water depth less than 20 cm, which is not part of the PREVENE (2001) methodology.

Table 34: Debris Flow Event Hazard Level.

Hazard Level	**Description**	**Depth H (m)**		**Depth*Velocity V * H (m^2/s)**
Low	People at low risk. Minor damage to buildings.	0.2 < H < 1.0	and	0<V*H < 0.2
Medium	People in danger outside their homes. Structural damage and possible destruction.	0.2 < H < 1.0	and	0.2 < V*H < 1.0
High	People in danger inside and outside homes. Structures destroyed.	H > 1.0	or	V*H > 1.0

The second component of the physical vulnerability is the population density, which definition is straightforward and corresponds to the number of people per km^2 in Huaraz. Areas with more population density are more vulnerable than area with less population density.

The third component is related to the houses materials for which we are going to use the information available in the 2007 census. There are three main types of construction listed in the Census for Huaraz: concrete, anchored wood, and adobe and non-anchored buildings. We are going to assign a score of 1, 2 and 3 to concrete,

anchored wood, and adobe and non-anchored buildings, which will be multiply for the fraction of houses with each material in each block. Finally, the scores will be summed obtaining an aggregated score for each block. The blocks with a higher score are more vulnerable than the one with a lower score.

3.5.1.2 Social Vulnerability

The proximity to the source of risk does not explain or determine by itself the vulnerability of a population at risk; social vulnerability, which describes the characteristics of the population also helps to understand the impacts of natural disaster (Yoon 2012). It is broadly accepted that social vulnerability is a multidimensional concept, which involves parameters related with poverty, race and ethnicity, gender, age for mentioning some of them (Cutter 1996; Cutter et al. 2003; Luers 2005; Adger 2006; Fuchs et al. 2007; Cutter and Finch 2008; Fuchs et al. 2012). As it is mentioned in Yoon (2012) an assessment of vulnerability without considering these factors is going to be at insufficient. For example, women and men, people in different age and ethnic groups, and those with different levels of physical and cognitive ability, experience disaster differently (ISDR 2004; Ionescu et al. 2005; Cutter and Finch 2008).

Social Index Vulnerability (SOVI) is used to estimate the social vulnerability (Cutter 1996). SOVI was created by first finding social characteristics consistently identified within the research literature as contributing to vulnerability. These target variables were used to identify a set of 42 normalized independent variables that influence vulnerability, from which 11 components were considered the most relevant since they explained the 76% of the vulnerability (Schmidtlein et al. 2008). Fekete (2009)

compared the SOVI index to real data from areas affected by floods in Germany in 2002 concluding that social vulnerability indexes, which he called SVI instead of SOVI, are effective to evaluate the differences in social vulnerability within a group of people as a consequence of flood events. SOVI can be adapted to the characteristics of the population affected by a hazard, this is particularly advantageous because we cannot used the same components that Cutter (1996) used in The USA or Fekete (2009) in Germany in the areas in which we are implementing our work.

SOVI calculation requires census information, which may be difficult to find in some countries; fortunately for this work we had access to the 2007 census in Peru for the city of Huaraz at a block level. Schmidtlein et al. (2008) and Fekete (2009) describe the procedure to calculate SOVI, starting from a principal component analysis (PCA) of the census variables in order to reduce the number of variables and group them in components that explain the heterogeneity existent within the population that could be affected by a flood. In this work, a multi collinearity test of the census variables is added in order to avoid that two or more variables are linearly perfect correlated, adding redundant weight to some characteristic of the population studied. The multi collinearity test is performed using NumXL add on Excel. We want a condition number lower than 30 and a value inflation factor (VIF) lower than 10. Additionally we calculate the Kaiser-Meyer-Olkin Measure of Sampling Adequacy (KMO) index and Bartlett's test of sphericity. The Bartlett's sphericity test and the KMO index enable to detect if it is possible to summarize the information provided by the initial variables, census variables in our case, in a few number of factors using PCA. A KMO above 0.5 indicates that the variables selected are suitable for factor analysis, although for better performance a KMO

value of 0.7 or above is desired. Also, the Bartlett's test of sphericity is performed to test the null hypothesis that the correlation matrix is the identity matrix. We want to reject this null hypothesis; that is, we want its associated probability to be less than 0.05. KMO index and Bartlett's test are calculated using a script in Matlab available online by Trujillo-Ortiz and Hernandez-Walls. (2003) and; Trujillo-Ortiz et al. (2006).

After performing the multi collinearity analysis, Bartlett's test and calculate KMO index we follow Schmidtlein et al. (2008). They list 6 steps for what they called SOVI algorithm, which are

1. Standardize all input (census) variables to z-scores, each with mean 0 and standard deviation 1.

2. Perform the PCA with the standardized input variables.

3. Select the number of components to be further used based.

4. Rotate the initial PCA solution (in our work we used a normal Kaiser Varimax rotation)

5. Interpret the resulting components on how they may influence the social vulnerability and assign signs to the components accordingly.

6. Combine the selected component scores into a univariate score using a predetermined weighting scheme.

7. Standardize the resulting scores to mean 0 and standard deviation 1

All the steps but step 6 are straightforward. In step 6, we need to decide how we want to combine the different components. Cutter et al., (2003) use factor analysis just for the selection of the variables assigning the same weight to them in the SOVI calculation. The second criterion is to use the scores from the PCA analysis adding them

but assuming that all the components have the same contribution to the SOVI. A Third criterion considers just the first component factors in an additive model since this is a linear combination that explain the largest amount of variation of the original data (Schmidtlein et al. 2008). Finally the fourth criteria uses the scores from the PCA analysis, but it assigns different weight to the principal components according with the fraction of variability that they explain (Schmidtlein et al. 2008).

For this work, the fourth criterion is used with the intention of using as much information as possible from the statistical analysis. Once the SOVI is calculated for each block on the census, the results are plot geographic system in order to visualize the distribution of the social vulnerability in Huaraz.

3.5.1.3 Combination of different vulnerability components

The Peruvian regulation requires that vulnerability calculations show four level of vulnerability. The vulnerability index will be calculated adding the different component of the physical and social vulnerability assuming the same weight for all of them. In order to have the same metric, four levels in each component of the vulnerability are going to be calculated. For the hazard calculation, this has already been defined; for the population density, house material and SOVI the scores calculated are going to be divided into quartiles. Then, a score from 1 to 4 is assigned to each quartile depending on the position of the quartile, 1 for the first, 2 for the second and so on. Finally, the scores for the four components in each block are added obtaining the total vulnerability. The blocks with higher values are more vulnerable than the ones with lower values.

3.5.1.4 Vulnerability Results using INDECI approach

Hazard results

The hazard identification method described in the previous section, using the maximum inundation depth and the maximum water velocity, is used to determine the level of hazard at different points in the city. Figure 72 shows the computed hazard levels for the expected breach scenario. As shown in Figure 72, almost all of the inundated areas within the city are in a high hazard zone (red). Very small areas on the fringe of the flooded area are in the medium (yellow), low (green) or very low (light blue) hazard zones. This hazard methodology is based on the inundation intensity, and it does not consider the time that people have to escape from the hazard zone.

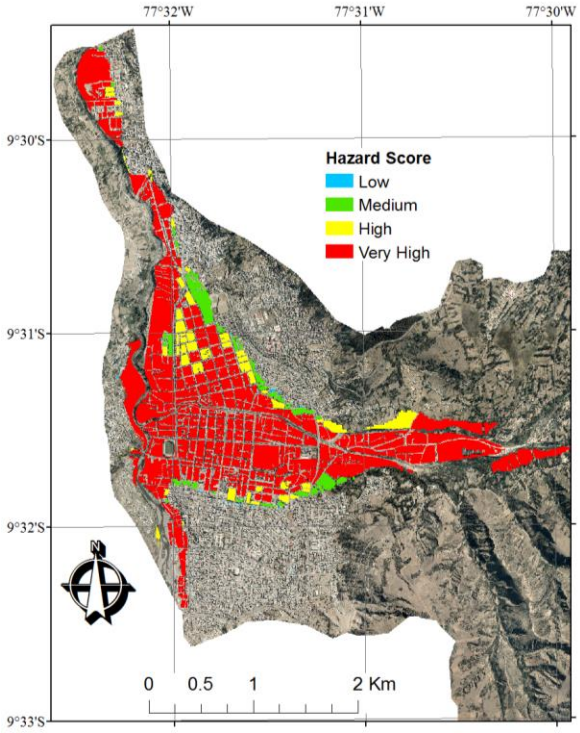

Figure 72: Hazard level in Huaraz for the expected breach scenario.

Population Density

Figure 73 shows a map with population density. The values are in people per square kilometer. The areas near the river in the city are more densely populated especially to the south side of the Quilcay River where the inundation would have more intensity. The areas to the east side of the city are less populated because they are more rural. The same happens at the north end of the city. To the north side of the Quilcay River, which corresponds to the Independencia municipality, the distribution of people is more homogenous going from 13520 to 24510 people per square kilometer.

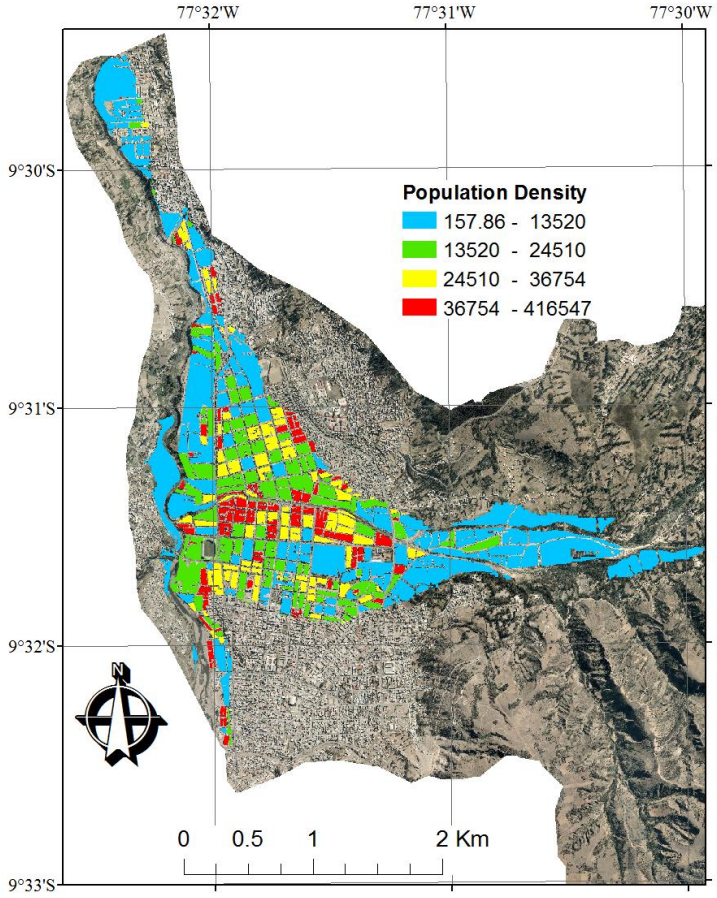

Figure 73: Population Density in number of people per square kilometer.

Building materials.

For the calculation of the building vulnerability, the information from the Census 2007 was used. In Huaraz there are several types of material in the building walls, which were aggregated in 3 categories: concrete wall (concrete and rock-concrete mix building walls), Anchored wood wall, and unanchored walls (adobe, mud and grass mix, rocks with no adhesive mix building walls). A score of 1, 2 or 3 was multiple for the fraction of concrete, anchored wood and unanchored building's wall respectively in each block. The results were summed in each block obtaining a general score. For the final results the general scores were classified in quartiles. The buildings located in the lowest quartile have more resistance therefore they are less vulnerable (Figure 74). The opposite happens to the fourth quartile. According to Figure 74, the area corresponding to the east side of the city, which would receive the impact of a GLOF first, has less resistant building; therefore, they are more vulnerable for this item. At the city, along the river Quilcay where the inundation would be more intense, buildings are more vulnerable. In general the south side of the river, corresponding to the Huaraz municipality, has better quality buildings than the north side. Also, it is possible to observe clear separations between the areas with better and lower quality constructions.

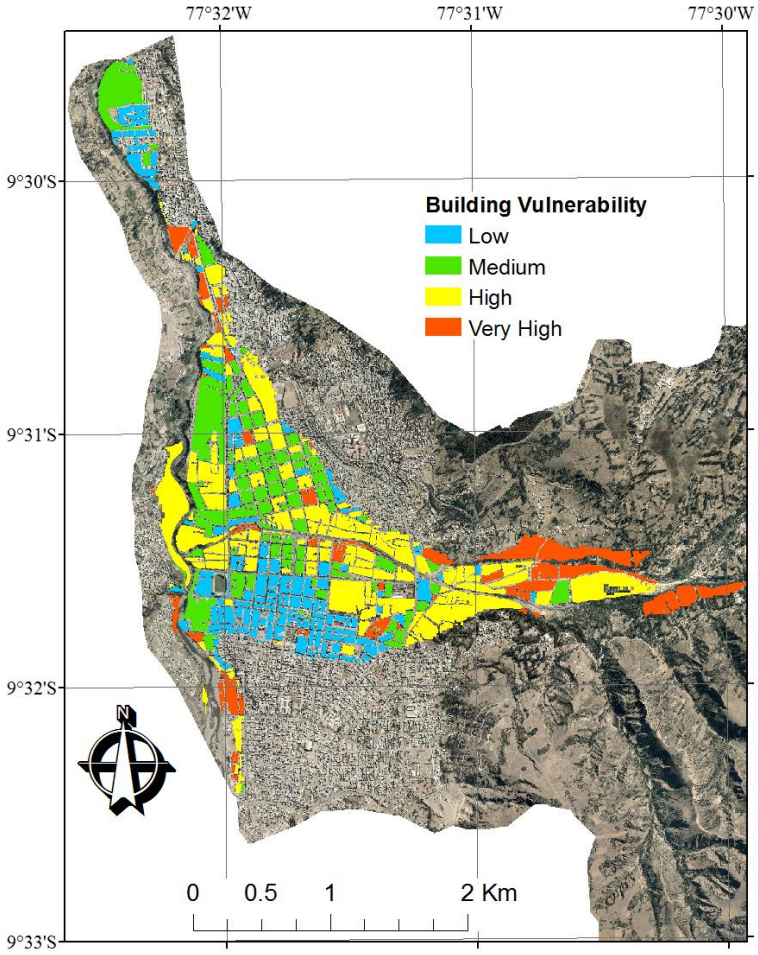

Figure 74: Building vulnerability generated with the information from the 2007 Census.

SOVI

For the calculation of the SOVI index, the information provided by the 2007 census of Peru at block level was used. The Census has 233 variables with information related to the characteristic of people and building in which people live. From those 233 variables, 173 variables are potential candidates for calculate SOVI. Some of the 233 variables were disregard since they did not represent, to the author criterion, information

that can explain the variability in the population. For example, the information related to religion was disregard, also questions such as the place in which the person sensed was born, or his/her mother was born were ignored. From the 173 variables, the ones that represent events mutually exclusive and collectively exhaustive were disregard; for example in the case of the number of male and female, the number of females was used and the number of males was ignored. The variable that increases vulnerability was generally used. For example between the variables “number of people that can read” and “number of people that cannot read," the variable “number that cannot read” was used and the variable “number of people that can read” was ignored. Also, other variables were aggregated, for example, a variable that includes the number of houses that are owned by the habitants of the houses was created, without considering how they acquired the property. Doing this process, the number of variables was reduced to 90. Then the values for the remaining variables were transformed to z scores subtracting the mean value and dividing by the standard deviation. These 90 variables were tested for collinearity. It turned out that many of them present collinearity problems; consequently they were taken out as well ending with 52 variables (Table 35 left column). Then a PCA analysis was performed with the remaining 52 variables resulting in that some variables could not be associated to any component, so they needed to be disregarded as well ending with 25 variables (Table 35 center column).

Table 35: Variables reduction from Peru census 2007.

52 Variables After Collinearity Analysis	25 Variables After PCA	19 Variables Selected
Population Density	Population Density	Population Density
Improvised construction	Improvised construction	+ Improvised construction
Hotel, hostel	Hotel, hostel , Hospital, Prison, Elder-houses, Children Village	+ Hotel, hostel , Hospital, Prison, Elder-houses, Children Village
Hospital, Prison, Elder-houses, Children Village		
Houses with people living on them		
Potable Water outside the house	Potable Water outside the house	+ Potable Water outside the house
No potable Water	No potable Water	+ No potable Water
No drainage system outside the house	No drainage system outside the house	+ No drainage system outside the house
No drainage system		
Public illumination		
# People per room	# People per room	+ # People per room
No own the house	No own the house	- No own the house
Radio	No electronic/electric device	+ No electronic/electric device
TV		
Sound system		
Washer machine		
Refrigerator		
Computer		
No internet, TV cable or phone line	No internet, TV cable or phone line	
Kerosene	Kerosene, Charcoal, Wood, Dung	
Charcoal		
Wood		
Dung		

Table 35 (Continued)

52 Variables After Collinearity Analysis	25 Variables After PCA	19 Variables Selected
At least 1 disable at home	At least 1 disable at home	+At least 1 disable at home
# family leader	# family leader	
Partner		
Children		
Son in law		
Grand children		
Parents, Parents in law		
Other relatives		
Other no relatives		
Women	Women	+ Women
0-14 year	0-14	+ 0-14 year
45-64 year		
>65 year	>45	+ >45 years
No medical insurance	No medical insurance	+ No medical insurance
Indigenous	Indigenous	
Cannot read	Cannot read	+ Cannot read
Primary School or less	Primary School or less	+ Primary School or less
Unemployed	Unemployed	+ Unemployed
Government employees	High Level Jobs	- High Level Jobs
Professors, scientists, intellectuals		
Technical laborers	Medium Level Jobs	
Office employees		
Work on sales		
Farmers	Lower level Jobs	+ Lower level Job
Mining workers		
Construction, manufactures workers		
Worker with no qualification		

Table 35 (Continued)

52 Variables After Collinearity Analysis	25 Variables After PCA	19 Variables Selected
Worker not specified		
Married/Partner	Married/Partner	

A second PCA analysis was performed using the variables from Table 35 (center). The variables were tested to know if they were suitable for PCA analysis. Table 36 shows the results for the Bartlet's test of sphericity rejecting the null hypothesis. Additionally the Kaiser-Meyer-Olkin Measure of Sampling Adequacy results was 0.8043, which means that the KMO test yields a degree of common variance meritorious. Therefore, the tests results imply that the 24 variables selected are suitable for PCA analysis.

Figure 75 shows the contribution to the variance of each of the 24 component using PCA. The first eleven components were selected since they explain 76.5 % of the variance; this is the same criteria used by Cutter et al. (2003). Kaiser criteria could have been used eliminating the component which eigenvalues are less than 1 but that would have reduced considerably, maybe too much, the number of variables used in the SOVI calculation leaving us with just 7 components.

Finally using the first 11 component, the resulting factor matrix was rotated in order to concentrate the weight of the variables in one component as possible. The results are indicated in Table 37. As Fekete (2009) suggested, factors above 0.3 were used ignoring the ones below 0.3. Therefore, factors smaller than 0.3 were not written down which also helps to keep Table 37 easier to read.

Table 36: Bartlet's test of sphericity

Component	Eigenvalue
1	5.4786
2	2.2514
3	1.8171
4	1.6270
5	1.4285
6	1.1582
7	1.1213
8	0.9713
9	0.9272
10	0.8226
11	0.7574
12	0.7303
13	0.6703
14	0.5798
15	0.5309
16	0.4701
17	0.4604
18	0.4305
19	0.3820
20	0.3514
21	0.3273
22	0.2835
23	0.2494
24	0.1735

Sample-size	Variables	X2	df	P
1257	24	10170.9152	276	0.0000

With a given significance level of: 0.05
Assumption of sphericity is not tenable.

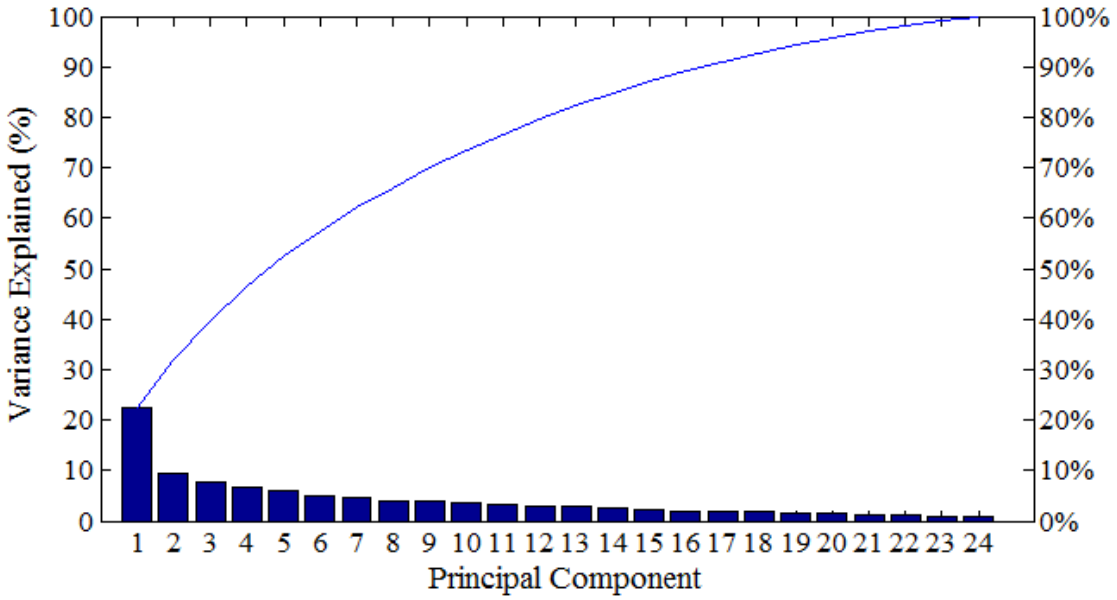

Figure 75: Variance explained by each factor. Continues line show the cumulative variance contribution.

The next step is the calculation of the SOVI, for doing so the z-score of the variable studied were multiply by the factor value associated to the variable and by the fraction of the variance explained by the component to where the variable belong. For example, population density has a factor of 0.9, and it belongs to Component 9; therefore, the z-scores are multiply by 0.9 and 0.0445. Also, if the population density increases the vulnerability increases as well, so the sign of this component variable is positive. This procedure was repeated for the 19 variables obtaining the SOVI index. Once all the indexes were aggregated the results were normalized and plotted in a map (Figure 76). In Figure 76 the final SOVI result is showed, the map is divided into 4 categories from more vulnerable (red) to less vulnerable (light blue). It is important to mention that these levels

of vulnerability are related or referenced to the characteristic of the population in Huaraz and is not comparable to the SOVI index in another group of people.

Table 37: Result summary of the PCA Analysis.

Selected Census Variables after PCA analysis to compose SOVI and presumed direction toward vulnerability + more vulnerable - less vulnerable	Component										
	1	2	3	4	5	6	7	8	9	10	11
+ Population Density									0.90		
+ Improvised construction										0.87	
+ Hotel, hostel , Hospital, Prison, Elder-houses, Children Village						0.63					
+ Potable Water Outside					0.71						
+ No potable Water				-0.51							
+ No drainage system					0.70						
+ People per room						0.63					
- No own the house								0.85			
+ No electronic/electric device				-0.66							
+ At least 1 disable											0.97
+ Women							-0.67				
+ 0-14 year			-0.57								
+ >45 years			0.66								
+ No medical insurance	0.50										
+ No read		0.53									
+ Primary School or less		0.43									
+ No Job							-0.56				
- High Level Jobs	-0.45										
+ Lower Level Job	0.48										
Factor Scores	2.80	2.47	1.98	1.88	1.61	1.58	1.40	1.22	1.15	1.06	1.04
% of variance explained by component	11.8	10.4	8.34	7.91	6.78	6.63	5.90	5.15	4.83	4.45	4.4
Cumulative Variance	11.8	22.2	30.5	38.4	45.2	51.8	57.7	62.9	67.7	72.2	76.5

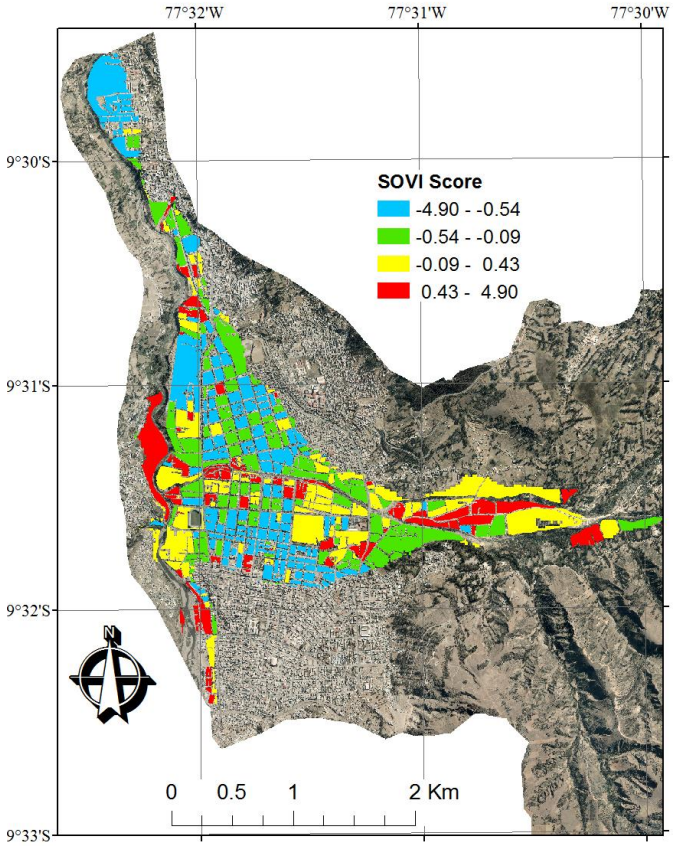

Figure 76: SOVI map, the lower scores indicate less vulnerable.

Total Vulnerability

Figure 77 shows the Total Vulnerability levels in Huaraz. The Total Vulnerability is the result of combining four indicators of vulnerability following the INDECI framework in Peru. The indicators are social vulnerability, which was calculated using SOVI, building vulnerability, population density vulnerability, and hazard levels. The last three component of the total vulnerability corresponds to physical vulnerability. Four levels of vulnerability were generated in each component and assigned a score of 4, 3, 2 and 1 to the very high, high, medium and low level of vulnerability. Then the scores from the four components were added for each block. The final result was divided into

quartiles as it is shown in Figure 77. The first quartile corresponds to low vulnerability, and the last quartile corresponds to Very High Vulnerability.

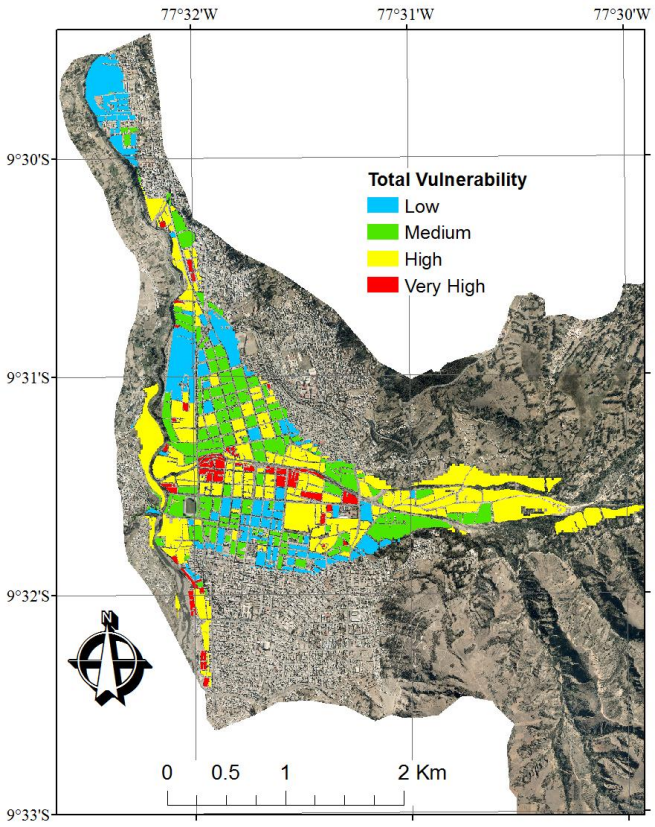

Figure 77: Total vulnerability levels.

The most vulnerable areas are located along the river, going from high to very high in some areas near the confluence between the Quilcay River and Santa River, which is explained for the high population density and high level of social vulnerability. In general, the inundation hazard level is very high for most of the city; therefore, it does not help to recognize where the vulnerability is higher or lower. However, it was included in this work in any case.

Then there is low and medium vulnerability to the south and north of the city respectively away from the river, which is mainly the result of the better quality in the construction materials and lowers SOVI.

3.5.2 Risk Analysis using LifeSIM adapted.

3.5.2.1 Background

In a previous section, the level of vulnerability in Huaraz due to a potential GLOF was calculated using an INDECI methodology. Although there is no doubt in the usefulness of that approach it is a qualitative identification of the areas in major risk, which does not allow quantifying the impact that a risk reduction effort could lead to. After several since the government of Peru declared Palcacocha Lake at high risk level, local organizations are taking the initiative to implement risk reduction measurements. These initiatives are going to be put in place in different stages. The first stage is to implement an early warning system (EWS), followed up by training of the population to improve the time of reaction and understanding of the activities that they should follow in the case that an alarm is giving by the authorities. A second stage would consider the intervention of the lake to reduce its volume, so the infrastructures and properties are also protected.

Although the benefits of an EWS may seem evident, they have strong opposition in some part of the population for reasons that are unknown and also they respond to the unknown effects that risk reduction measurements could bring to the population. In order to partially fill this gap is that this work includes the evaluation of the effects that an EWS may have in the expected number of people that potentially can lose their life. Also

quantify the number of people that may be killed by a GLOF and how that number changes if the authorities in charge of the population safety in Huaraz release an alarm that can initiated an evacuation process before the GLOF reaches the city.

An adaptation of the LIFESim is used to evaluate the impacts that an EWS could have in Huaraz. LIFESim was developed at Utah State University and funded by the Corps of Engineering. The model is a modular, spatially-distributed, dynamic simulation system for estimating potential life loss from natural and dam and levee failure floods (Aboelata and Bowles 2005)a. LIFESim has three modules, 1) Loss of Shelter, including prediction of building performance; 2) Warning and Evacuation; and 3) Loss of Life calculation. This model can perform in a deterministic or an uncertainty mode. A modification of the LIFESim model, called simplified LIFESim, is used by the Corp of Engineers in the software HEC-FIA (Lehman and Needham 2012; USACE 2012). LIFESim model overcomes the limitations of using of empirical equations, for example in (Graham 1999), for calculating the loss of life and use detailed inundation data, as well as building characteristics. Also in the evacuation process include a calculation of the number of affected people that initiate the evacuation, but cannot reach a safe area.

Graham (2009) and USDHS (2011) give reviews of the LIFESim, and the simplified LIFESim used in HEC-FIA strength and weakness. Among the strengths highlighted:

- The model is based on almost 60 flooding cases.
- Important factors that influence loss of life are modeled.
- Warning and evacuation curves can be adjusted to local characteristic of the population analyzed.

- The model evaluates the level of protection that a building can give to the population that has not evacuated.
- It gives fatality rates for different levels of building destruction.

Among the disadvantages are:

- In order to know the evacuation and mobilization curves the local authorities or dam owners should have some knowledge of the system analysis, however dam break is not a frequent process so probably the people managing a dam do not have experience in this type of problems.
- LIFESim does not give guidance of when the alarm needs to be release to the population.

3.5.2.2 Methodology

In this work, the same workflow that LIFESim and the Simplified LIFESim models used. The main modifications are based on the lack of information that there is in Huaraz since LIFESim was developed for the level of information available in the US. For example, HEC-FIA, which uses the simplified LIFESim model, can read census information in the same format that the official online Census publication (USACE 2012). The information for the intensity of the inundation is extracted from the simulation performed using FLO-2D (Section3.4). There are 3 modules or stages in the life loss number calculation: 1) Loss of Shelter, 2) Warning and Evacuation; and 3) Loss of Life calculation

Loss of Shelter

The aim of this module is to evaluate the impact on the building in the inundation area. Here concept of lethally zone is used, which is an indication of the level of destruction that the inundation could produce to the buildings. The model defines three lethally zones (Aboelata and Bowles 2005):

Chance Zones: In which the building are practically washed away, and the survival depends on chance. The fatality rate in chance zones ranges from about 38 percent to 100 percent, with an average rate over 91 percent.

Compromised Zones: In which the building has been partially damaged. The historic fatality rate in Compromised Zones ranges from zero to about 50 percent, with an average rate near 12 percent.

Safe Zones: In which the inundation practically does not reach or the water is shallow enough to unlikely sweep people off their feet. Fatality rate in Safe Zones is virtually zero.

A summary of the probability for the different zones is given in Figure 71, the safe zone is not included since the lethally is virtually 0. The fatality rates follow triangular probability distribution. In LIFESim, all the parameters follow triangular distribution unless otherwise mentioned (Aboelata and Bowles 2005).

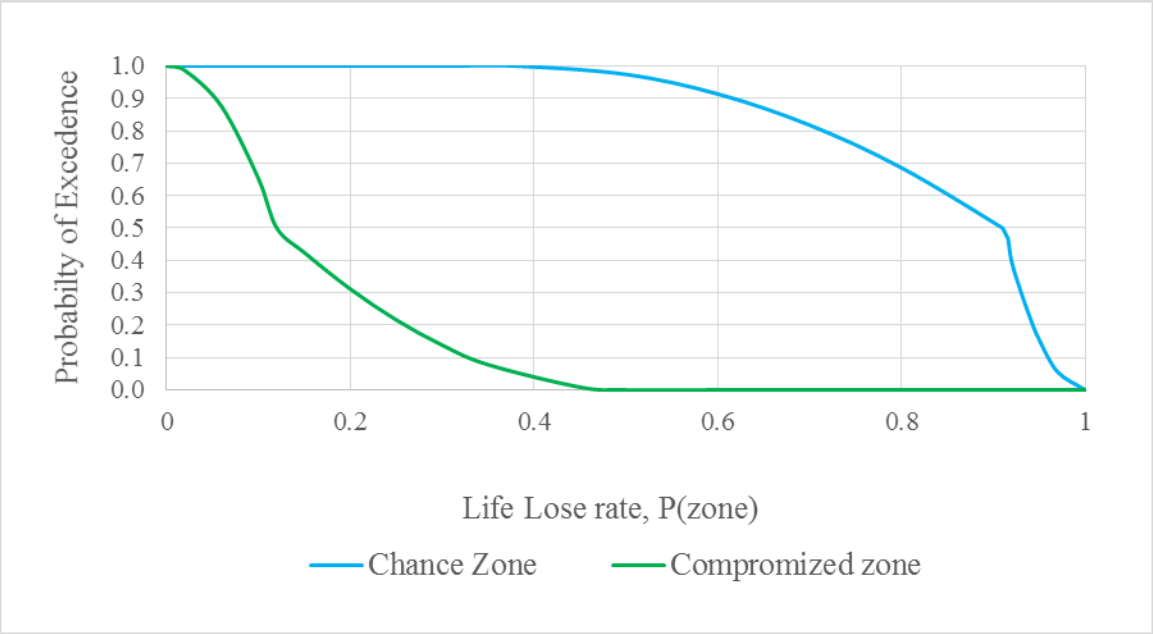

Figure 78: Probability of exceedance for the chance and compromised zones life lose rate (McClelland and Bowles 2002; Aboelata and Bowles 2005)

The information from Table 38 was used in order to define the lethally zones Table 38 defines three types of building, Wood-Framed Unanchored, Wood-Framed Anchored, and Masonry, Concrete and Brick buildings. The information related to wall materials in Huaraz building was extracted from the Peruvian Census 2007.

The number of floors is not included in the Census information available; therefore in this work the information related to the number of flats was not used. The level of damage, partial or total, is calculated based on the flood intensity (depth*velocity) criteria described in RESCDAM (2000) (Aboelata et al. 2003). Additionally bounds of uncertainty are added following Aboelata and Bowles (2005).

Table 38: Damage calculation using RESCDAM (2000) criteria (Aboelata et al. 2003; Aboelata and Bowles 2005)

Building Type	Velocity (m/s)	Velocity * Depth (m^2/s)					
		Partial Damage			Total Damage		
		Lower	Best	Upper	Lower	Best	Upper
Wood-Framed							
Unanchored	-	2.5	3	5	6	7	20
Anchored	-	1.65	2	3.2	2.5	3	5
Masonry, Concrete and Brick	>2	2.5	3	5	6	7	20

Warning and Evacuation

In LIFESim the warning and evacuation process is divided into four main components: warning, mobilization, evacuation-transportation, and high-rise building evacuation. In this work, the three first components are calculated. The fourth component cannot be considered because it was not possible to access the information related to the number of flats and building elevation. The high-rise building component is important for calculating the number of people that cannot leave the buildings before the inundation arrives, but they can escape vertically to a second or third floor that is not inundated.

The first process analyzed is the warning penetration in the population. Once the warning alarm is released there is a period for the population to associate it to an imminent hazard. The following equation from Rogers and Sorensen (1991) calculates the rate of penetration that an EWS has in the population, it is also suitable for several types of warning systems and activities in which the population is involved at the moment of the warning (Table 39 and 40):

$$dn/dt = k\,(a_1 * a_1 f\,(N - n)) + (1 - k)\,(a_2\, n\,(N - n)) \qquad \text{Equation 6}$$

Where:

dn/dt= is the fraction warned rate

k = fraction of population alerted via the broadcast process (Table 39),

(1-k) = represents the fraction of people left to be warned,

a_1=effectiveness of the warning system (Table 40),

$a_1 f$ = adjustment factor by location and activity (Table 40)

a_2= effectiveness of the contagion warning process (Table 40),

N = fraction that the system is designed to warned in the first 30 minutes after issuance of the warning, also referred to in Table 40 as the 30-min limit, and,

n = the fraction warned at the beginning of the time step.

The time step is 1 minute.

This equation has two components, the first one is the fraction of people that identifies that the warning alarm means that there is an imminent danger; and a second component that considers the fraction of people that will react after receiving the alarm from a secondary sources such as the ones that reacts in previous time steps (Aboelata and Bowles 2005).

Table 39: Fraction of population alerted via the broadcast process (Rogers and Sorensen 1991)

	Home Asleep	Indoors	Outdoors	in Transit	Working Shopping	Watching TV	Listening to Radio
Sirens	0.691	0.8	0.9	0.9	0.6		
Tone alert radios	0.85	0.9	0	0	0.7		
Auto-dial telephones	0.933	0.95	0	0	0.8		
Emergency Broadcast System	0	0.4	0.2	0.2	0.1	1	1
Sirens and tone alert radios	0.9	0.9	0.9	0.9	0.7		
Sirens and auto-dial telephones	0.933	0.85	0.9	0.9	0.8		

Table 40: Parameters used in the warning penetration calculation for different warning systems (Rogers and Sorensen 1991)

	k (fraction per min)	a1	a2	30 min Limit (N)	Release Rate after 30 min.
Sirens	0.2	0.2	0.3	0.75	0.3
Tone alert radios	0.4	0.3	0.2	0.9	0.1
Auto-dial telephones	0.3	0.2	0.25	0.5	0.5
Emergency Broadcast System	0.4	0.35	0.2	0.93	0.1
Sirens and tone alert radios	0.4	0.3	0.3	0.95	0.1
Sirens and auto-dial telephones	0.4	0.35	0.3	0.95	0.1

People in Huaraz are planning to install a siren system replicating the system installed in Carhuaz, a town near Huaraz. Therefore, just a siren system was analyzed from Table 40. Additionally there is not information that allows knowing in which activities people are involved during the day. HEC-FIA, for example, assumes the

distribution shown in Table 41 which is based in the US census information. In order to know, the influence of each activity in the alarm penetration rate a curve was plot for each activity in which the time after the warning is released versus the % of people warned is shown; and the differences for a siren system are small. In Figure 79, it is shown in blue the average and black the maximum and minimum curves for the different activities presented in Table 39. The different are small; consequently the average curve and the maximum and minimum bounds are used in this work.

Table 41: Percentages of people involved in different activities as functions of the time of the day use in HEC-FIA (USACE 2012)

Time	Home Asleep	Indoors	Outdoors	In Transit	Working	Watching TV	Listening Music
12:00 AM	91.7	0	2.1	0	4.2	2.1	0
2:00 AM	96.6	1.4	0	0	1.4	0.7	0
4:00 AM	93.1	0	2.1	0	4.9	0	0
6:00 AM	50	0.7	7.9	4.6	32.9	2	2
8:00 AM	12	3.8	25.3	7	43	3.8	5.1
10:00 AM	3.2	7.6	31.2	7.6	40.8	5.7	3.8
12:00 PM	3.8	7.6	29.7	8.2	38.6	7.6	4.4
2:00 PM	5.7	36.1	8.2	8.9	28.5	8.9	3.8
4:00 PM	3.8	5.7	17.7	10.8	46.8	12	3.2
6:00 PM	2.6	3.8	9.6	8.3	51.3	21.8	2.6
8:00 PM	8.6	1.3	7.9	4.6	43	33.1	1.3
10:00 PM	53	0	3.4	2	22.1	18.8	0.7

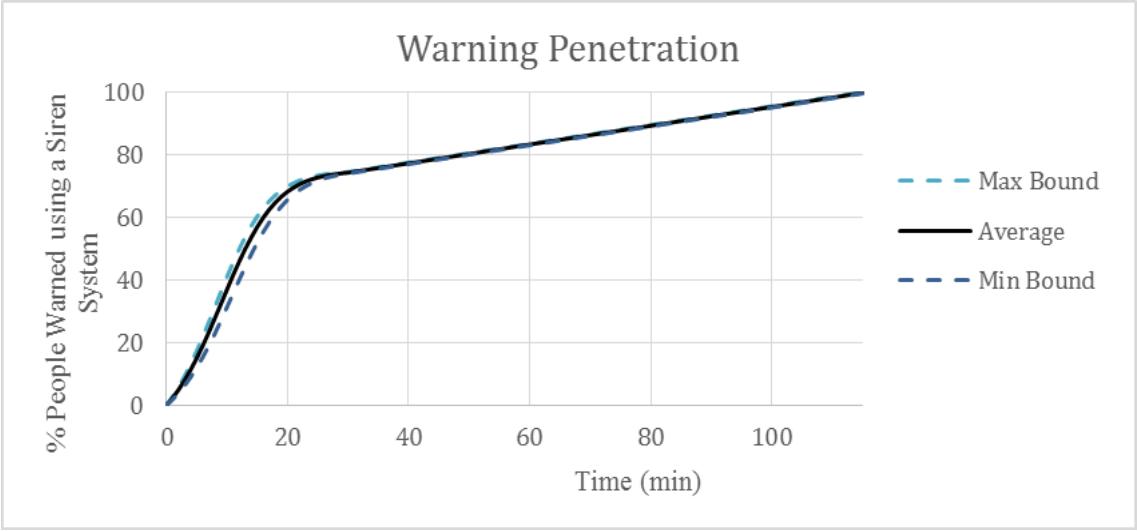

Figure 79: Penetration bounds of the early warning system.

The second process analyzed is the mobilization rate. When people internalize that there is an imminent threat, they start preparing for evacuation to a safety area. This process, as well as the warning penetration, is not immediate, and it can take for some people longer to get ready to leave or take the decision to leave the place in where they are at the moment of the alarm. USACE (2012) defines the curve of mobilization used in this work (Figure 80).

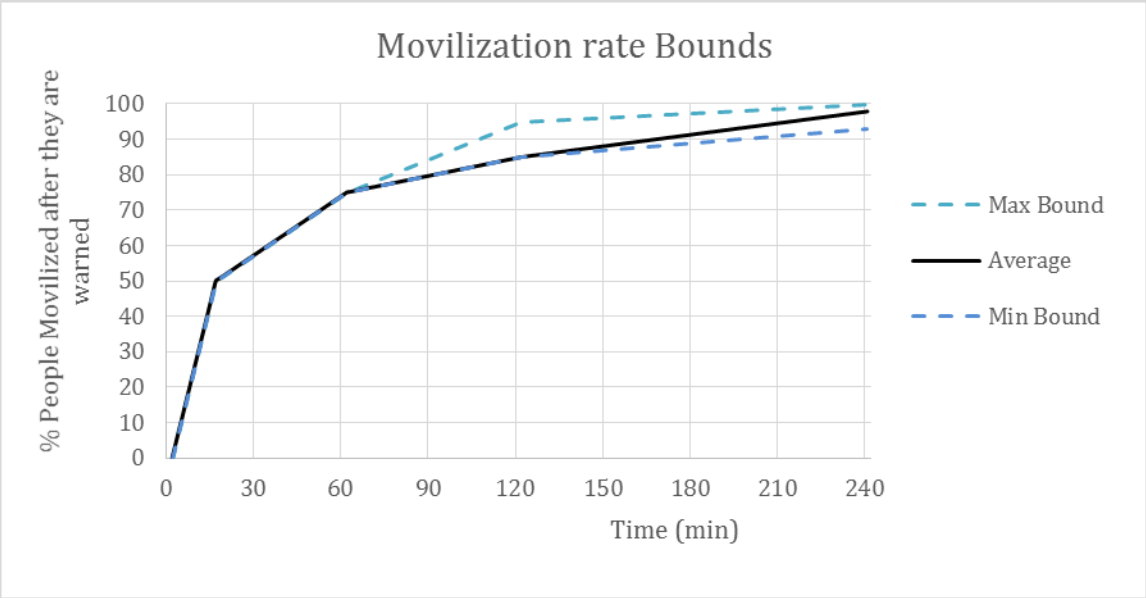

Figure 80: Mobilization rates (USACE 2012)

Since there are uncertainty bounds for the warning penetration and mobilization curves, a Monte Carlo simulation was implemented to combine them in order to calculate the evacuation rate curve (Figure 81).

The last component of the warning and evacuation process is the time that population takes to reach a safe area. LIFESim considers evacuation by: using cars, sport utility vehicles (SUVs), by foot and vertical evacuation. It is assumed that people would walk to a non-inundated area since it is the easiest and fastest way to reach a safe area, beside there is not information of the car density and the velocity of the car evacuation in Huaraz. Vertical evacuation is not considered either because as it was mentioned there is not information available for this work that allows knowing the number of floors in each building.

The walking velocity used ranges from 3-7 with an average of 4 mph or 80-187 with an average of 107 meters per minute (Aboelata and Bowles 2005). The shortest maximum

and minimum distance for each block to a no-inundated area were measured manually, which is used to calculate the time that people in each block would take to walk out of the danger zones.

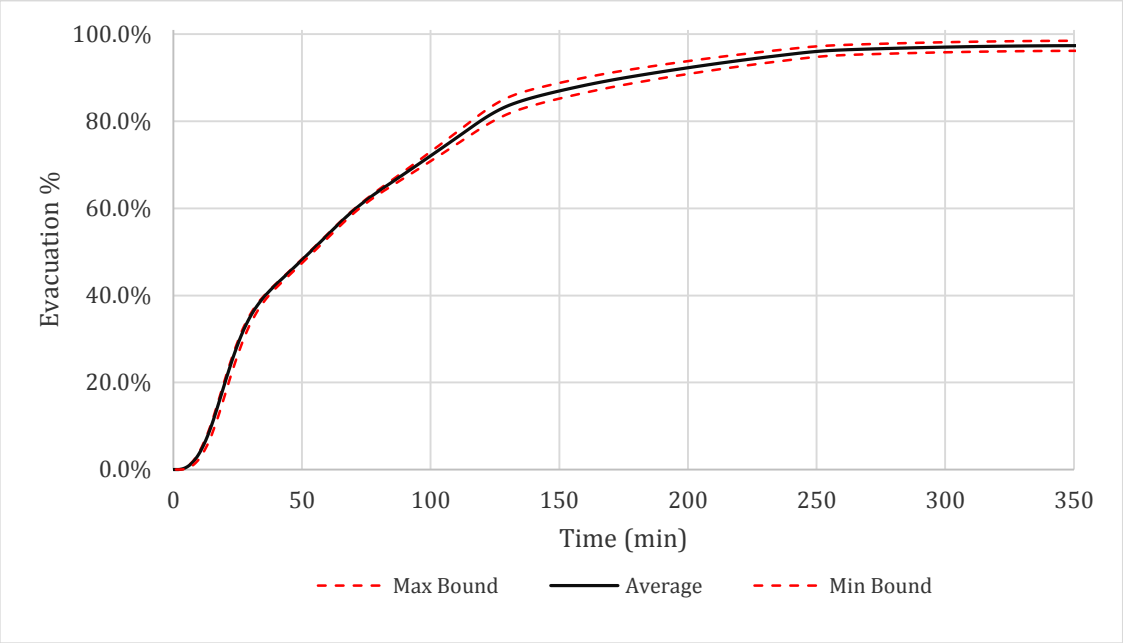

Figure 81: Evacuation % vs time calculated using 20000 samples in a Monte Carlo Simulation.

Loss of Life calculation

In this section the loss of shelter, the warning and evacuation calculations with the population at risk (PAR) are combined. Population at risk is defined as the people that live in the inundation zone; therefore, it can be affected by the GLOF. The aim of this analysis is to quantify the reduction in loss of life if an EWS were to be installed in Huaraz. Therefore, first the number of people that can lose their life without alarm and consequently no evacuation was calculated. The result will depend upon mainly the

building characteristics. Second, the EWS is evaluated by calculating the number of people that can evacuate the danger zone to a safe area, and the consequent reduction in life losses. It is important to mention that the population that initiated the evacuation but cannot reach a safe area will be considered as if they did not leave their original location.

Also for the discussion section, artificially it was generated an improved mobilization curve that assumes that 100% of people will leave the hazard zone in one hour after they recognize from the warning system that there is an imminent risk (Figure 82).

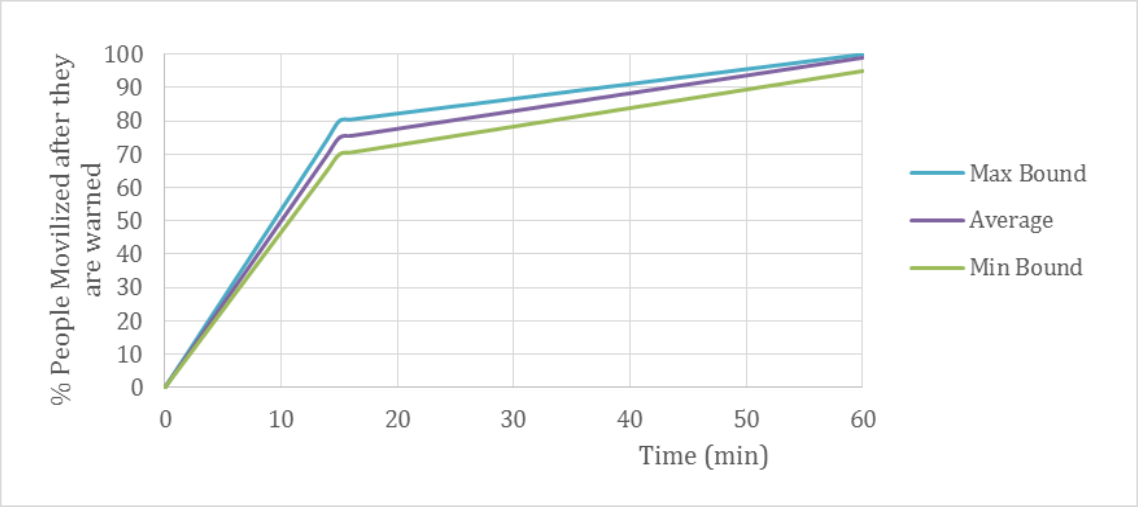

Figure 82: Improved mobilization curve.

For doing the calculations all the uncertainty ranges were considered using Monte Carlo simulation with 20000 samples.

3.5.2.3 Results

No early warning system

The first step is to calculate how the inundation would affect the building, destroying completely, partially or not destroying them with the respective fatality rate associated to each situation. The number of people living in the inundated area is 40646 people. In Figures 76, 77, 78 the lethally percentage is shown for the different building wall materials. There is an evident high lethally rate in the center of the city where the inundation would destroy the building and reduces as the inundation spreads out far from the river. These results are similar to what happened in 1941 (Figure 46). Each block has houses with different wall material composition; consequently lethality the percentage for each wall material was multiply by the fraction of houses that are built with those materials. Then the percentages for each of the three materials are summed to generate a weighted lethality percentage (Figure 79). This weighted lethality percentage is multiply by the PAR in each block resulting in a potential loss of lives of 19773 with a standard deviation of 1191 people. Also, the loss of life was calculated, in a deterministic process for comparison, in 22036 people using the average values.

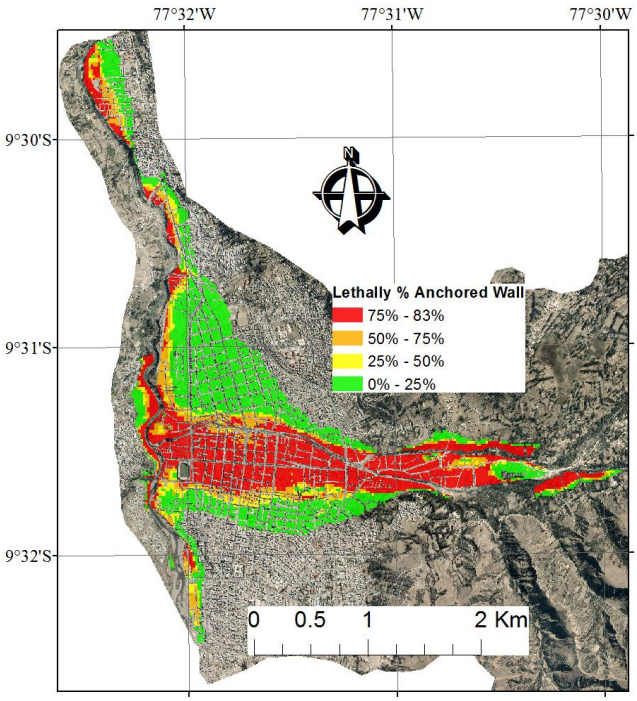

Figure 83: Lethally % for anchored wood walls

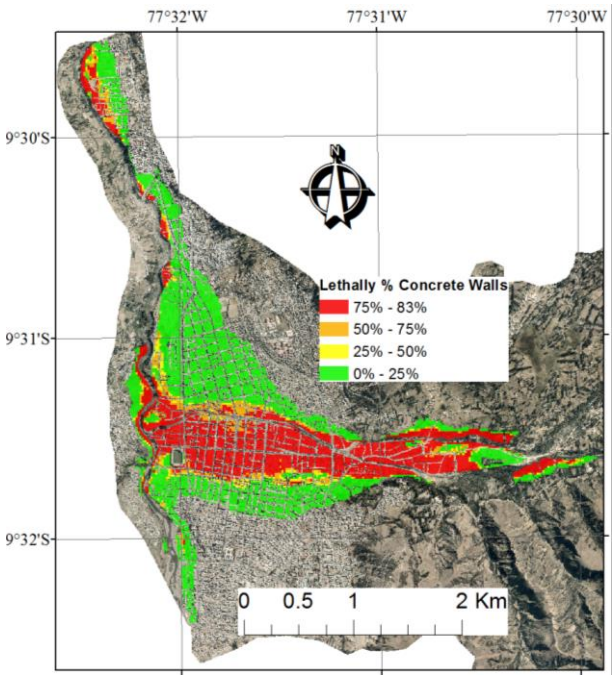

Figure 84: Lethally % for concreted walls

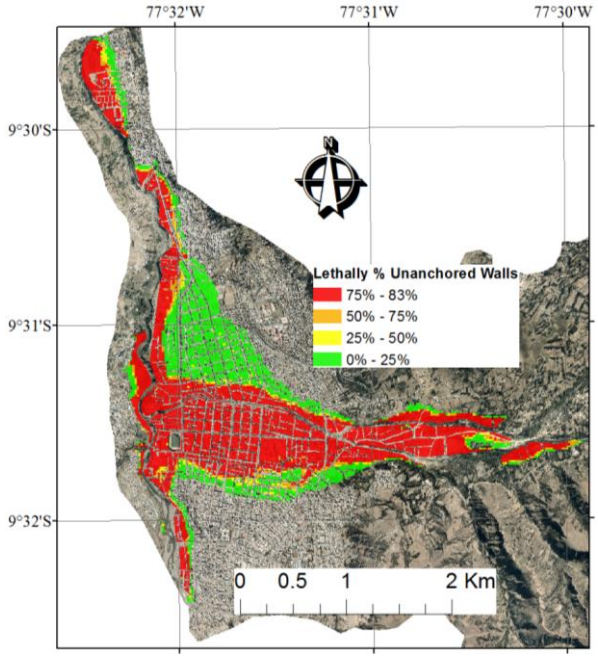

Figure 85: Lethally % for unanchored wood walls

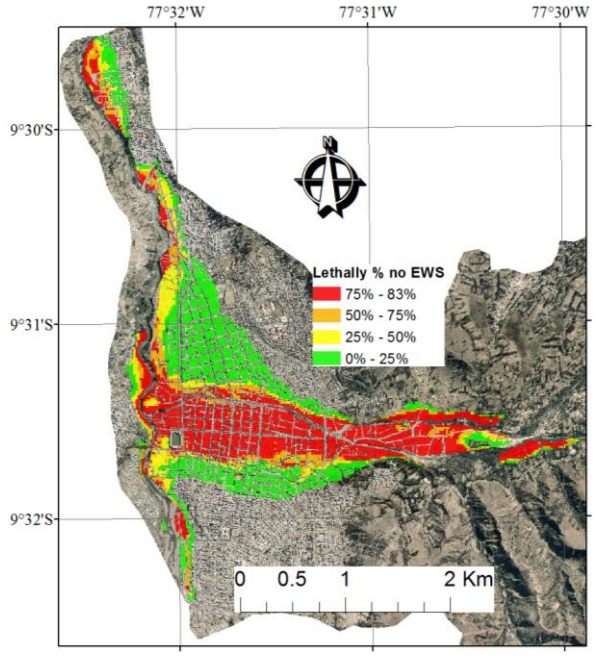

Figure 86: Lethally % for the inundation for no early warning system (EWS) in Huaraz.

Early Warning System

In order to calculate the lethally percentage, the percentage of people that would evacuate the inundation area before the inundation arrives needs to be estimated (Figure 79). There is a lower rate of evacuation to the east of the city that is a consequence of the earlier arrival of the inundation in that area. Figure 80 shows the lethally rate if a siren alert were released immediately after the dam break is produced. The average number of potential life losses is 7344 people with a standard deviation of 1446 people. Figure 81 shows the reduction in the life loss percentage which goes up to 67.9 % in some areas.

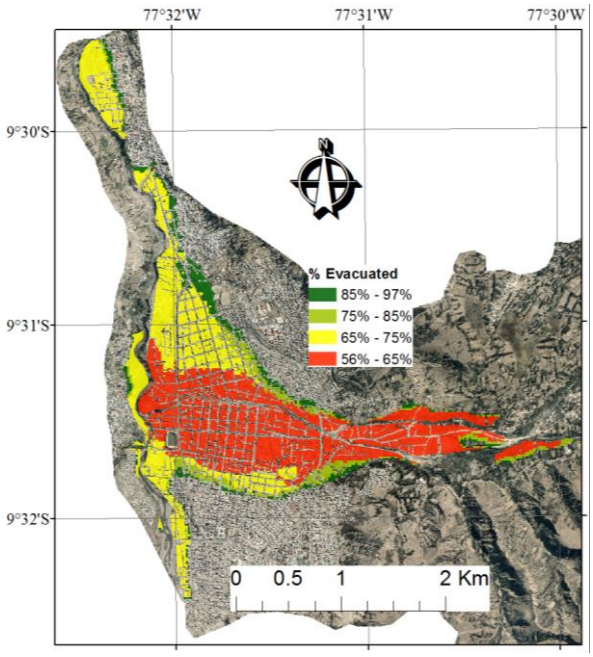

Figure 87: Percentage of people that are able to evacuated the inundation area if the alarm were release at the time the GLOF is release at the lake.

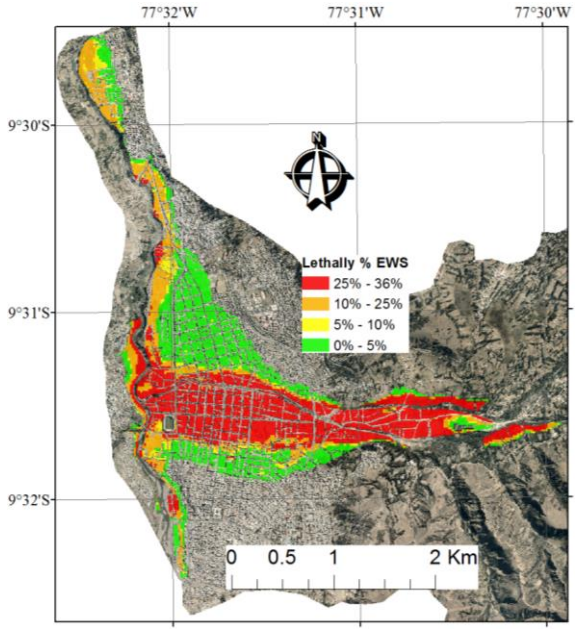

Figure 88: Lethally rate considering an early warning system (EWS) in Huaraz.

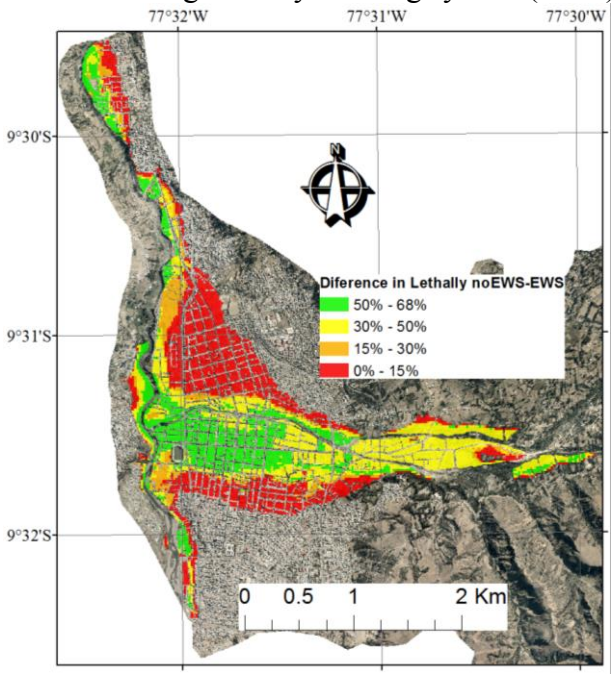

Figure 89: Differences in lethally percentage between a scenario that does not have a EWS and one that has a EWS.

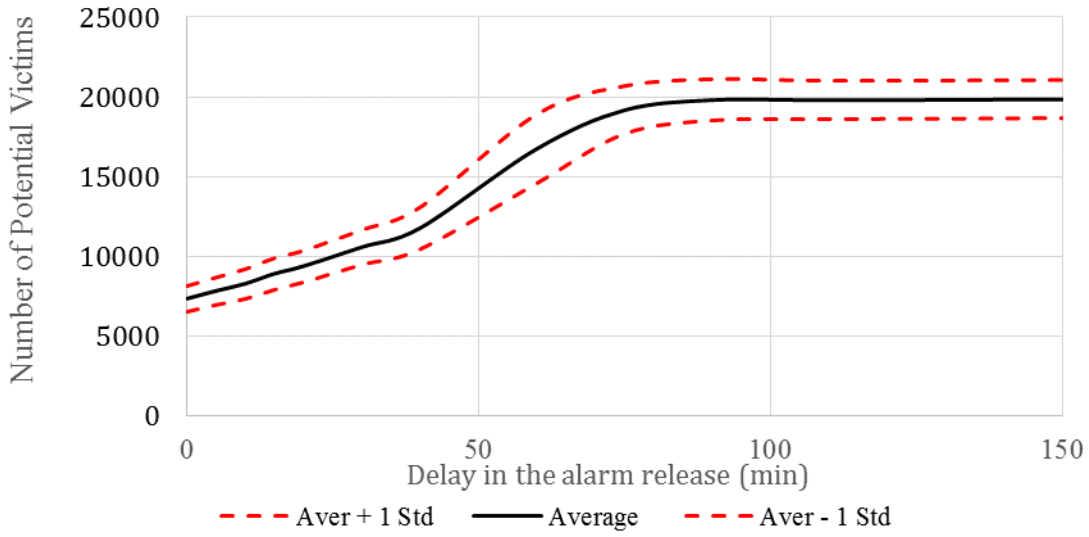

Figure 90: Number of people killed for different alarm time lapses after initiated the GLOF.

Another case analyzed is the case in which the alarm is not released immediately after the moraine collapses at Palcacocha Lake. The results are shown in figure 82. The number of people killed by the GLOF will double if the alarm is given 50 minutes after the moraine breach process starts and triple is the alarm is released 90 minutes after, which is almost equivalent to not have an EWS at all.

Finally using the modified mobilization curve from Figure 75 the number of people killed by a GLOF reduces from 7344 in average to 2865 people in an average with a standard deviation of 462. This last result highlights the importance that training and information dissemination to how to react in an emergency situation has in the success of an EWS

3.6 CONCLUSIONS

In this Chapter, a GLOF from Palcacocha Lake affecting the city of Huaraz was simulated. The GLOF is triggered by an avalanche that generates a wave, which overtops and erodes the terminal moraine releasing more than 15 million of cubic meters of water. Empirical equations were used combined with Hec-RAS dam breaking module to generate the hydrographs resulting in the moraine breaching process. Uncertainty in the peak flow calculation was also included. The inundation is model using FLO-2D. The results indicate that the flow takes about one hour after the GLOF process starts, at the lake, to arrive at the city, and the maximum peak arrives six to eight minutes later. The inundation crosses the city from east to west in around 20 minutes expanding to the north and south as it progresses through the city. Approximately 40646 people live in the inundation area.

Using the flow simulation and the Peru Census 2007, a map of vulnerability was generated. This Map indicates that the most vulnerable areas are near to the river, especially where the Quilcay River meets with Santa River, which is explained by the high population density, high SOVI index and the high inundation intensity.

Finally using an adaptation of the LIFESim methodology, the number of people that can be killed by a GLOF from Palcacocha Lake was calculated. A second scenario in which a siren system is installed as an EWS was calculated as well as a scenario that assumes that the population is more prepared to escape when they received the alarm. In the scenario with no EWS, the expected life loss is 19773 people with a standard deviation of 1191 people. Considering that an EWS is installed and the alarm is released as soon as the GLOF process starts, the expected life loss number reduces to 7344 people

with a standard deviation of 1446 people. Finally, if the evacuation curve is improved the expected life loss reduces to 2865 people in average with a standard deviation of 462.

The results of this work involve a high number of people that can be killed if a GLOF event occurs in Huaraz; therefore, it is pertinent to mention the restrictions that are involved in this work (Table 42).

Table 42: List of assumptions and restrictions that are involved in this work.

Variable	Description
Probability of occurrence	There is not enough information to calculate the probability of occurrence of GLOF events; therefore this work was limited to estimate the extension of an inundation and the number of people that may be killed by the event given that a GLOF happens.
Moraine breach	There is not information of the composition of the moraine. In this work the worst scenario was analyzed, which considers that whole moraine height can breach. This could be overestimating the real problem.
Sediment concentration	This parameter is important for the inundation in Huaraz because it affects the volume of the flow, and consequently the area inundated. In this work, a fixed concentration of 50% by volume was used, which is a good upper limit according to the literature, but it may be too big if the solid material available for erosion is not sufficient in the inundation path.
Buildings blocking the flow	Although the model FLO-2D allows including building and obstacles that can affect the inundation trajectory, it was not clear in this work if the building were strong enough to support the impact and, therefore, deviate the flow. In some areas, it is highly probable that the flow will destroy the buildings especially near the river, but far from the river that may be more difficult to happen. On the other hand, in this work an area reduction factor of 20% was included in the areas with buildings. Also, the debris generated by the building can change the rugosity coefficient.
Census from 2007	The census information is almost 7 years old, so it may out of date. Ideally this work should have been done with more recent information.
Number of flats	The census available does not have the information related to the number of flats, so the vertical evacuation could not be calculated.
Mobilization and evacuation curves	The mobilization and evacuation curves are not locally adjusted. This is also a limitation of the LIFESim model. Ideally the calculations include curves that are calibrated to the condition of Huaraz.
Evacuation transport	This work considers walking as the only way to evacuate. It would have been ideal to include cars as well.

Table 42 (Continued)

Variable	Description
Building materials	The material classification needs to be revised and calibrated with surveys since the census information may be too general.
Damage curves	The damage curves used in this work were not created for the Peruvian standards; consequently they need to be adjusted with local data. Also it would be good to include other methodologies such as the U.S. Corp of Engineering methodologies.
Evacuation routes	The evacuation routes need to be design in the field in consultation with the local authorities and communities. In this work they were extracted manually from the maps using GIS.
People evacuated but not leave safe area	The calculation does not consider the case in which a person evacuates, but meets the inundation when it is walking to a safe area. Also, it considers that if a person cannot walk to a safe area before the water reaches its building, that person never leave the building.
Differences in social vulnerability	The evacuation module does not consider the differences between one group of people and other within the city of Huaraz.

Chapter 4: Conclusions

4.1 RESEARCH SUMMARY AND OBJECTIVES

Through this research we apply a logic process using scarce available data in order to generate information that could help in the analysis of GLOF risk at Imja Lake and Palcacocha Lake. The objectives of this dissertation research are to:

1. Generate basic physical information that allows us to understand and model potential GLOF events from Imja Lake predicting future conditions.
2. Evaluate the effectiveness of an UNDP proposal to reduce Imja Lake risk lowering the lake by 3 meters.
3. Quantify the magnitude of a potential GLOF from Lake Palcacocha in Peru and map the vulnerability using INDECI framework.
4. Evaluate the benefits of an early warning system (EWS) in the risk reduction in Huaraz including uncertainty analysis

4.2 DISCUSSION

4.2.1 Objective 1

The objective 1, to generate basic physical information that allows to understand and model potential GLOF events from Imja Lake predicting future conditions was addressed in the first part of Chapter 2. One of the main problem of working in remote areas of Nepal such as Imja Lake near Mount Everest is the data scarcity, which is a consequence of the distance and difficulties to get to the lake and the natural difficulties

of working in areas above 5000 m.a.s.l. Imja Lake was visited three times. In the first one in September 2011, data were not collected but the lake was inspected, and discussions were held with other researchers and experts in lake safety related to the issues that it needs to be addressed. As a result the lake was visited again on May 2012, after visiting Tama Pokhari where a GLOF occurred in 1998, to collect GPR data on the terminal moraine with the idea of clarifying how extensive was the ice underneath the terminal moraine. Originally it was planned to set a model to know the resistant of the moraine to water static pressure and liquefaction due to earthquake knowing that the lake is likely to join the outlet lakes, which is expanding continuously. Unfortunately, there were not enough good data to map the moraine ice core, so the moraine soil mechanic model was disregard. Additionally some short GPR transects were taken at the glacier that fortunately show that the GPR equipment was suitable for measuring the depth of the glacier. On September 2012 visit to Imja Lake using sonar equipment, mounted in a rafting boat; a bathymetry survey was performed to update the previous successful bathymetry from 2002. Due to calving processes the glacier lost a considerable amount of mass that was floating in the lake, and it was impossible to reach the end of the lake at the east side, so several assumption had to be made related to the ice ramp underneath in order to calculate the final lake volume. The results of the 2012 bathymetric survey of Imja Lake show that the lake deepened from 98 m in 2002 to 116 m in 2012. Likewise, the volume has increased from 35.8 million m3 to 61.6±1.8 million m3 over the past decade as well, 70 percent increase. The lake volume is increasing at a rate of 2.51 million m^3/yr., and the average depth is increasing by 0.86 m/yr. Additionally, a GPR survey at Imja and Lhotse-Shar glaciers were performed from north to south obtaining a

good transect, which shows the thickness of the glacier. The thickness of the glacier varies from 40-60 m thick near the lateral moraines to over 200 m thick in the center of the glacier. The GPR results indicate that the lake potentially can be expanded his length many hundreds of meters increasing his volume, which means that in the future the lake can release more water in a potential GLOF.

The importance of the information collected is that in order to set an inundation model a basic parameter to know is the volume of the water available for the inundation or potential GLOF water (PGW). If the lake is dangerous with the current conditions, it is an open discussion, and in this work the discussion was expanded to a future scenario. Statistically, the major dam trigger is avalanches of ice or rock that generate waves that overtop the terminal moraine producing the failure. The data shows that the glacier continues retreating at a rate of 45-50 m/year expanding the lake to the east side where steep hills are located. With the GPR data collected, it was showed that the glacier is depth enough that the lake will stop growing when:

1) The glacier stop retreating, which won't happen according with the data available or

2) When the lake reaches the hills so the glacier will hang that will increase the risk of avalanches falling into the lake.

Therefore, the first objective was successfully answered, with the information collected it was possible to generate a conceptual model that allows setting an inundation model to answer the second objective.

4.2.2 Objective 2

The objective 2, to evaluate the effectiveness of a UNDP proposal to reduce Imja Lake risk lowering the lake by 3 meters was addressed in the second part of Chapter 2. With the conceptual model of Imja Lake and Imja, Lotse-Shar Glaciers a 2 dimensional model was set to simulate a potential GLOF. The village of Dingboche was used as a point of comparison for the different scenarios. The project proposed by the government of Nepal and UNDP seeks to lower the lake by three meters. The goal was to show in a map how much the inundation will be reduced by the project or in case the reduction was not sufficient, how much the lake should be lowered. Four scenarios were considered: no lowering (current conditions), lowering the lake 3 meters (UNDP project), lowering the lake by 10 meters and lowering the lake by 20 meters. Additionally, two future scenarios were created in which the lake reach an area of 2 km^2. The first one keeps the current water elevation, and the second has a 20 m lower lake elevation.

This work proves that the project proposed by UNDP and the government of Nepal of lowering the lake by three meters does not show any considerable reduction in the inundation at Dingboche compared to the scenario in which the lake is not lowered. Lowering the lake by 10 and 20 meters reduce the inundation area. In consultation with the local communities, the idea of risk reduction for them means that a GLOF should not inundate any land. The only scenario that reduces the inundation to that level is the one in which the lake water level is lower by 20 meters. Additionally, the same inundation area is obtained for the future scenario with 20 m lower lake model. Therefore, lowering the lake by 20 meters is a scenario that will reduce the risk to the levels that the communities expect for the actual lake conditions and future lake conditions.

Finally, this work proved that lowering the lake by three meters will conduct to the same mistake that was made in the project at Tsho Rolpa Lake. A considerable amount of money will be spent to carry out this work with no effective risk reduction for the communities and the fragile ecosystem downstream the lake. In this work is proposed that the lake should be lowered by 20 meters, which answers objective 2.

4.2.3 Objective 3

Objective 3, to quantify the magnitude of a potential GLOF from Lake Palcacocha in Peru and map the vulnerability using INDECI framework was addressed in Chapter 3. There is a consensus in the local authorities, scientist and specialist in risk that Palcacocha Lake represents an imminent risk of GLOF. There is a previous experience from 1941 when Palcacocha Lake burst killing more than 5000 people. However, there was not a model that shows the extension of the inundation with the current size of the lake. With the support of the Peruvian Ministry of Environment and the Inter-American Development Bank, it was possible to generate high resolution topographic information for the model. A GLOF that is trigger by an avalanche into the lake was simulated. Empirical equations were used putting especial attention to the uncertainty of such equations. In the sensitivity analysis it is possible to see the inundation is more sensitive to the breaching process than the roughness coefficient or the sediment concentration. For the moraine breach, Hec-RAS model was used and for the inundation the FLO-2D model was used. The results indicate that the flow takes about one hour after the GLOF process starts, at the lake, to arrive at the city, and the maximum peak arrives six to eight minutes later. The inundation crosses the city from east to west in around 20 minutes expanding to

the north and south as it progresses through the city. Approximately 40646 people live in the inundation area.

For the vulnerability analysis, the INDECI framework was used. The INDECI approach combined the population density, building material's resistance, intensity of the inundation and the SOVI Index. A map of vulnerability was generated. This map indicates that the areas more vulnerable are near to the river, especially where the Quilcay River meets with Santa River, which is explained by the high population density, high SOVI index and the high inundation intensity.

This research generated information that allows mapping the vulnerability in Huaraz using physical and social information addressing objective 3.

4.2.4 Objective 4

Objective 4, to evaluate the benefits of an early warning system (EWS) in the risk reduction in Huaraz including uncertainty analysis was addressed in Chapter 3. One of the motivations to work in this objective was the possibility that the 1941 GLOF, which killed more than 5000 people, could be repeated. Consequently, it was thought that the final result for this work needed to be a quantification of the impacts that a GLOF could have in Huaraz generating information that allows to implement public policies to reduce GLOF related risks. Ideally, the frequency of GLOFs needed to be calculated; however, that was not possible due to the lack of data available. Therefore, the work was restricted to answer what the expected losses would be if a GLOF were to occur. Inundation calculations were intercepted with the information from the Peru Census 2007 using LIFESim methodology. The case in which the population does not receive a warning

alarm was analyzed so the mortality rate is dependent mainly on the protection that building can provide. The calculation shows that 19733 people with a standard deviation of 1191 people could die under these conditions. Then the effects of early warning system were calculated. The results indicate that the EWS reduces the expected life loss number to 7344 people with a standard deviation of 1446 people. Finally using the same assumption but improving the mobilization curve, in which now it is assumed that 100% of the people would leave the risk area in less than 1 hour after they internalize the alarm. The expected number of life decreases to 2865 people in average with a standard deviation of 462. This calculation shows the effectiveness of an EWS and the necessity of implementing the system with an associated plan of training for the people living in Huaraz to reduce the risk addressing objective 4.

4.3 FUTURE WORK

The work done in both, Peru and Nepal, represents a big step forward to understand the impacts from potential GLOFs from Imja Lake in Nepal and Palcacocha Lake in Peru. However, the work in both locations has a major deficiency, which is the probability of occurrence calculation for GLOF events. Although, it was part of the goals of this work when it started a couple of years ago, the little or non-available data related to the frequency of GLOF events made impossible to calculate, for example, returning period. Also, it is important to think in how these events are going to evolve as the temperatures in high elevation continue increasing. Statistically the main trigger of moraine dam breaks is the overtopping due to waves generated from avalanches of rock and ice. As the temperature increases these events are going to be more frequent,

however there is not reliable information in Nepal nor Peru that allows to undertake such calculation. Consequently, it is important to consider in a future work the calculation of the avalanche of ice/rock probability of occurrence that allows knowing the probability that an event of certain size occurs in a given period of time.

Another component that needs to be studied with more attention is the probability of moraine failure given that the moraine is overtopped. In this work, it was analyzed a case in which a GLOF is generated at the lake by breaching the moraine when this is overtopped by a wave. However, a remaining question from this work is, when and how a moraine would breach, what is the flow that needs to overtop a moraine to make it fail and what is the probability that the moraine will collapse. This is important because then the probability of a trigger (i.e. avalanche) can be combined with the probability of failure to obtain the total GLOF probably of occurrence. Having the total probability will allow to carry out a full risk analysis study.

The two tasks described in the previous two paragraphs are the most difficult remaining tasks. However, there are many other components that need to be studied in more details. For example in Nepal, it is not clear what communities are going to be affected by a GLOF, except for Dingboche village. Therefore, it is important to generate information that allows decision makers to quantify the real impacts that a GLOF would have in order to justify the projects that can help to reduce the risk from Imja Lake. Also, it is important to generate digital elevation model with better resolution and accuracy that allows extending the inundation simulation downstream.

In Peru the life risk assessment needs to be refined, especially because the results indicate that a GLOF could kill almost 4 times more people than the previous event in

1941. It is necessary to generate information that can apply to Huaraz. For example, it is important to generate evacuation curves with local data. Also, it is important to spread this first approximation to the problem to the local organizations in Huaraz in order to define evacuation routes. This process will become iterative since once the population and authorities learn from this work, the information and procedures will be probably improved so the calculations will need to be done again with the updated data. The new results will start a new process of diffusion improving even further the population preparedness.

Appendix

APPENDIX A: FLO-2D

The conservation of mass equation solved in FLO-2D is

$$\frac{\partial h}{\partial t} + \frac{\partial (hV)}{\partial x} = i \tag{A1}$$

And the conservation of linear momentum equation is

$$S_f = S_o - \frac{\partial h}{\partial x} - \frac{V}{g}\frac{\partial V}{\partial x} - \frac{1}{g}\frac{\partial V}{\partial t} \tag{A2}$$

Where h (m) is the flow depth, V (m/s) is the depth-averaged velocity in one of the flow directions, i is the excess rainfall intensity (m/s), S_f is the friction slope, S_o is the bed slope. We are considering the effects of sediments; consequently, the characteristics of sediment and its concentration in the fluid are included. Thus the total friction slope can be expressed as (Flo-2, 2012; Julien 2010; O'Brien *et al*. 1993)

$$S_f = S_y + S_v + S_{td} = \frac{\tau_y}{\gamma_m h} + \frac{K\eta\omega}{8\gamma_m h^2} + \frac{n^2\omega^2}{h^{4/3}} \tag{A3}$$

where S_y is the yield slope, S_v is the viscous slope, S_{td} is the turbulent-dispersive slope, τ_y is the Mohr Coulomb yield stress, γ_m is the specific weight of the sediment mixture, K is the resistance parameter (K = 2,285 for urban studies (Flo-2D 2012)), η is the Bingham dynamic viscosity, ω is the depth-averaged velocity, n is the Manning roughness coefficient.

Rheological properties, Bingham dynamic viscosity (η) and Mohr Coulomb yield stress (τ_y), can be formulated as exponential functions of the sediment volume concentration (Julien and Leon 2000; Julien 2010). The yield stress and the dynamic viscosity are represented as

$$\eta = \alpha_2 e^{\beta_2 c_v} \tag{A4}$$

$$\tau_y = \alpha_1 e^{\beta_1 c_v} \quad \text{(A5)}$$

where α_i and β_i are empirical coefficients defined by laboratory experiment (FLO-2D 2012).

Although the geometry of the grid within the Flo-2D model is two dimensional, the flow is modeled in eight directions and it solves the one-dimensional equation in each direction. Each velocity computation is essentially one-dimensional in nature and is solved independently of the other seven directions. The continuity and momentum equations are solved with a central, finite difference method with an explicit time-stepping scheme, which uses a Courant-Friedrich-Lewy (CFL) condition for numerical stability. The CFL condition relates the flood wave celerity to the model time and spatial increments. The physical interpretation of the CFL condition is that a particle of fluid should not travel more than one spatial increment in one time step (Flo-2D 2012).

$$\Delta t = \frac{C\Delta x}{\beta V + c} \quad \text{(A6)}$$

Where C is the Courant number ($C \leq 1.0$), Δx is the square grid element width, V is the computed average cross section velocity, β is a coefficient (5/3 for a wide channel), and c is the computed wave celerity.

References

Aboelata M, Bowles DS (2005) LIFESim: A Model for Estimating Dam Failure Life Loss. 1–274.

Aboelata M, Bowles DS, McClelland DM (2003) A model for estimating dam failure life loss. Aust. Comm. Large Dams Risk Work.

Adger W (2006) Vulnerability. Glob Environ Chang 16:268–281. doi: 10.1016/j.gloenvcha.2006.02.006

Armstrong RL (2010) Melting Glaciers: Current Status and Future Concerns. Europe 1850:1–20.

Awal R, Nakagawa H, Fujita M, et al. (2010) Experimental Study on Glacial Lake Outburst Floods Due to Waves Overtopping and Erosion of Moraine Dam. Annu. Disas. Prev. Res Inst. Kyoto Univ.

Bajracharya B, Shrestha AB, Rajbhandari L (2007a) Glacial Lake Outburst Floods in the Sagarmatha Region. Mt Res Dev 27:336–344. doi: 10.1659/mrd.0783

Bajracharya B, Uddin K (2010) Study of Land Cover Dynamics in Sagarmatha National Park and Buffer Zone. 10th Int. Symp. High Mt. Remote Sens. Cartogr. pp 125–132

Bajracharya SR, Mool P (2009) Glaciers, glacial lakes and glacial lake outburst floods in the Mount Everest region, Nepal. Ann Glaciol 50:81–86.

Bajracharya SR, Mool PK, B. R. Shrestha (2007b) Impact of climate change on Himalayan glaciers and glacial lakes: Case studies on GLOF and associated hazards in Nepal and Bhutan. 127.

Bajracharya SR, Mool PK, Shrestha BR (2008) Global Climate Change and Melting of Himalayan Glaciers. Sci York 28–46.

Ball GH, Hall DJ (1965) ISODATA, a novel method of data analysis and pattern classification. Menlo Park, Ca.

Barnett TP, Adam JC, Lettenmaier DP (2005) Potential impacts of a warming climate on water availability in snow-dominated regions. Nature 438:303–9. doi: 10.1038/nature04141

Bell WW, Donich T, Groves KL, Sytsma D (2000) Tsho Rolpa GLOF Warning System Project. Proc. 28th IAHR Congr.

Benn DI, Bolch T, Hands K, et al. (2012) Response of debris-covered glaciers in the Mount Everest region to recent warming, and implications for outburst flood hazards. Earth-Science Rev 114:156–174. doi: 10.1016/j.earscirev.2012.03.008

Benn DI, Warren CR, Mottram RH (2007) Calving processes and the dynamics of calving glaciers. Earth-Science Rev 82:143–179. doi: 10.1016/j.earscirev.2007.02.002

Benn DI, Wiseman S, Hands KA (2001) Growth and drainage of supraglacial lakes on debris-mantled Zgozumpa glacier, Khumbu Himal, Nepal. J. Glaciol. 47:

Bolch T, Buchroithner MF, Peters J, et al. (2008) Identification of glacier motion and potentially dangerous glacial lakes in the Mt. Everest region/Nepal using space borne imagery. Nat Hazards Earth Syst Sci 8:1329–1340. doi: 10.5194/nhess-8-1329-2008

Bolch T, Kulkarni A, Kääb A, et al. (2012) The state and fate of Himalayan glaciers. Science (80-) 336:310–314.

Bolch T, Pieczonka T, Benn DI (2011) Multi-decadal mass loss of glaciers in the Everest area (Nepal Himalaya) derived from stereo imagery. Cryosph 5:349–358. doi: 10.5194/tc-5-349-2011

Bradley RS, Vuille M, Diaz HF, Vergara W (2006) Threats to Water Supplies in the Tropical Andes. Science (80-) 312:1755–1756.

Budhathoki KP, Bajracharya OR, Pokharel BK (2010) Assessment of Imja Glacier Lake outburst Flood (GLOF) risk in Dudh Koshi river basin using remote Sensing Techniques. J Hydrol Meteorol 7:75–91.

Byers A (1987) Geoecological Study of Landscape Change and Man-accelerated Soil Loss: The Case of the Sagarmatha (Mt. Everest) National Park, Khumbu, Nepal. 354.

Byers AC (2007) An assessment of contemporary glacier fluctuations in Nepal's Khumbu Himal using repeat photography. Himal J Sci 4:21–26. doi: 10.3126/hjs.v4i6.979

Byers AC, McKinney DC, Somos-Valenzuela M, et al. (2013) Glacial lakes of the Hinku and Hongu valleys, Makalu Barun National Park and Buffer Zone, Nepal. Nat Hazards 69:115–139. doi: 10.1007/s11069-013-0689-8

Calvo B, Savi F (2009) A real-world application of Monte Carlo procedure for debris flow risk assessment. Comput Geosci 35:967–977. doi: 10.1016/j.cageo.2008.04.002

Carey M (2010) In the Shadow of Melting Glaciers: Climate Change and Andean Society. Oxford Univ. Press, New York, NY

Carey M (2005) Living and dying with glaciers: people's historical vulnerability to avalanches and outburst floods in Peru. Glob Planet Change 47:122–134.

Carey M, Huggel C, Bury J, et al. (2012) An integrated socio-environmental framework for glacier hazard management and climate change adaptation: lessons from Lake 513, Cordillera Blanca, Peru. Clim Change 112:733–767. doi: 10.1007/s10584-011-0249-8

Carey M, Huggel C, Bury J, et al. (2011) An integrated socio-environmental framework for glacier hazard management and climate change adaptation: lessons from Lake 513, Cordillera Blanca, Peru. Clim Change 112:733–767. doi: 10.1007/s10584-011-0249-8

Carrivick JL (2006) Application of 2D hydrodynamic modelling to high-magnitude outburst floods: An example from Kverkfjöll, Iceland. J Hydrol 321:187–199. doi: 10.1016/j.jhydrol.2005.07.042

Casassa G, López P, Pouyaud B, Escobar F (2009) Detection of changes in glacial run-off in alpine basins: examples from North America, the Alps, central Asia and the Andes. Hydrol Process 23:31–41. doi: 10.1002/hyp.7194

Catania G, Hulbe C, Conway H (2010) Grounding-line basal melt rates determined using radar-derived internal stratigraphy. J Glaciol 56:545–554. doi: 10.3189/002214310792447842

Cenderelli D, Wohl E (2001) Peak discharge estimates of glacial-lake outburst floods and "normal" climatic floods in the Mount Everest region, Nepal. Geomorphology 40:57–90. doi: 10.1016/S0169-555X(01)00037-X

Chander G, Markham B (2003) Revised landsat-5 tm radiometric calibration procedures and post calibration dynamic ranges. IEEE Trans Geosci Remote Sens 41:2674–2677. doi: 10.1109/TGRS.2003.818464

Chander G, Markham BL, Helder DL (2009) Summary of current radiometric calibration coefficients for Landsat MSS, TM, ETM+, and EO-1 ALI sensors. Remote Sens Environ 113:893–903. doi: 10.1016/j.rse.2009.01.007

Chen Y, Xu C, Chen Y, et al. (2010) Response of glacial-lake outburst floods to climate change in the Yarkant River basin on northern slope of Karakoram Mountains, China. Quat Int 226:75–81. doi: 10.1016/j.quaint.2010.01.003

Chikita K, Joshi S, Jha J, Hasegawa H (2000) Hydrological and thermal regimes in a supraglacial lake: Imja, Khumbu, Nepal Himalaya. Hydrol Sci J 45:507–522.

Chow VT (1959) Open Channel Hydraulics. The Blackburn Press, Caldwell, New Jersey, USA

Clague J, Evans S (2000) A review of catastrophic drainage of moraine-dammed lakes in British Columbia. Quat Sci Rev 19:2763–1783.

Coudrain A, Francou B, Kundzewicz Z (2005) Glacier shrinkage in the Andes and consequences for water resources-Editorial. Hydrol Sci J 50:925–932. doi: 10.1623/hysj.2005.50.6.925

Cox JH (1999) An assessment of habitats and human interaction in the Hinkhu, Hongu, Kasuwa and Barun Kholas of Makalu-Barun National Park and Conservation Area. Kathmandu: Makalu Barun Conservation Project.

Cutter SL (1996) Vulnerability to environmental hazards. Prog Hum Geogr 20:529–539. doi: 10.1177/030913259602000407

Cutter SL, Boruff BJ, Shirley WL (2003) Social Vulnerability to Environmental Hazards. Soc Sci Queartely 84:242–161.

Cutter SL, Finch C (2008) Temporal and spatial changes in social vulnerability to natural hazards. Proc Natl Acad Sci U S A 105:2301–6. doi: 10.1073/pnas.0710375105

Davis JL, Annan AP (1989) Ground-penetrating radar for high resolution mapping of soil and rock stratigraphy. Geophys Prospect 37:531–551.

Diario la Republica (2010) La republica. Retrieved 04 24, 2010, <www.larepublica.pe/regionales/20/04/2010/declaran-en-emergencia-la-laguna-palcacocha-en-huaraz>.

Emmer A, Vilímek V (2013) Review Article: Lake and breach hazard assessment for moraine-dammed lakes: an example from the Cordillera Blanca (Peru). Nat Hazards Earth Syst Sci 13:1551–1565. doi: 10.5194/nhess-13-1551-2013

Emmer A, Vilímek V (2014) New method for assessing the potential hazardousness of glacial lakes in the Cordillera Blanca, Peru. Hydrol Earth Syst Sci Discuss 11:2391–2439.

Eriksson M, Jianchu X, Shrestha A, et al. (2009) The changing Himalayas – Impact of climate change on water resources and livelihoods in the Greater Himalayas. Perspectives on water and climate change adaptation. 5th World Water Forum

Eriksson M, Xu J (2008) Climate Change Impact on the Himalayan Water Tower. Stock Water Front A Forum Glob Water 2:11–12.

Fekete A (2009) Validation of a social vulnerability index in context to river-floods in Germany. Nat Hazards Earth Syst Sci 9:393–403. doi: 10.5194/nhess-9-393-2009

Fiebiger G (1997) Hazard Mapping in Austria. J Torrent, Avalanche, Landslide Rockfall Eng 61:153–164.

Fischer L, Huggel C, Kääb A, Haeberli W (2013) Slope failures and erosion rates on a glacierized high-mountain face under climatic changes. Earth Surf Process Landforms n/a–n/a. doi: 10.1002/esp.3355

Fischer L, Purves RS, Huggel C, et al. (2012a) On the influence of topographic, geological and cryospheric factors on rock avalanches and rockfalls in high-mountain areas. Nat Hazards Earth Syst Sci 12:241–254. doi: 10.5194/nhess-12-241-2012

Fischer L, Purves RS, Huggel C, et al. (2012b) On the influence of topographic, geological and cryospheric factors on rock avalanches and rockfalls in high-mountain areas. Nat Hazards Earth Syst Sci 12:241–254. doi: 10.5194/nhess-12-241-2012

FLO-2D (2012) Flo-2D Pro Reference Manual.

FLO-2D (2009) FLO-2D reference manual. 1–69.

Forzieri G, Degetto M, Righetti M, et al. (2011) Satellite multispectral data for improved floodplain roughness modelling. J Hydrol 407:41–57. doi: 10.1016/j.jhydrol.2011.07.009

Forzieri G, Moser G, Vivoni ER, et al. (2010) Riparian Vegetation Mapping for Hydraulic Roughness Estimation Using Very High Resolution Remote Sensing Data Fusion. J Hydraul Eng 136:855–867. doi: 10.1061/(ASCE)HY.1943-7900.0000254

Fread DL, Lewis JM (1998) NWS FLDWAV Model, Theoretical Development, User Document. Silver Spring, MD

Froehlich DC (1995) Peak Outflow from Breached Embankment Dam. J Water Resour Manag 121:90–97.

Fuchs S, Birkmann J, Glade T (2012) Vulnerability assessment in natural hazard and risk analysis: current approaches and future challenges. Nat Hazards 64:1969–1975. doi: 10.1007/s11069-012-0352-9

Fuchs S, Heiss K, Hübl J (2007) Towards an empirical vulnerability function for use in debris flow risk assessment. Nat Hazards Earth Syst Sci 7:495–506. doi: 10.5194/nhess-7-495-2007

Fujita K, Sakai A, Nuimura T, et al. (2009) Recent changes in Imja Glacial Lake and its damming moraine in the Nepal Himalaya revealed by in situ surveys and multi-temporal ASTER imagery. Environ Res Lett 4:045205 (7pp). doi: 10.1088/1748-9326/4/4/045205

Fushimi H, Ikegami K, Higuchi K, Shankar K (1985) Nepal case study: catastrophic floods. AHS Publ 149:125–130.

Gades A, Conway H, Nereson N, et al. (2000) Radio echo-sounding through supraglacial debris on Lirung and Khumbu Glaciers , Nepal Himalayas. Debris-Covered Glaciers. IAHS, Seattle, Washington, USA, pp 13–22

Gallopín GC (2006) Linkages between vulnerability, resilience, and adaptive capacity. Global Environmental Change. Glob Environ Chang 16:293–303.

Garcia R, Lopez J. (2005) Debris Flows of December 1999 in Venezuela. Chapter 20th Debris-flow Hazards Relat. Phenomena. Jakob, Matthias, Hungr, Oldrich Eds. Springer Verlag Praxis, Berlin.

Garcia R, López JL, Noya M, et al. (2003) Hazard mapping for debris flow events in the alluvial fans of northern Venezuela.pdf. "Hazard Mapp. debris flow events Alluv. fans North. Venez. Third Int. Conf. Debris-Flow Hazards Mitig. Mech. Predict. Assessment. Davos, Switzerland. Sept. 10-12

García R, López JL, Noya ME, et al. (2002) “Hazard maps for mud and debris flow events in Vargas State and Caracas.” Avila Project Report. Caracas, Venezuela, (In Spanish).

Gardner AS, Moholdt G, Cogley JG, et al. (2013) A Reconciled Estimate of Glacier Contributions to Sea Level Rise: 2003 to 2009. Science (80-) 340:852–857. doi: 10.1126/science.1234532

Georges C (2004) 20th-Century Glacier Fluctuations in the Tropical Cordillera Peru Glacier Fluctuations. Arctic, Antarct Alp Res 36:100–107.

Goldenberg S (2011) Glacier lakes: Growing danger zones in the Himalayas, Guardian. <http//www.guardian.co.uk/environment/2011/oct/10/glacier-lakes-melt-himalayas (last accessed 27 July 2012)>

Gov. Pro. Huaraz (2005) Ordenanza municipal #3-2005-GPH.

Grabs WE, Hanisch J (1993) Objectives and Prevention Methods for Glacier Lake Outburst Moods (GLOFs). Snow Glacier Hydrol. IAHS, Kathmandu, pp 341–352

Grabs WE, Hanisch J (1992) Objectives and Prevention Methods for Glacier Lake Outburst Moods (GLOFs). Snow Glacier Hydrol 218:341–352.

Graham WJ (1999) "A procedure for estimating loss of life caused by dam failure" Rep. No. DSO-99-06. 1–46.

Graham WJ (2009) A comparison of methods for estimating loss of life from dam failure. Manag. Our Water Retent. Syst. Cover. 29th Annu. USSD Conf. April 20-24, 2009. USSD-U.S. Society on Dams, Nashville, Tennessee, pp 1143–1166

Haeberli W (1983) Frequency and characteristics of glacier floods in the Swiss Alps. Ann Glaciol 4:85–90.

Haeberli W (2013) Mountain permafrost — research frontiers and a special long-term challenge. Cold Reg Sci Technol 96:71–76. doi: 10.1016/j.coldregions.2013.02.004

Haeberli W, Clague JJ, Huggel C, Kääb A (2010) Hazards from lakes in high-mountain glacier and permafrost regions : Climate change effects and process interactions. Av. la Geomorfol. en España 2008-2010 XI Reun. Nac. Geomorfol. Solsona 2010

Haeberli W, Somos-Valenzuela M, Portocarrero C (2013) Glacial lakes and emerging risks in the Cordillera Blanca. High Mountain Glacial Watershed Program's Community of Practice conference "Managing Climate Change in High Mountain Glacial Watersheds: Promoting Social, Scientific, and Institutional Collaborati.

Hagen T, Dyrenfurth GO, Von Fiirer-Haimendorf, C. Schneider E (1963) Mount Everest: Formation, Population and Exploration of the Everest Region. Oxford University Press, London.

Hamandawana H, Eckardt F, Ringrose S (2006) The use of step-wise density slicing in classifying high-resolution panchromatic photographs. Int J Remote Sens 27:4923–4942. doi: 10.1080/01431160600857436

Hambrey MJ, Quincey DJ, Glasser NF, et al. (2008) Sedimentological, geomorphological and dynamic context of debris-mantled glaciers, Mount Everest (Sagarmatha) region, Nepal. Quat Sci Rev 27:2361–2389. doi: 10.1016/j.quascirev.2008.08.010

Hammond J (1988) Glacial lakes in the Khumbu region, Nepal: An assessment of the hazards. MA Thesis. University of Colorado, Boulder, CO.

Hegglin E, Huggel C (2008) An Integrated Assessment of Vulnerability to Glacial Hazards. Mt Res Dev 28:299–309. doi: 10.1659/mrd.0976

Horizons - Horizons South America S.A.C (2013) Informe Técnico del Proyecto, Consultoría Para El Levantamiento Fotogramétrico Detallado De La Sub Cuenca Del Río Quillcay Y La Ciudad De Huaraz Para El Proyecto, Implementación de Medidas de Adaptación al Cambio Climático y Gestión de Riesgos en la Sub-c.

Horritt MS, Bates PD (2002) Evaluation of 1D and 2D numerical models for predicting river flood inundation. J Hydrol 268:87–99. doi: 10.1016/S0022-1694(02)00121-X

Hossain AKMA, Jia Y, Chao X (2009) Estimation of Manning's roughness coefficient distribution for hydrodynamic model using remotely sensed land cover features. 2009 17th Int. Conf. Geoinformatics. IEEE, pp 1–4

Huggel C, Haeberli W, Kääb A, et al. (2004) An assessment procedure for glacial hazards in the Swiss Alps. Can Geotech J 41:1068–1083. doi: 10.1139/t04-053

Huggel C, Kääb a., Haeberli W, Krummenacher B (2003) Regional-scale GIS-models for assessment of hazards from glacier lake outbursts: evaluation and application in the Swiss Alps. Nat Hazards Earth Syst Sci 3:647–662. doi: 10.5194/nhess-3-647-2003

Huggel C, Kääb A, Haeberli W, et al. (2002) Remote sensing based assessment of hazards from glacier lake outbursts : a case study in the Swiss Alps. Can Geotech J 39:316–330. doi: 10.1139/T01-099

Huggel C, Salzmann N, Allen S, et al. (2010) Recent and future warm extreme events and high-mountain slope stability. Philos Trans R Soc A Math Phys Eng Sci 368:2435–2459.

Huss M (2011) Present and future contribution of glacier storage change to runoff from macroscale drainage basins in Europe. Water Resour Res 47:n/a–n/a. doi: 10.1029/2010WR010299

ICIMOD (2011) Glacial Lakes and Glacial Lake Outburst Floods in Nepal. Kathmandu

ICIMOD (2009) Adaptation to climate change impacts and regional cooperation on water and hazards in the Himalayan region. Kathmandu, Nepal

INDECI (2006) Manual basico para la estimacion del riesgo.

Instituto Nacional de Defensa Civil (2011) Informe de peligro N°003-12/05/2011/COEN-SINADECI/ 15:00 horas (Informe N° 01): Peligro por aluvión en el departamento de Ancash. Huaraz-Peru: COEN-SINADECI. 1–15.

Ionescu C, Klein RJT, Hinkel J, et al. (2005) Towards a Formal Framework of Vulnerability to Climate Change. NeWater Working Paper 2 and FAVAIA Working Paper 1. 24.

IPCC (2001) Climate Change 2001: Impacts, Adaptation and Vulnerability. Contribution of Working Group II to the Third Assessment Report of the Intergovernmental Panel on Climate Change. 1032.

IPCC (2007) Climate Change 2007 : Synthesis Report. 23–73.

ISDR (2004) Living with risk, a global review of disaster reduction initiatives. International Strategy for Disaster Reduction initiatives. 1:457.

Ives JD (1986) Jokulhlaup disasters in the Himalaya and their identification, a case study: The Langmoche Jokulhlaup of 4th August 1985, Khumbu Himal, Nepal. ICIMOD Occasional Paper. Kathmandu: International Centre for Integrated Mountain Development (ICIMOD). (ICIMOD 1.

Ives JD, Shrestha RB, P. K. Mool (2010) Formation of Glacial Lakes in the Hindu Kush-Himalayas and GLOF Risk Assessment. 66.

Julien PY (2010) Erosion and Sedimentation, second edition. 371.

Julien PY, Leon CA (2000) Mud floods, mudlows and debris flows classification, rheology and structural design. Invit. Pap. Int. Work. Mudflows debris flows, Caracas, Venez. Novemb. 27- December 1.

Kääb A (2005) Combination of SRTM3 and repeat ASTER data for deriving alpine glacier flow velocities in the Bhutan Himalaya. Remote Sens Environ 94:463–474.

Kattelmann R (2003) Glacial Lake Outburst Floods in the Nepal Himalaya: A Manageable Hazard ? Nat Hazards 28:145–154.

Kattelmann R, Watanabe T (1998) Approaches to reducing the hazard of an outburst flood of Imja Glacier Lake, Khumbu Himal. Chalise, S.R. and Khanal, N.R. Eds.: Ecohydrology of high mountain areas. ICIMOD. 359–366.

Kattelmann R, Watanabe T (1996) Draining Himalayan glacial lakes before they burst. Destr. V/ater Water-Caused Nat. Disasters, their Abat. Control. Mammoth Lakes, pp 337–343

Khadka NS (2012) Everest Sherpas in glacial lake study warning. BBC News: Science and Environment. September 12, 2012.

Kirkbride (1993) The Temporal Significance of Transitions from Melting to Calving Termini at Glaciers in the Central Souther Alps of New Zealand. The Holocene 3:232–240.

Kirkbride MP, Warren CR (1997) Calving processes at a grounded ice cliff. Ann Glaciol 24:116–121.

Lamsal D, Sawagaki T, Watanabe T (2011) Digital terrain modelling using Corona and ALOS PRISM data to investigate the distal part of Imja Glacier, Khumbu Himal, Nepal. J Mt Sci 8:390–402. doi: 10.1007/s11629-011-2064-0

Lehman W, Needham J (2012) Consequence Estimation for Dam Failures Using HEC-FIA 2.2.

Lenearts J, Angelen J van, van den Broeke M, et al. (2013) (2013) Geophysical Research Letters, 40:1–5. 40 1-5:

Lin P-S, Lee J, Chang C-W (2011) An application of the FLO-2D model to debris-flow simulation- a case study of Song-Her district in Taiwan. 5th Int. Conf. Debris-Flow Hazards "Mitigation, Mech. Predict. Assessment." Padua, Italy, pp 947–956

Linsbauer a., Paul F, Haeberli W (2012) Modeling glacier thickness distribution and bed topography over entire mountain ranges with GlabTop: Application of a fast and robust approach. J Geophys Res 117:F03007. doi: 10.1029/2011JF002313

Luers AL (2005) The surface of vulnerability: An analytical framework for examining environmental change. Glob Environ Chang 15:214–223. doi: 10.1016/j.gloenvcha.2005.04.003

Matambo S, Shrestha A (2011) "World Resources Report Case Study. Nepal: Responding Proactively to Glacial Hazards" World Resources Report, Washington DC. Available online at http://www.worldresourcesreport.org (accessed online 19 October 2011).

McClelland DM, Bowles DS (2002) Estimating life loss for dam safety risk assessment--a review and new approach. 420.

Mool P, Bajracharya S, Joshi S (2001) Inventory of glaciers, glacial lakes, and glacial lake outburst floods: Monitoring and early warning systems in the Hindu Kush-Himalayan region, Nepal. 375.

Mussetter Enginnering Inc. (2009) Cornet Creek watershed and alluvial fan debris flow analysis. 1–58.

Neal A (2004) Ground-penetrating radar and its use in sedimentology: principles, problems and progress. Earth-Science Rev 66:261–330. doi: 10.1016/j.earscirev.2004.01.004

O'Brien G, O'Keefe P, Rose J, Wisner B (2006) Climate Change and Disaster Management. Disasters 30:64–80.

O'Brien JS, Julien PY, Fullerton WT (1993) Two-Dimensional water Flood and mudflow simulation. J Hydraul Eng 119:244–261.

O'Brien K, Eriksen S, Schjolden A, Nygaard L (2004) What's in a word? Conflicting interpretations of vulnerability in climate change research. Working Paper 2004:04. 19.

O'Connor J, Hardison J, Costa J (2001) Debris flows from failures of Neoglacial-age moraine dams in the Three Sisters and Mount Jefferson Wilderness Areas, Oregon. 117.

OFEE, OFAT, ODEFP (1997) Prise en compte des dangers dus aux crues dans le cadre des activités de l'aménagement du territoire. Bienne, Switzerland

Osti R, Egashira S (2009) Hydrodynamic characteristics of the Tam Pokhari Glacial Lake outburst flood in the Mt . Everest region, Nepal. Hydrol Process 23:2943– 2955. doi: 10.1002/hyp

Peng S-H, Lu S-C (2013) FLO-2D simulation of mudflow caused by large landslide due to extremely heavy rainfall in southeastern Taiwan during Typhoon Morakot. J Mt Sci 10:207–218. doi: 10.1007/s11629-013-2510-2

Petrascheck AW, Sydler PA (1984) Routing of Dam Break Floods. Int Water Power Dam Constr 36:29–32.

Portocarrero C (2014) The Glacial Lake Handbook: Reducing Risk from Dangerous Glacial Lakes in the Cordillera Blanca, Peru, United States Agency for International Development, Washington, DC.

PREVENE (2001) Contribution to "Natural" Disaster Prevention in Venezuela. Cooperation: Venezuela - Switzerland - PNUD (Project VEN/00/005).

Quincey DJ, Richardson SD, Luckman A, et al. (2007a) Early recognition of glacial lake hazards in the Himalaya using remote sensing datasets. Glob Planet Change 56:137–152. doi: 10.1016/j.gloplacha.2006.07.013

Quincey DJ, Richardson SD, Luckman A, et al. (2007b) Early recognition of glacial lake hazards in the Himalaya using remote sensing datasets. Glob Planet Change 56:137–152.

Rabatel A, Francou B, Soruco A, et al. (2013) Current state of glaciers in the tropical Andes: a multi-century perspective on glacier evolution and climate change. Cryosph 7:81–102. doi: 10.5194/tc-7-81-2013

Racoviteanu AE, Arnaud Y, Williams MW, Ordon J (2008) Decadal changes in glacier parameters in the Cordillera Blanca, Peru, derived from remote sensing. J Glaciol 54:499–510.

Rana B, Shrestha AB, Reynolds JM, et al. (2000) Hazard assessment of the Tsho Rolpa Glacier Lake and ongoing remediation measures. J Nepal Geol Soc 22:563–570.

RESCDAM (2000) The Use of Physical Models in Dam-Break Flood Analysis. Rescue Actions Based on Dam-Break Flood Analysis, Final Report of Helsinki University of Technology, Helsinki, Finland.

RGSL (2003) Development of glacial hazard and risk minimization protocols in rural environments Guidelines for the management of glacial hazards and risks. 69.

Richardson SD (2010) Remote sensing approaches for early warning of GLOF hazard in the Hindu Kush – Himalayan region, United Nations International Strategy for Disaster Reduction (UN/ISDR).

Richardson SD, Reynolds JM (2000) An overview of glacial hazards in the Himalayas. Quat Int 65/66:31–47.

Rickenmann D (1999) Empirical Relationships for Debris Flows. Nat Hazards 19:47–77.

Robertson CM, Benn DI, Brook MS, et al. (2012) Subaqueous calving margin morphology at Mueller , Hooker and Tasman glaciers in Aoraki / Mount Cook National Park , New Zealand. J Glaciol 58:1037–1046. doi: 10.3189/2012JoG12J048

Rogers GO, Sorensen JH (1991) Diffusion of Emergency Warning: Comparing Empirical and Simulation Results. In Risk Analysis Prospects and Opportunities, C. Zerros et al. (eds.), Plenum Press, New York, p. 117 - 134.

Röhl K (2006) Thermo-erosional notch development at fresh-water-calving Tasman Glacier, New Zealand. J Glaciol 52:203–213. doi: 10.3189/172756506781828773

Rouse JW, R.H H, Deering DW, Schell JA (1973) Monitoring the vernal advancement and retrogradation (green wave effect) on natural vegetation. 1–87.

Sakai A, Fujita K (2010) Formation conditions of supraglacial lakes on debris covered glaciers in the Himalaya. J Glaciol 56:177–181.

Sakai A, Fujita K, Yamada T (2005) Expansion of the Imja glacier in the east Nepal Himalayas. 7th GLACKIPR Symp.

Sakai A, Fujita K, Yamada T (2003) Volume change of Imja Glacial Lake in the Nepal Himalayas. Comput Inf Sci c:556–561.

Sakai A, Saito M, Nishimura K, et al. (2007) Topographical survey of end moraine and dead ice area at Imja glacier in 2001 and 2002. Bull Glaciol Res 24:29–36.

Sass O (2007) Bedrock detection and talus thickness assessment in the European Alps using geophysical methods. J Appl Geophys 62:254–269. doi: 10.1016/j.jappgeo.2006.12.003

Schmidtlein MC, Deutsch RC, Piegorsch WW, Cutter SL (2008) A sensitivity analysis of the social vulnerability index. Risk Anal 28:1099–114. doi: 10.1111/j.1539-6924.2008.01072.x

Schneider D, Huggel C, Cochachin A, et al. (2014) Mapping hazards from glacier lake outburst floods based on modelling of process cascades at Lake 513, Carhuaz, Peru. Adv Geosci 35:145–155. doi: 10.5194/adgeo-35-145-2014

Shrestha AB, Aryal R (2010) Climate change in Nepal and its impact on Himalayan glaciers. Reg Environ Chang 11:65–77. doi: 10.1007/s10113-010-0174-9

Shrestha AB, Aryal R (2011) Climate change in Nepal and its impact on Himalayan glaciers. Reg Environ Chang 11:65–77. doi: 10.1007/s10113-010-0174-9

Shrestha BB, Nakagawa H, Kawaike K, Baba Y (2010) Glacial Lake Outburst due to Moraine Dam Failure by Seepage and Overtopping with Impact of Climate Change. Annu Disas Prev Res Inst Kyoto Univ 569–582.

Silverio W, Jaquet J-M (2005) Glacial cover mapping (1987–1996) of the Cordillera Blanca (Peru) using satellite imagery. Remote Sens Environ 95:342–350. doi: 10.1016/j.rse.2004.12.012

Singh P, Bengtsson L (2004) Hydrological sensitivity of a large Himalayan basin to climate change. Hydrol Process 18:2363–2385.

Somos-Valenzuela M, Chisolm RE, McKinney DC, Rivas D (2014a) Hazard Mapping of a Potential Glacial Lake Outburst Flood in Huaraz, Peru. CRWR Online Report 14-01.

Somos-Valenzuela MA, McKinney DC, Rounce DR, Byers AC (2014b) Changes in Imja Tsho in the Mt. Everest region of Nepal. Cryosph Discuss 8:2375–2401. doi: 10.5194/tcd-8-2375-2014

Tacsi A, Zapata M, Arnaud Y (2008) Inventario de glaciares y lagunas alto andinas de la Cordillera Blanca (Ancash-Peru). VII ENCUENTRO Int. Investig. DEL Group. Trab. NIEVES Y HIELOS Am. Lat. DEL PHI-UNESCO 26 al 30 Agosto 2008

Timmerman P (1981) Vulnerability, resilience and the collapse of society. Environmental Monograph I.

Trujillo-Ortiz A, Hernandez-Walls R, Castro-Perez A, et al. (2006) kmo: Kaiser-Meyer-Olkin Measure of Sampling Adequacy. A MATLAB file. [WWW document]. URL http://www.mathworks.com/matlabcentral/fileexchange/loadFile.do?objectId=12736 .

Trujillo-Ortiz A, Hernandez-Walls. R (2003) Sphertest: Sphericity tests menu. A MATLAB file. [WWW document]. URL

http://www.mathworks.com/matlabcentral/fileexchange/loadFile.do?objectId=3694&objectType=FILE.

U.S.B.R. (1988) Downstream Hazard Classification Guidelines, ACER Technical Memorandum No. 11, Assistant Commissioner-Engineering and Research. 57.

UNDP (2013) Community Based Glacier Lake Outburst and Flood Risk Reduction in Nepal. Project Document, UNDP Environmental Finance Services, Kathmandu, Nepal.

USACE (2003) Uncertainty in Bathymetric Surveys, Coastal and Hydraulics Engineering Technical Note ERDC/CHL CHETN-IV-59.

USACE (2010) HEC-RAS River Analysis System User's Manual (Version 4.1). Davis, CA, U.S.A.

USACE (2012) HEC-FIA Flood Impact Analysis User's Manual. 1–352.

USDHS (2011) Dams Sector. Estimating loss of life for dam failure scenarios. 1–94.

Valderrama P, Vilga O (2012) Dinamica e implicancias del aluvion de la Laguna 513, Cordillera Blanca, Ancash Peru. Rev la Asoc Geológica Argentina 69:400–406.

Vergara W, Valencia A, Haeussling S, et al. (2009) Latin America and Caribbean Region Sustainable Development Working Paper 32: Assessing the Potential Consequences of Climate Destabilization in Latin America.

Vogel C, Moser SC, Kasperson RE, Dabelko GD (2007) Linking vulnerability, adaptation, and resilience science to practice: Pathways, players, and partnerships. Glob Environ Chang 17:349–364. doi: 10.1016/j.gloenvcha.2007.05.002

Vuichard D, Zimmermann M (1986) The Langmoche Flash-Flood, Khumbu Himal, Nepal. Mt Res Dev 6:90–94.

Vuichard D, Zimmermann M (1987) The 1985 Catastrophic Drainage of a Moraine-Dammed Lake, Khumbu Himal, Nepal: Cause and Consequences. Mt Res Dev 7:91. doi: 10.2307/3673305

Vuille M, Francou B, Wagnon P, et al. (2008) Climate change and tropical Andean glaciers: Past, present and future. Earth-Science Rev 89:79–96. doi: 10.1016/j.earscirev.2008.04.002

Wahl TL (1998) Prediction of Embankment Dam Breach Parameters - A Literature Review and Needs Assessment. 67.

Wahl TL (2004) Uncertainty of Predictions of Embankment Dam Breach Parameters. J Hydraul Eng 130:389. doi: 10.1061/(ASCE)0733-9429(2004)130:5(389)

Wang W, Yao T, Gao Y, et al. (2011) A First-order Method to Identify Potentially Dangerous Glacial Lakes in a Region of the Southeastern Tibetan Plateau A First-order Method to Identify Potentially Dangerous Glacial Lakes in a Region of the Southeastern Tibetan Plateau. Mt Res Dev 31:122–130.

Warren CR, Kirkbride MP (2003) Calving speed and climatic sensitivity of New Zealand lake-calving glaciers. Ann Glaciol 36:173–178. doi: 10.3189/172756403781816446

Watanabe T, Ives JD, Hammond JE (1994) Rapid growth of a glacial lake in Khumbu Nepal, Nepal Himalaya: prospects for a catastrophic flood. Mt Res Dev 14:329–340.

Watanabe T, Kameyama S, Sato T (1995) Imja Glacier dead-ice melt rates and changes in a supra-glacial lake, 1989-1994, Khumbu Himal, Nepal: danger of lake drainage. Mt Res Dev 15:293–300.

Watanabe T, Lamsal D, Ives JD (2009) Evaluating the growth characteristics of a glacial lake and its degree of danger of outburst flooding: Imja Glacier, Khumbu Himal, Nepal. Nor Geogr Tidsskr - Nor J Geogr 63:255–267. doi: 10.1080/00291950903368367

WGMS (2008) Global glacier changes: facts and figures. M. Zemp, I. Roer, A. Kääb, M. Hoelzle, F. Paul and W. Haeberli Eds. UNEP and WGMS, Nairobi and Zurich. Free download from UNEP and WGMS homepages.

Woodward J, Burke MJ (2007) Applications of Ground-penetrating Radar to Glacial and Frozen Materials. J Environ Eng Geophys 12:69–85. doi: 10.2113/JEEG12.1.69

Wu Y-H, Liu K-F, Chen Y-C (2013) Comparison between FLO-2D and Debris-2D on the application of assessment of granular debris flow hazards with case study. J Mt Sci 10:293–304. doi: 10.1007/s11629-013-2511-1

Xin W, Shiyin L, Wanqin G, Junli X (2008) Assessment and Simulation of Glacier Lake Outburst Floods for Longbasaba and Pida Lakes, China. Mt Res Dev 28:310–317. doi: 10.1659/mrd.0894

Yamada T (1998) Glacier lakes and its outburst flood in the Nepal Himalaya. Monograph No.1.

Yamada T, Sharma CK (1993) Glacier Lakes and Outburst Floods in the Nepal Himalaya, in Snow and Glacier Hydrology. Proc. Kathmandu Symp. Nov. IAHS Publ. No. 218.

Yoon DK (2012) Assessment of social vulnerability to natural disasters: a comparative study. Nat Hazards 63:823–843. doi: 10.1007/s11069-012-0189-2

Zemp M, Haeberli W, Hoelzle M, Paul F (2006) Alpine glaciers to disappear within decades? Geophys Res Lett 33:L13504. doi: 10.1029/2006GL026319

Zhou R, Judge D, Donelly CR (2005) Comparison of HEC-RAS with FLDWAV and DAMBRK Model for Dam Break Analysis. CDA2005 Annu. Conf. p 13